Norwegian University of Life Sciences
Faculty of Science and Technology

Philosophiae Doctor (PhD)
Thesis 2023:5

Raman spectroscopy for in-line food quality characterization

Raman spektroskopi for målinger av matkvalitet i prosesslinjen

Tiril Aurora Lintvedt

Raman spectroscopy for in-line food quality characterization

Raman spektroskopi for målinger av matkvalitet i prosesslinjen

Philosophiae Doctor (PhD) Thesis

Tiril Aurora Lintvedt

Norwegian University of Life Sciences

Faculty of Science and Technology

Ås 2023

Thesis number 2023:5

ISSN 1894-6402

ISBN 978-82-575-2033-5

"Ask the right questions, and nature will open the doors to her secrets"

— C. V. Raman

Abstract

A major challenge in the food industry is to effectively handle massive streams of food raw materials and products of different origin and quality. In-line sensor systems for food analysis can potentially measure and collect critical quality and safety parameters throughout the processes. This information can be used for sorting, product differentiation, process optimisation and product control. One emerging technology that shows great promise for future in-line food sensor systems is Raman spectroscopy. The overall goal of this thesis was to elucidate the feasibility of Raman spectroscopy as a tool for detailed quality evaluation of heterogeneous food raw materials, under in-line industrial conditions. To this end, two main application areas were chosen, including A1) in-line measurements of fatty acid features in salmon fillets and A2) in-line characterization of a poultry rest raw material stream.

A central element in both application areas was the use of a Wide Area Illumination (WAI) Raman probe to obtain representative measurements of the heterogeneous raw materials and to tackle variations in working distance. Variations in working distance may easily happen in an industrial process line with samples of varying thicknesses and streams of varying production volumes. The limited measurement volume of the WAI probe was increased by scanning over the sample surface. We showed that this strategy was successful with respect to obtaining representative measurements. This was demonstrated through obtaining good performances for EPA+DHA estimation in salmon fillets of varying thickness (± 1 cm) and through characterization (fat, protein, bone and collagen) of poultry rest raw material with larger variations in working distances (± 3 cm). For the latter study, the method was also tested in-line at a real hydrolysis facility with promising results. For the study on salmon fillets, the varying fat deposition across the fillets was shown to have implication for choice of scanning strategy at shorter exposure times due to impact on signal-to-noise ratio (SNR). This illustrates the importance of considering the heterogeneity of the food product in a given application, and of optimizing measurement strategies accordingly.

Another main objective was to elucidate the ability of Raman measurements to tackle short exposure times. This is of particular importance for measurements of single samples at a conveyor belt, where exposure time is strictly limited. This was investigated in paper I and II, where we measured single salmon and poultry samples at exposure times down to 1 s. While exposure times around 2-1 s in these cases did give acceptable performances, it was evident that these low exposure times reduced SNR and performance and that SNR was a critical parameter. This indicates that at shorter exposure times, the surface scanning with the WAI Raman probe might be less robust with respect to tackling samples of varying sample sizes or lower analyte concentrations. Therefore, for such single samples, WAI Raman spectroscopy is currently better suited for fast at-line or on-line measurements.

However, such measurements could also have high value for the industry, as it represents a frequent quality feedback, which is currently lacking.

Overall, it was found that further efforts on calibration development, SNR optimization and practical measurement setup are needed to unlock the full potential for in-line measurements in the two application areas. Still, this thesis has shown that it is feasible to use a WAI Raman probe for detailed characterization of very heterogeneous streams of raw material, at industrially relevant speeds and in presence of moderate variations in working distance and probe tilt. It was shown that WAI Raman spectroscopy is promising, both for measurements of continuous raw material streams and single food products on a conveyor belt. This introduces many new application opportunities for Raman spectroscopy within quality documentation, sorting, process analysis and real-time process control in the food industry.

Sammendrag

En stor utfordring for matindustrien er å håndtere store strømmer av råvarer og produkter av forskjellig opprinnelse og kvalitet på en effektiv måte. Sensorsystemer som kan brukes direkte på prosesslinjene, såkalt "in-line", kan potensielt måle og samle kritisk informasjon om matkvalitet og mattrygghet. Resultatet er verktøy for sortering, produktdifferensiering, prosessoptimering og produktkontroll. Raman spektroskopi er en lovende teknologi under utvikling med stort potensiale som sensorsystem i matindustrien. Målet med dette doktorgradsprosjektet var å undersøke mulighetene for å bruke Raman-spektroskopi som et verktøy for kvalitetsmålinger av heterogene matråvarer direkte i prosesslinjen. For å nå dette målet ble to bruksområder valgt, inkludert A1) in-line målinger av fettsyreprofil i laksefileter og A2) in-line karakterisering av råvarestrømmer fra fjærfe-produksjon.

Et sentralt tema for begge bruksområdene var bruken av en Raman-probe med bredt belysningsområde (WAI) for å oppnå representative målinger av heterogene råvarer og for å takle variasjoner i arbeidsavstand. Variasjoner i arbeidsavstand kan fort oppstå i en industriell prosesslinje med prøver av varierende tykkelse og for stømmer med varierende produksjonsvolum. Fokusvolumet til WAI-proben ble økt ved å skanne over prøveoverflaten. Vi viste at denne strategien fungerte godt for å oppnå representative målinger. Dette ble demonstrert ved å oppnå lave prediksjonsfeil for EPA + DHA-estimering i laksefileter med varierende tykkelse ($\pm$ 1 cm) og for karakterisering (fett, protein, bein og kollagen) av kyllingråstoff med større variasjoner i arbeidsavstand ($\pm$ 3 cm). For sistnevnte studie ble metoden også testet in-line på et industrielt hydrolyseanlegg, med lovende resultater. For studien på laksefileter ble det vist at det varierende fettinnholdet på filletoverflaten hadde betydning for valg av skannestrategi ved kortere eksponeringstider, grunnet effekten på signal-støy-forholdet. Dette illustrerer hvor viktig det er å gjøre nøye vurderinger av heterogeniteten til et gitt matprodukt, og å optimalisere målestrategien deretter.

Et annet hovedmål var å undersøke hvordan Raman-målingene håndterte kortere eksponeringstider. Dette er av spesiell betydning for målinger av enkeltprøver på et transportbelte, der eksponeringstiden er sterkt begrenset. Dette ble undersøkt i artikkel I og II, der vi målte enkeltprøver av laks og fjærfe-restråstoff ved eksponeringstider ned til 1 s. Selv om eksponeringstider rundt 2-1 s i disse tilfellene ga akseptable prediksjonsfeil, var det tydelig at disse lave eksponeringstidene reduserte signal-støy-forholdet og dermed prediksjons-prestasjonen. Signal-støy-forholdet er altså en kritisk faktor, og dette indikerer at skanning med WAI Raman-proben kan være mindre robust når det gjelder å håndtere prøver med varierende prøvestørrelser eller lavere analytt-konsentrasjoner, ved slike korte eksponeringstider. Derfor er Raman-målingene foreløpig bedre egnet for hurtige målinger ved siden av produksjonslinjen ("at-line" eller "on-line"), for enkeltprøver. Slike målinger kan også ha høy verdi for industrien, da det representerer et system

som gir hyppig tilbakemelding på kvalitet, noe som det for øyeblikket ikke finnes løsninger for.

En videre innsats innen kalibreringsutvikling, SNR-optimering og utvikling av praktisk måleoppsett er nødvendig for å realisere det fulle potensialet for in-line Raman-målinger i de to applikasjonsområdene. Likevel har dette doktorgradsprosjektet vist at det er mulig å bruke en Raman probe med bredt belysningsområde til detaljert karakterisering av av svært heterogene strømmer med råvaremateriale, ved industrielt relevante eksponeringstider og med moderat variasjon i arbeidsavstand. Det ble vist at WAI Raman spektroskopi er lovende både for målinger på kontinuerlige råvarestrømmer og enkeltprøver på et transportbelte. Dette muliggjør en rekke nye applikasjoner for WAI Raman spektroskopi innen kvalitetsdokumentasjon, sortering, prosessanalyse og sanntids prosesskontroll i matindustrien.

Preface

The past three years, from 2020 to 2023, have been an incredible learning experience. I would like to express my deepest gratitude to my supervisors at Nofima, Jens Petter Wold and Nils Kristian Afseth for their dedication and patience throughout my PhD work. I would also like to extend my appreciation to my main supervisor at NMBU, Achim Kohler, for his invaluable guidance. Special thanks to Petter Vejle Andersen and Erik Tengstrand for stimulating helpful discussions about chemometrics and spectroscopy. I am so grateful to the extended research team at Nofima for the warm welcome, even though I showed up during the initial months of the COVID-19 lockdown and there weren't many high-fives or warm handshakes to go around. A big thank you to Katinka Dankel for always being a great office buddy and also for helping me out with all those dummy chemistry questions I had. I would also like to give a shoutout to my fellow PhD students, the "Kids of Covariance". Thank you for the great camaraderie and support. I hope that I can be of help when it's your turn to defend your theses.

This research have been funded by the Research Council of Norway through projects SFI Digital Food Quality and the Food Pilot Plant, as well as the Norwegian Agricultural Food Research Foundation through the project Precision Food Production. I have been especially excited to be involved in the Digital Food Quality (DigiFoods) centre for research-based innovation (SFI). This center aims to develop sensor solutions for food quality assessment directly in the processing lines, throughout the food value chains. It is envisioned that real-time analysis and utilization of large-scale industrial data collected from connected sensors and machines, will significantly increase productivity and reduce food loss. I would like to direct a special thanks the industry partners in the DigiFoods project, particularly Bioco, Nortura and Lerøy Aurora, for welcoming me and other colleagues into their facilities and teaching us about the inner workings of the food industry. I would also like to express a special thanks to Brian Marquardt and MarqMetrix Inc. for providing Raman instrumentation through the partnership in DigiFoods.

I am forever grateful for the guidance and support of my colleagues, and I hope that the results of my research will make a meaningful contribution to the field of food science and technology. Last but not least, a big big thanks to my cohabitant and partner Zakarias, without whom I would not have eaten a decent meal these past months.

Tiril Lintvedt

Ås, February 2023

Contents

List of Papers

Paper I

[1] Tiril Aurora Lintvedt, Petter Vejle Andersen, Nils Kristian Afseth, Brian Marquardt, Lars Gidskehaug, and Jens Petter Wold. Feasibility of In-line Raman Spectroscopy for Quality Assessment in Food Industry - How Fast Can We Go? *Applied Spectroscopy*, 76(5):559–568, 2022

Paper II

[2] Tiril Aurora Lintvedt, Petter Vejle Andersen, Nils Kristian Afseth, Karsten Heia, Stein-Kato Lindberg, and Jens Petter Wold. Raman Spectroscopy and NIR Hyperspectral Imaging for In-line Estimation of Fatty Acid Features in Salmon Fillets. *Talanta*, 254:124113, 2023

Paper III

[3] Tiril Aurora Lintvedt, Petter Vejle Andersen, Nils Kristian Afseth, and Jens Petter Wold. In-line Raman Spectroscopy for Characterization of an Industrial Poultry Raw Material Stream. *Submitted to Talanta*

Additional Scientific Work

Poster Presentations

Tiril Aurora Lintvedt, Petter Vejle Andersen, Nils Kristian Afseth, Karsten Heia, Stein-Kato Lindberg, and Jens Petter Wold. Raman Spectroscopy for In-line Food Quality Sensing on a Conveyor Belt. In *SciX Conference*, Providence, RI, 2021

Tiril Aurora Lintvedt, Petter Vejle Andersen, Nils Kristian Afseth, Brian Marquardt, Lars Gidskehaug, and Jens Petter Wold. Feasibility of In-line Raman Spectroscopy for Quality Assessment in the Food Industry. In *European Biosensor Symposium*, 2021

Tiril Aurora Lintvedt, Petter Vejle Andersen, Nils Kristian Afseth, Karsten Heia, Stein-Kato Lindberg, and Jens Petter Wold. Raman Spectroscopy for In-line Estimation of Fatty Acid Features in Salmon Fillets. In *The International SensorFINT Conference*, Izola, Slovenia, 2022

List of Abbreviations

ALS	Asymmetric Least Squares
ANOVA	Analysis of Variance
CCD	Charge-Coupled Device
CV	Cross Validation
DHA	Docosahexaenoic Acid
EMSC	Extended Multiplicative Signal Correction
EPA	Eicosapentaenoic Acid
FA	Fatty Acid
HSI	Hyperspectral Imaging
HYP	Hydroxyproline
LV	Latent Variables
MUFA	Monounsaturated Fatty Acid
NA	Numerical Aperture
NIRS	Near Infrared Spectroscopy
PAT	Process Analytical Technology
PLSR	Partial Least Squares Regression
PUFA	Polyunsaturated Fatty Acid

SAT	Saturated Fatty Acid
SG	Savitzky–Golay
SNR	Signal to Noise Ratio
SNV	Standard Normal Variate
TAG	Triacylglycerol
WD	Working distance

Chapter 1

Background

1.1 General introduction

There is an increasing pressure on the food processing sector to be more competitive, to reduce costs, to be more sustainable and to prevent food waste. This can only be met with new innovative technology. A major challenge in this industry is to effectively handle massive streams of food raw materials and products of different origin and quality. The inherent raw material variation can reduce process efficiency, give variable end quality and food loss. The raw material can account for as much as 75% of the cost of the final food product [7], illustrating the importance of controlling and utilizing this variation. A crucial part of the new digital transformation in the food industry is the use of sensors to measure the critical quality and process parameters. In-line sensor systems for food analysis can potentially measure and collect critical quality and safety parameters throughout the processes. This information can be used for sorting, product differentiation, process optimisation and product control, leading to a more sustainable and profitable food industry.

One emerging technology that shows great promise for food sensor systems is Raman spectroscopy. Raman spectroscopy relies upon inelastic scattering of photons, known as Raman scattering. By illuminating the sample with a laser beam and detecting Raman scattered photons, vibrational modes of molecules can be determined. Raman is gaining increasing interest for its ability to capture subtle chemical distinctions in foods. Recent feasibility studies show how the various Raman techniques can be used to quantify complex food quality features like fatty acids in muscle foods [8, 9], describe protein structure related to water holding capacity in pork meat [10] and quantify mineral, bone and collagen content [11, 12] in meat slurries. However, in those studies the focus was not to measure under industrial conditions, while in this thesis we elucidate the feasibility of using Raman spectroscopy for food quality measurements directly in the processing lines.

1.2 Main goal and challenges

Traditionally, Raman spectroscopy requires expensive instrumentation and has therefore been used mostly in academic and industrial laboratories. Recently, however, robust and more low-cost Raman instrumentation has become available

and paves the way for affordable and practical in-line sensor solutions in the food industry. There are still some main challenges connected to successful in-line applications in the food industry, as elaborated below.

Raman scattering is an optical phenomenon with low probability. It is well known that for this reason, measurements can suffer from low signal-to-noise-ratio (SNR). Biological tissues (e.g. foods) typically yield low-to-moderate Raman signal intensities, depending on the analyte [13]. Therefore, reported literature on quality measurements for such samples typically employ minute-long exposure times, to increase signal intensity as much as possible [9,14,15]. Generally, signal intensities can be increased either by employing higher laser power, shorter laser excitation wavelengths or prolonged exposure times. However, the laser power may be limited due to occurrence of burning effects [16,17] or ultimately by complying with the conventional laser hazard class (3B according to the FDA), which restricts the maximum laser power [18]. The choice of laser is also often restricted to longer laser wavelengths since this helps avoid strong disturbances from fluorescence, commonly present in spectra from biological tissues [19–21]. This is why adjusting exposure time is often the easiest way to control signal intensity for food samples. However, for in-line applications, measurements might be needed within seconds. Therefore a challenge is to **obtain adequate SNR for quantitative analysis on detailed food quality features at short enough exposure times**.

Furthermore, food raw materials can consist of many types of tissues and may be spatially very heterogeneous [22, 23]. Since Raman spectroscopic techniques illuminate the sample with a small laser spot, the sampling volume is very limited. Wide area illumination (WAI) Raman probes, for which the laser spot size can be increased up to 6 mm, have been suggested as a way to obtain more representative measurements [24–26]. This has in recent studies been combined with a surface scanning approach to further increase sample coverage [12,15,23]. Still, the sampling volume is limited, and a challenge is to **ensure representative measurements of larger heterogeneous food products or streams**.

Due to the combination of the two main challenges stated above, Raman spectroscopy has not yet gained particular attention for in-line measurements of heterogeneous foods. There is generally a lack of literature on detailed food quality measurements for heterogeneous foods at short exposure times. Literature reports in-line type applications where longer exposure times are employed and less complex sample matrices are considered, such as monitoring of fermentation processes [27] and monitoring of degradation processes of frying oils [28]. Therefore, the investigation of Raman spectroscopy employed for quality measurement of more complex raw material streams is needed to elucidate the full potential and limitations of Raman spectroscopy for in-line food applications.

The main research goal of this thesis was to elucidate the feasibility of Raman spectroscopy as a tool for detailed quality evaluation of heterogeneous food raw materials, under in-line industrial conditions. Related to the above challenges,

three subgoals were defined:

G1 Develop effective Raman sampling regimes for heterogeneous foods suitable for industrial in-line conditions

G2 Develop analysis strategies for in-line evaluation of food quality parameters based on Raman measurements

G3 Evaluate performance of developed strategies in a real in-line industry setting.

The challenges and feasibility of in-line Raman measurements will depend on the chemical compounds of interest, the sample composition and the practical measurement situation. Therefore, two main application areas were chosen for this thesis:

A1 In-line measurements of fatty acid features in salmon fillets

A2 In-line characterization of a poultry rest raw material stream

These applications represent two considerably different measurement tasks, both with respect to the raw material, analytes of interest and the practical measurement situation. In the salmon application, we aim to measure specific fatty acids in single fillets that pass by on a conveyor belt. This limits the exposure time greatly. The salmon fillets vary little in thickness, but are spatially heterogeneous. However, the heterogeneity is known reasonably well [22], with fat distribution over the fillet being a main factor. For the poultry rest raw material application, we aim to measure several different analytes in a continuous stream. This does not limit the exposure time in the same way, but the material can be very heterogeneous and the stream can vary considerably in volume. In addition, the magnitude and frequency of variations are unknown.

Chapter 2

Theory and Methods

2.1 The theory behind Raman spectroscopy

2.1.1 Origin of the Raman spectrum

Raman spectroscopy relies upon inelastic scattering of photons, known as Raman scattering. This effect was discovered in 1928 by C.V. Raman and his research group [29]. They observed the scattering from a range of different liquids when focusing sunlight on the samples, and provided evidence that the scattering was different from the more commonly known fluorescence phenomenon. The significance of his work was quickly appreciated and C.V. Raman won a Nobel prize in 1930. Within a few years, chemists started to use Raman spectroscopy routinely for chemical analysis. The technique is typically used to determine vibrational modes of molecules and can provide a chemical fingerprint by which molecules can be identified. Raman scattering is an interaction process between an incoming electromagnetic wave and a molecule, which has very low probability. To effectively utilize this effect, one has to employ illumination sources such as lasers. In standard Raman spectroscopy, the incoming photons excite the molecule to a virtual energy state, which is not stable, and immediately prompts the emission of a scattered photon, as illustrated in Figure 2.1. The scattered photon gains a shift in frequency due to the energy transfer, which can be observed by the detector at the frequency ν, as described by

$$\nu = \nu_0 \pm \nu_m, \qquad \bar{\nu} = \frac{\nu_0}{c} \pm \frac{\nu_m}{c}, \tag{2.1}$$

where ν_0 is the frequency of the radiation source and ν_m is the frequency of the molecular vibration [30]. The alternative expression on the right expresses this shift in units of wavenumber (cm^{-1}), which is customary in the field. The difference $\nu - \nu_0$ is called the Raman shift. As the equation indicates, the photon can both gain and loose energy, depending on the initial vibrational state of the molecule. If the molecule is initially in the ground state vibration (v = 0), it may fall back to the first excited vibrational state (v = 1). This results in emission of a photon with lower frequency, a phenomenon referred to as the *Stokes* Raman effect. If instead the molecule is initially in the first excited state, the molecule may also fall back to the ground state with emission of a photon with higher

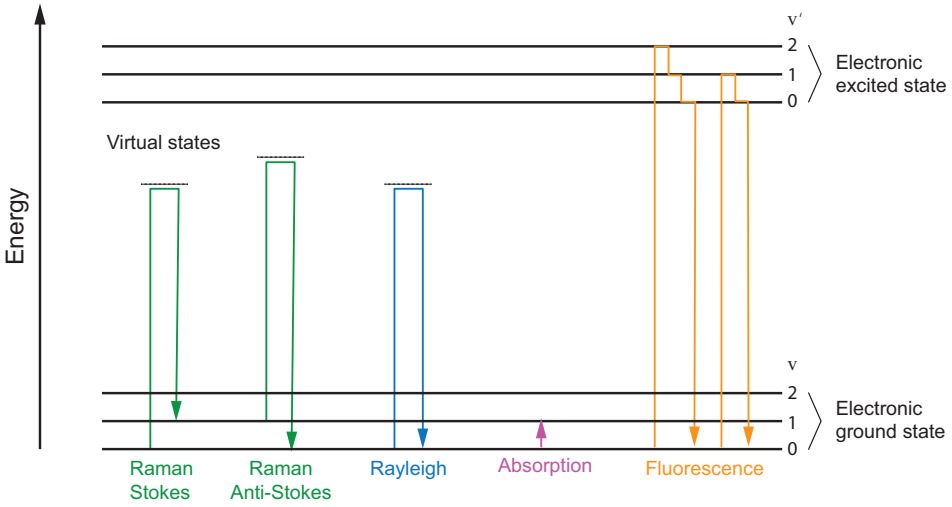

Figure 2.1: Diagram illustrating the energy level of a molecular vibration upon illumination, showing the possible and most relevant scattering and absorption phenomena with respect to Raman spectroscopic measurements. The vibrational energy levels are denoted v for the electronic ground state and v′ for the electronic excited state. The energy axis is not linear (distances between energy levels are not accurate).

frequency. This phenomenon is referred to as the *Anti-Stokes* Raman effect. At normal sample temperatures, most molecular vibrations are in the ground state, as described by Boltzmann's population law, which means that the Stokes scattering component usually has higher intensity and is therefore most utilized in Raman instruments. The Boltzmann's population law is given by

$$\frac{N_{\mathrm{v}=1}}{N_{\mathrm{v}=0}} = e^{-h\nu_m/kT}, \tag{2.2}$$

where N is the number of molecules in the respective state of a given vibration, h is Planck's constant, k is Boltzmann's constant and T is the absolute temperature of the sample [31]. The nature of the energy transfer during Raman scattering is the induction of a dipole moment in the electron cloud for the oscillating (ν_m) molecular bond by the incoming photon's oscillating (ν_0) electric field ($\boldsymbol{E}$). The induced dipole moment $\boldsymbol{p}$ can (simplified) be described by

$$\boldsymbol{p} = \alpha \boldsymbol{E} = \alpha \boldsymbol{E}_0 \cos(2\pi\nu_0 t), \tag{2.3}$$

where α is the polarizability (tensor) [31]. As the chemical bond vibrates, the polarizability may also vary. When the variation in polarizability as a function of molecule vibration is taken into account (and polarizability assumed to undergo

harmonic oscillation), it can be shown that this dipole moment will have three components, as described by

$$\begin{aligned} \boldsymbol{p} = \alpha_0 \boldsymbol{E}_0 \cos 2\pi\nu_0 t \quad &+ \quad 1/2 \quad \alpha_\nu^{'} \boldsymbol{E}_0 Q_{\nu 0} \cos(2\pi(\nu_0 + \nu_m)t + \varphi_v) \\ &+ \quad 1/2 \quad \alpha_\nu^{'} \boldsymbol{E}_0 Q_{\nu 0} \cos(2\pi(\nu_0 - \nu_m)t + \varphi_v), \end{aligned} \tag{2.4}$$

where the $\alpha_\nu^{'}$ is the derivative of the polarizability to the normal coordinate Q_ν under equilibrium, $Q_{\nu 0}$ is the amplitude of the normal vibration, ν_m is the vibrational frequency of the normal coordinate of the molecule and φ_ν is a phase difference [32]. The two latter terms in the above equation are associated with the Raman Anti-Stokes and Stokes effects, respectively. It is evident that these terms require a change in polarizability in order to have a non-zero amplitude, therefore rendering the bond Raman inactive if this is not the case. The first term is associated with a third possible event: the elastic Rayleigh scattering occurring at the same frequency as the incoming photon, which can give as much as 10^6 times stronger signals than Raman scattering [30]. This component of the signal is therefore filtered out, as it does not contain relevant information and would saturate the detector.

In general, the acquired signal from a bulk sample is not only comprised of the Raman and Rayleigh components. An acquired spectrum can be influenced by other competing phenomena, as summarized in Figure 2.1. Autofluorescence can disturb the Stokes Raman signal if there are fluorophores in the sample, and give rise to broad baseline signals. If the laser frequency corresponds to transitions between vibrational modes in some molecules of the sample, IR absorption can also occur and reduce the Raman intensities. See section 2.1.4 for an overview of possible spectrum disturbances. Disregarding such influences, the intensity I_m of the Stokes Raman component of the spectrum for a given molecular vibration obeys the following proportional relationship

$$I_m \propto \frac{I_0 N(\bar{\nu_0} - \bar{\nu_m})^4}{\bar{\nu_m}(1 - e^{-hc\bar{\nu_m}/kT})}, \tag{2.5}$$

where I_0 is the laser intensity, N is the number of scattering molecules present in the illuminated volume, $\bar{\nu_0}$ is the frequency of the laser in wavenumber, $\bar{\nu_m}$ is the frequency of the molecular vibration in wavenumber, h is Planck's constant, c is the speed of light, k is Boltzmann's constant and T is the absolute temperature [32]. From this equation one can readily see that the recorded spectrum intensity at the given Raman shift is proportional to the concentration of the molecule, which is the basis for quantitative modelling of constituents based on Raman spectra. Enhancing the Raman intensity as much as possible is usually important for accurate quantitative analysis. To enhance the Raman intensity, it is evident from Eq. 2.5 that one can increase the laser intensity (power), increase

the number of scattering molecules (i.e. by increasing exposure time) or increase the laser frequency. Although the intensity is proportional to the fourth power of the laser frequency, higher laser frequencies are also associated with increased autofluorescence, i.e. there's a higher chance that the incident laser frequency correspond with an electronic transition (Figure 2.1). This is generally a big challenge when acquiring Raman spectra of biological tissues [19, 20]. Usually, a 785 nm wavelength laser is considered a good compromise between Raman intensity and autofluorescence level.

2.1.2 Raman active groups

As explained in section 2.1.1, a molecular vibration is Raman active, if the polarizability of the molecule varies with the vibration. For such vibrations, the frequency of the vibration will generally depend on the bond strength (force constant) and the reduced mass of the bond. Since these are rather stable for a specific type of bond and functional group, it is helpful to determine so called group frequencies. This concept is based on the simplification that vibrations in a specific functional group are independent of the other vibrations in the molecule. The group frequencies for some important Raman active functional groups in organic compounds are shown in Table 2.1. It can be seen that vibrations involving atoms with smaller masses (e.g. hydrogen) generally have higher vibrational frequencies. In addition, the effect of bond strength is apparent through the carbon-carbon stretch series: $\nu(\mathrm{C}-\mathrm{C})$, $\nu(\mathrm{C}=\mathrm{C})$, $\nu(\mathrm{C}\equiv\mathrm{C})$, with stronger bonds having higher vibrational frequencies [32]. Methylene (CH_2) groups are common features in organic compounds, and as an example, the normal vibrational modes of this functional group are shown in Figure 2.2.

2.1.3 Instrumentation

Raman spectrometers exist in many variants, but the general setup consists of a radiation source (laser), sampling optics (Raman scattering collection), a wavelength dispersion system and a detector. The two main instrument groups differ in the dispersion system, with *dispersive* instruments utilizing a grating for the spatial separation of different wavelengths and *Fourier-Transform* (FT) instruments utilizing a Michelson interferometer for temporal separation of different wavelengths. Generally, FT-Raman is used for lasers with long wavelengths (above 900 nm), while dispersive instruments are used for shorter wavelengths due to the sensitivity of the respective detectors for different wavelength ranges. In this thesis, the main focus is on the dispersive instrument, for which an example setup is illustrated in Figure 2.3. The detector used for dispersive instruments is usually a Charge-Coupled Device (CCD). In addition, filters that can remove the contributions of Rayleigh scattering (band block filters) or ensure narrow laser bands

Vibration		**Raman shift** ($\mathbf{cm^{-1}}$)	**Raman intensity**[a]
$O-H$ stretch	$\nu(O-H)$	$3650-3000$	w
$N-H$ stretch	$\nu(\ N-H)$	$3500-3300$	m
$C-H$ stretch of alkenes	$\nu(=C-H)$	$3100-3000$	s
$C-H$ stretch of alkanes	$\nu(-C-H)$	$3000-2750$	s
$C\equiv C$ stretch of alkynes	$\nu(C\equiv C)$	$2250-2100$	vs
$C=C$ stretch of alkenes	$\nu(C=C)$	$1750-1450$	vs – m
$C-C$ stretch of aliphatic chains and cycloalkanes	$\nu(C-C)$	$1150-950$	s – m
CC stretch of aromates ((substituted) benzene molecules)	$\nu(C-C)$	1600,1580, 1500,1450, 1000	s – m m – w s
$C=O$ stretch	$\nu(C=O)$	1870-1650	s – w
Antisymmetric $C-O-C$ stretch	$\nu_{\text{asym}}(COC)$	1150-1060	w
Symmetrical $C-O-C$ stretch	$\nu_{\text{sym}}(COC)$	970-800	s – m
CH_2 bending vibrations, antisymmetric CH_3 bend	$\delta\,(CH_2)$, $\delta_{\text{asym}}\,(CH_3)$	1470-1400	m
Symmetric CH_3 bend	$\delta_{\text{sym}}\,(CH_3)$	1380	m – w
CH_2 in phase twist	$\delta\,(CH_2)$	1305-1295	m
CONH stretch[b]	Amide I	1670-1630	m – w
$C-N$ stretch, coupled with opening of the CNH angle [b]	Amide III	1350-1250	m – w

[a] s - strong, m - medium, w - weak, v - very
[b] vibrations of the bonds in an amide group cannot be considered independently.

Table 2.1: Group frequencies of some important functional groups in organic compounds. Adapted from Vandenabeele. [32]

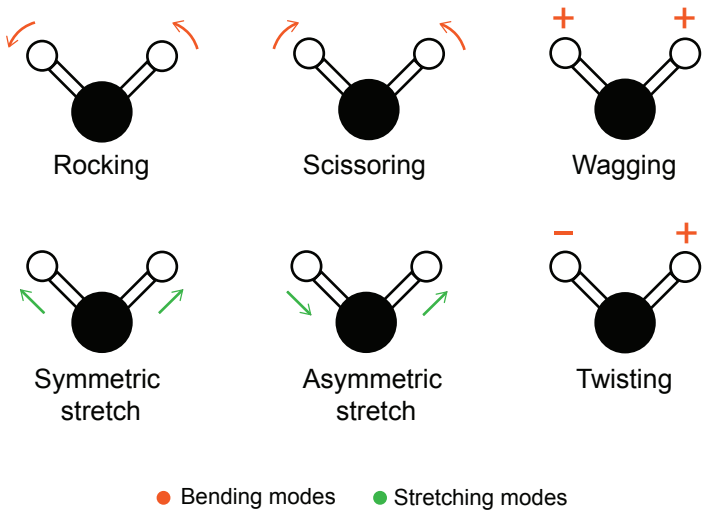

Figure 2.2: CH vibrations of CH_2 groups. The figure indicate the movement during the first half of the vibration. The +/- signs denote movements in and out of the plane, respectively.

(band pass filters) are important components of a Raman system. In the last decades, Raman instruments have become more affordable and robust, making Raman spectroscopy a tool relevant for process analytical technologies (PAT). As reviewed by Esmonde-White [33], this is due to the development of compact and stable laser sources, low-noise CCD detectors, volume holographic gratings and high-speed optical fibers. Stable lasers are important, as fluctuations in laser intensity lead to fluctuations in the acquired spectrum (Eq. 2.5), which can disturb quantitative analysis. Low noise CCDs enable applications for analytes and samples which are less effective Raman scatterers, such as foods. In addition, the development of NIR sensitive deep depletion CCDs has enabled more effective signal recovery when using longer laser wavelengths. This has been an important development for measurements of biological tissue prone to fluoresce, as fluorescence is better suppressed at longer wavelengths [34]. Volume holographic gratings can be used in several optical components and have for instance resulted in more effective pass/block filters compared to previous technologies. By effectively eliminating Rayleigh scattered laser light from single monochromators, holographic band block filters have contributed to the development of a new generation of compact, high performance Raman instruments [35]. The use of fiber optic cables in combination with lightweight probe heads facilitates industrial sampling away from the spectrometer and makes it a versatile tool. For many modern fiber optical Raman instruments, the probe head can also be easily interchanged which provides an additional sampling versatility. Some fiber optic instruments have enabled spectrum collection of samples as far as 250 m from the analytical spectroscopy laboratory [36]. However, background signals may arise from the fiber

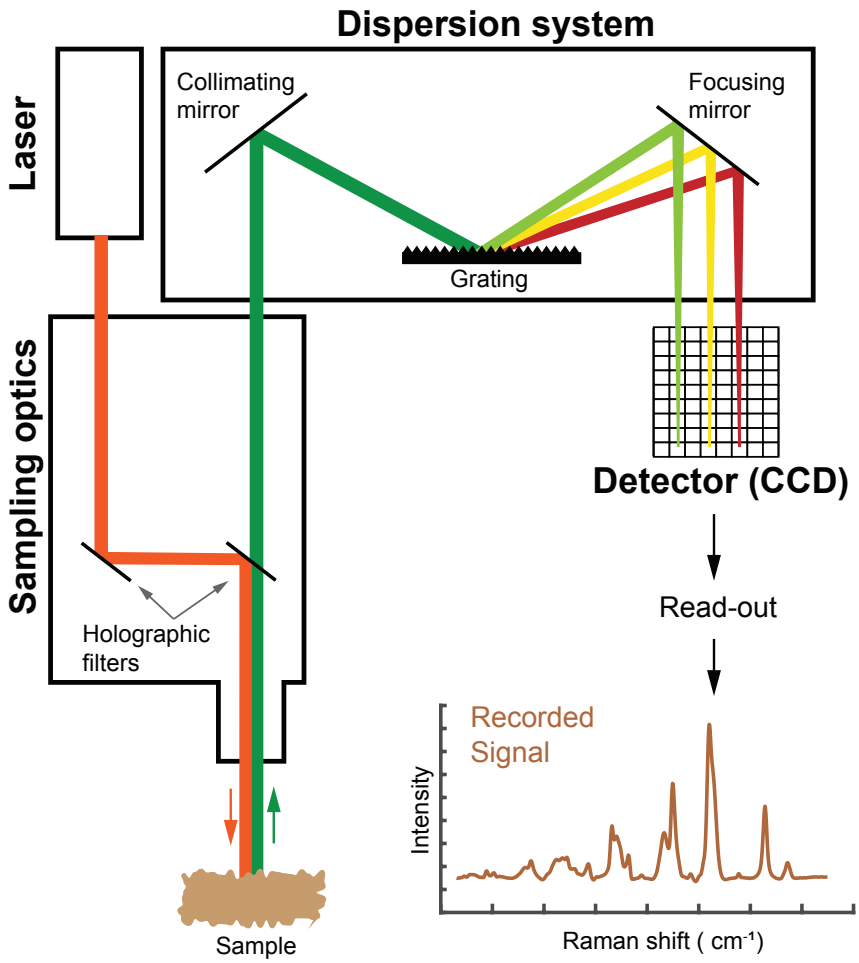

Figure 2.3: Schematic overview of a dispersive Raman instrument measuring a sample in back scattering mode.

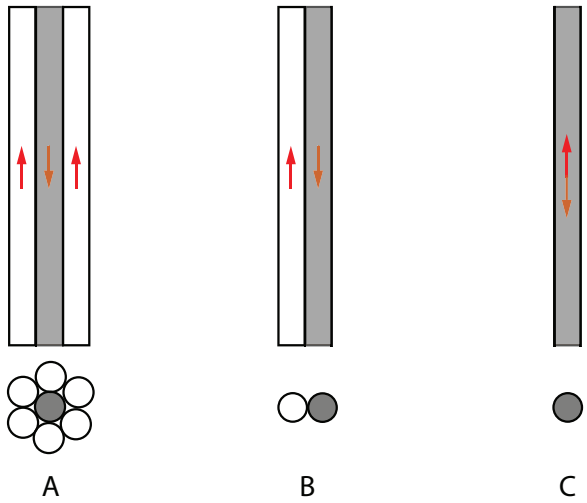

Figure 2.4: Examples of three different types of fiber optic probes: A) fiber bundle probe, B) double-fiber probe, and C) single fiber probe. The lower images represent the cross-sectional view. In A and B, the white and shaded areas represent collection and excitation fibers, respectively. Adapted from Li and Church [37].

optic material itself and wavelength filtering in the excitation and collection fiber is important. In addition, signal losses due to a limited transmission efficiency of the fibers occur. For samples with weaker Raman signals (e.g. foods), such long cables with optical fibers may be challenging with respect to the SNR and is not particularly needed in many applications.

Optical fibers transmit light both for laser excitation and for light collection. The exact design of a Raman fiber probe strongly depends on the application, and a plethora of different Raman probe configurations have been reported in the literature [34,39]. Examples of different fiber setups are illustrated in Figure 2.4 [37]. In general, a high collection efficiency is obtained by creating a good overlap between the excitation and collection volume, which can be realized by a single central excitation fiber with closely packed collection fibers (Figure 2.4A) or by a single fiber and a beamsplitter between excitation and collection paths (Figure 2.5 d). A major distinction can be made between confocal and non-confocal probes. Some probe configurations reported for in-vivo Raman applications in the medical domain [38] are shown in Figure 2.5, where an example of a basic non-confocal probe without a focusing lens (a) and several confocal probes with focusing lenses (b-d) are shown. In the case where the laser beam can be described as a Gaussian beam, the spot size can roughly be described by the radius of the narrowest region of the beam focus, called the beam waist (Figure 2.6). An important characteristic which

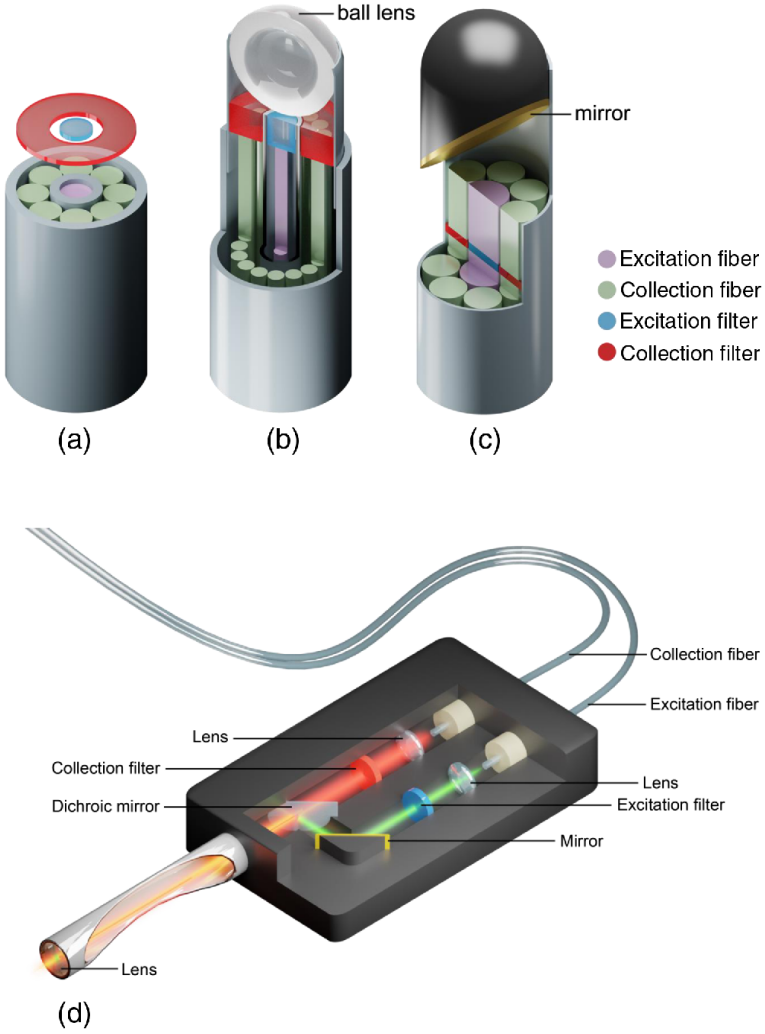

Figure 2.5: Examples of four different types of fiber optic probes, commonly used for in-vivo Raman measurements, including a basic probe without a focusing lens (a), a probe with a ball lens for focusing (b), a probe with side-view option, and (d) a handheld Raman probe. Reproduced from Cordero et al. [38]

describes the focusing optics, is the numerical aperture (NA), which is defined as

$$NA = n \cdot \frac{w_L}{f}, \tag{2.6}$$

where where w_L is the beam radius at the focusing lens and f is the focal length and n is the refractive index of the medium between the sample and the objective [40, 41]. For air, the refractive index is 1. The spot size radius is inversely proportional to the NA, while the focus depth is inversely proportional to the cube of the NA [40]. The larger the NA, the smaller the focal volume. Traditionally, the sampling optics focuses the laser on a point (50 - 500 μm), which makes spectrum intensity sensitive to out-of-focus working distances. An emerging term used in

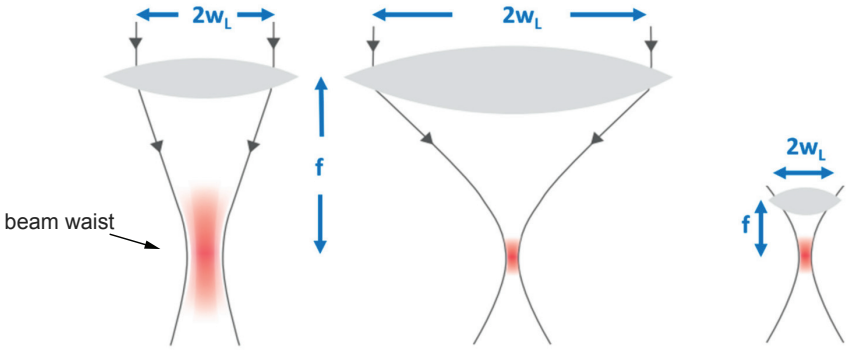

Figure 2.6: The focal volume (red) of a Gaussian laser beam scales with the numerical aperture $NA = n \cdot w_L/f$ of the focusing lens, where w_L is the beam radius at the focusing lens, f is the focal length, and n is the refractive index of the medium between the sample and the objective. The larger the NA, the smaller the focal volume. Reproduced from Latz et al. [40]

the literature for probes which do not focus the laser on a very small point and which have spot diameters up to 6 mm is "Wide Area Illumination" (WAI) probes. Although the exact definition of this term is somewhat unclear, these probes may employ an unfocused or loosely focused laser, which increases the sampling volume. Since the beam is not strongly focused, using many collection fibers (in case of config. A, Figure 2.4) is important for the collection efficiency. For example, the WAI probe from Kaiser Optical Inc. (Ann Arbor, MI, USA) employs 50 collection fibers [42]. The WAI probes are less sensitive towards variations in working distances [24, 39], a situation which could easily occur in an industrial process setting. Due to these advantages, the WAI scheme has proved to facilitate representative sampling [24, 25], and have resulted in enhanced performances in a variety of applications (e.g. in the pharmaceutical, polymer and agricultural domains), as reviewed by Shin and Chung [26]. Recently, the WAI scheme has also been employed with promising results for foods, such as for quality measurements of poultry and salmon rest raw materials [12, 15, 23], beef [12] and pork [23].

This makes the WAI probe the currently most promising alternative for process measurements of heterogeneous foods.

2.1.4 Signal disturbances and noise

As discussed in section 2.1.1, a recorded spectrum does not only contain Raman scattering signals. Other signals can originate from 1) the sample, 2) the instrument and 3) the environment. Table 2.2 summarizes the common phenomena which cause signal disturbances. Autofluorescence is perhaps the most challenging phenomenon for Raman spectroscopy of biological tissue. Foods contain a wide range of naturally occurring fluorophores, such as aromatic amino acids, vitamins and porphyrins [19]. Although longer laser wavelengths are generally associated with lower fluorescence level, Semenov et al. [21] recently demonstrated that oxidation products of organic components (e.g. lipid, proteins and amino acids) can contribute considerably to broad band fluorescence signal, particularly when excited by red or near infrared radiation. This is something to keep in mind when working with biological materials, as this may hamper the Raman measurement more as the sample decays and oxidation product are produced. This corresponds with the author's own experiences with fluorescence from salmon and poultry rest-raw material stored for a longer time. Other biological materials prone to fluoresce are for instance bones [11, 43]. Cosmic ray spikes are another type of disturbance. They are a result of high energy particles such as muons, protons or neutrons that directly hit the CCD detector and generate electron-hole pairs in the detector [44]. As a result they can occur at any wavelength in the spectrum. Ambient light could also be a challenge, as many commonly used light sources can contribute with strong signals to the Raman spectra. However, suitable light sources can be employed for minimal disturbance. For example, cold LEDs (4000K) can be when measuring in the near infrared range. Still, employing a shielding setup might be necessary as a safe guard in larger production halls in the industry.

Source	Disturbance phenomenon	Effect on spectrum
Environment	cosmic ray spikes ambient light	sharp features (few pixels wide) depending on source
Sample	fluorescence other absorption other scattering	broad baseline intensity variations intensity variations
Instrument	dark current laser fluctuations	low intensity uniform baseline intensity variations

Table 2.2: Examples of possible disturbance phenomena in an acquired Raman spectrum.

In literature, the term noise is used with varying meanings. It is often used as a collective term for all possible disturbances to the Raman signal. When addressing noise in this introduction, it is referred strictly to the phenomena with random behaviour. Other signals or influences on the signal are called *spectrum disturbances*. The uncertainty, i.e. noise, on a spectral signal is by statistical theory on stochastic processes given by

$$\sigma_S = \sqrt{S}, \tag{2.7}$$

where S is the signal intensity [41]. Such a noise source is called *shot noise* and may stem from the statistical variation in photon-to-electron conversion at the detector (photon noise) or from the statistical variation in the number of electrons thermally generated within the silicon structure of the CCD (dark noise). For dispersive instruments, shot noise is pixel-specific and may vary over the Raman spectrum depending on a variety of signals. This could be Raman or autofluorescence signals from the sample or ambient light signals. Normally, many noise and disturbance phenomena can be corrected for or reduced by pre-processing of the spectra (see chapter 2.1.5). The SNR can be a limiting factor for the performance of models based on spectroscopic measurements. In this context, only the Raman signal is of interest, and if measurements are dominated by shot noise we can generally express the SNR of the CCD detector by

$$SNR = \frac{S_{Raman}}{\sqrt{S}}, \tag{2.8}$$

where the signal intensity S will depend on factors such as the exposure time, laser power and quantum efficiency of the detector. In addition to shot noise, the process of converting electrons to a digital signal can also introduce a random noise component, so called *read noise*. However, such noise is usually not a limitation unless the exposure time is very low.

2.1.5 Pre-processing of Raman spectra

As outlined in section 2.1.4, many disturbing signals and noise phenomena can contribute to the acquired spectrum. If not removed, these may disturb further analysis and interpretation of the spectra. Pre-processing steps that are frequently employed for removing disturbing effects are summarized below. Some of the main phenomena and the effect of one possible pre-processing strategy is shown as an example in Figure 2.7.

Dark subtraction

Before any further pre-processing of a spectrum, it is customary to subtract a dark spectrum which is acquired without illumination of the sample. Such subtraction is

often automatically done directly by the instrument, and contains a dark current signal and potential ambient light. By subtracting, one can remove the main signal component, but it is important to note that the random error associated with these signals are not removed. Additionally, if ambient light signals are not stable over time, and the dark spectrum is acquired at a slightly different time than the sample spectrum, the obtained dark spectrum may not correspond completely to the sample spectrum. Therefore, dark subtraction can sometimes introduce additional disturbances to the spectrum.

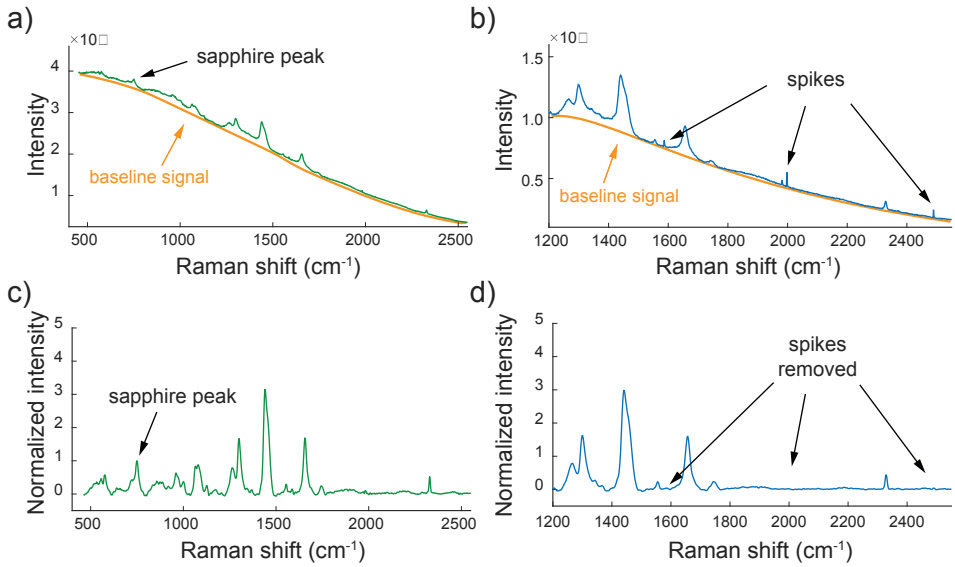

Figure 2.7: Examples of two different spectra from measurements of poultry rest raw material from paper III (green, blue). The spectra are shown without any pre-processing (a-b) and with pre-processing (c-d). The pre-processing included spike removal, smoothing by the Savitzky-Golay [45] method, baseline correction by the Asymmetric Least Squares [46] method and normalization by the sapphire peak intensity. For the spectra without pre-processing, broad baseline signals (i.e. autofluorescence) and spikes can be seen. The baseline is drawn in for conceptual illustration.

Spike removal

Spikes are unpredictable, sharp, positive spectral features, usually spanning only a couple of pixels. Many methods have been proposed for detection of such spikes [44, 47–50]. In this thesis, an approach similar to Whitaker and Hayes [44] was followed. In this method, spikes are detected and removed for each spectrum separately. To detect the spike locations, the second derivative is calculated, for which sharp spectral features are enhanced compared to broader spectral features. A threshold must be carefully determined. Instead of using a threshold based on the derivative value directly, Whitaker and Hayes proposed to use a commonly

employed outlier detection method based on normal distribution statistics. In this method, a modified Z value for each spectrum index is calculated, in this case according to

$$Z_i = \frac{0.6745 \cdot (\nabla^2 x_i - M(\nabla^2 x))}{M(|\nabla^2 x_i - M(\nabla^2 x)|)}, \tag{2.9}$$

where $\nabla^2 x_i$ denotes the second derivative value of the spectrum x at the index i and $M(\nabla^2 x)$ denotes the median of the spectrum derivative values [51]. Any spectrum location with a larger value than the chosen threshold is defined as a spike, and subsequently each spike is replaced by a fitted line. In this approach, the choice of threshold value is important and it is not always possible to employ one single threshold for the entire data set. For example, narrow peaks of high-intensity analyte bands (e.g. in spectra of high fat samples) might not be removed by the derivative operation. Such peaks can then obtain similar modified Z values to spikes, and caution must be made. Similar challenges with defining an optimal threshold are found for other approaches as well [50]. For this reason, many suggested approaches are not suitable for full automation and in-line measurements. As a counter-proposal to such methods, Mozharov et al. [52] suggested to exploit the sparsity of spikes in the temporal domain in stead. As spikes occur suddenly, particularly in the time domain, they use the derivative in the time domain, in combination with a multi-step approach for filtering out ”falsely” detected cosmic spikes. In addition, this method has an automatic threshold routine, and can in theory be used without any user-defined parameters.

Denoising

Reduction of random fluctuations on a signal might be advantageous for SNR optimization. *Savitzky–Golay* (SG) filtering [45] is a method widely used in the spectroscopic domain, which can be used for signal smoothing, but also estimation of signal derivatives. In this approach, a polynomial of a predefined order is fitted locally in each point of the spectrum and a certain number of left- and rightward points are used combined with a specific weighting for estimating the parameters for each polynomial. The number of spectrum points included in these portions are called the window size. Note that the fitting that is done is never perfect in practice. For a given choice of polynomial degree and window size, the fit might be very good at broad features, while the fit at narrow Raman peaks might be less successful and introduce intensity errors in stead. Therefore, moderate smoothing parameters are usually used in Raman spectra, and an example of a commonly applied parameter combination is a 2nd order polynomial and a 9-point window size. Recently, it was suggested by Barton et al. [53], to combine the SG algorithm with Maximum Likelihood Estimation to obtain stronger smoothing while maintaining sharp Raman bands.

Another strategy to reduce noise while keeping the signal component constant is

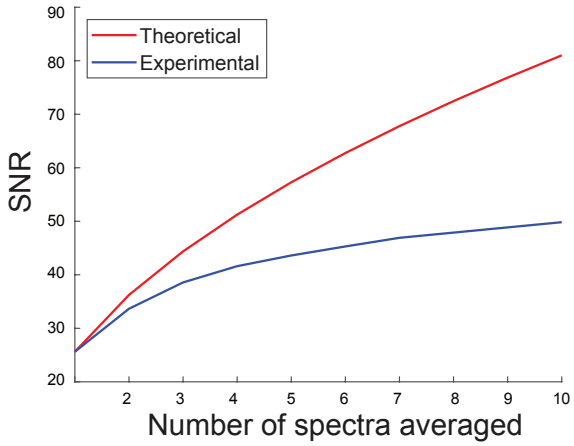

Figure 2.8: Theoretical and experimental effect of averaging a 4s exposure time signal (after pre-processing) up to 10 times. The SNR was estimated through the same method as in the papers in this thesis.

to average signals acquired in several consecutive time intervals, i.e. increasing the total exposure time. This can be useful when higher SNR is needed, but increasing the single exposure time interval would saturate the detector. The ideal improvement due to averaging is

$$SNR_n = \sqrt{n} \cdot SNR, \tag{2.10}$$

where n is the number of measurements being averaged [54]. In Figure 2.8, the experimental improvement due to averaging of spectra of homogenized poultry samples (from paper III) is shown together with the theoretical improvement based on Eq. 2.10. As can be seen, the experimental SNR does increase with increasing number of averages, however, the indicated SNR enhancement is not as strong as expected. This is mainly a result of the inexactness of the SNR estimation method used. The noise component of the spectrum is estimated by fitting a smoothed spectrum obtained by the SG method and subtracting this from the original spectrum. It is expected that the noise will be overestimated since the fitting of the smoothed spectrum is not exact. The fitting error will likely dominate the estimated noise more for low noise spectra.

Baseline and intensity correction

Broad baseline and intensity disturbances can either be corrected separately or simultaneously. Examples of baseline correction approaches which do not include any multiplicative corrections are the modified polynomial curve fitting method suggested by Lieber and Mahadevan-Jansen (Modpoly) [20] and the Asymmetric

Least Squares (ALS) suggested by Eilers [46]. Since the correction of multiplicative effects are often needed as well, these are often used in combinations with methods such as the Standard Normal Variate (SNV) [55] or other peak intensity/area normalization methods. Other methods correct for baselines and multiplicative effects simultaneously, such as the Extended Multiplicative Signal Correction [56]. The methods used in this thesis are described in the following.

Asymmetric least squares (ALS) is an iterative method based on least squares which in each iteration aims to minimize the cost function

$$S = \sum_i w_i (x_i - b_i)^2 + \lambda \sum_i \nabla^2 b_i, \tag{2.11}$$

where x_i is the original spectrum, b_i is the current estimation of the baseline, w_i is the asymmetric weighting of the residual and $\nabla^2 b_i$ is the second derivative of the current baseline [46, 57]. The first term in the equation represents the fit to the original spectrum and the second term represents the smoothness of the fitted baseline. In each iteration, the baseline fit is updated and the weighting w_i is changed according to the new fit. An important part of the weighting is that it is asymmetric, i.e. positive residuals are weighted by a parameter p, and negative residuals are weighted by $(1 - p)$. For baseline correction, the fit to the original spectrum is not important and a small value of p (e.g. 0.01) and large smoothing parameter λ (e.g. 6) is needed. An interesting aspect of this method is that it can work as a smoothing method by setting $p = 0.5$, for which positive and negative residuals are weighted symmetrically.

Extended Multiplicative Signal correction (EMSC) is a well established pre-processing method based on the least squares fit of a predefined number of model components to the measured spectrum, i.e. according to

$$x(\bar{\nu}) = a + b \cdot m(\bar{\nu}) + d_1 \cdot \bar{\nu} + d_2 \cdot \bar{\nu}^2 + \cdots + d_n \bar{\nu}^n + e(\bar{\nu}), \tag{2.12}$$

where $x(\bar{\nu})$ is the measured spectrum, $m(\bar{\nu})$ is a stabilising reference spectrum (e.g. mean spectrum), a represents a constant baseline shift, b represents multiplicative effects (e.g. laser intensity fluctuations) of the reference spectrum, and $d_1 .. \ d_n$ are constants representing the polynomials of the Raman shifts [56–58]. Together these polynomials can account for complex baselines, as needed to remove fluorescence from the Raman spectrum. The information about the chemical differences between the reference spectrum and the measured spectrum is ideally captured by the residual $e(\bar{\nu})$. Liland et al. [57] found that an EMSC model including polynomials of the Raman shifts ranging from 1st up to 6th order was needed to handle the complexity of the baselines associated with example Raman spectra of milk.

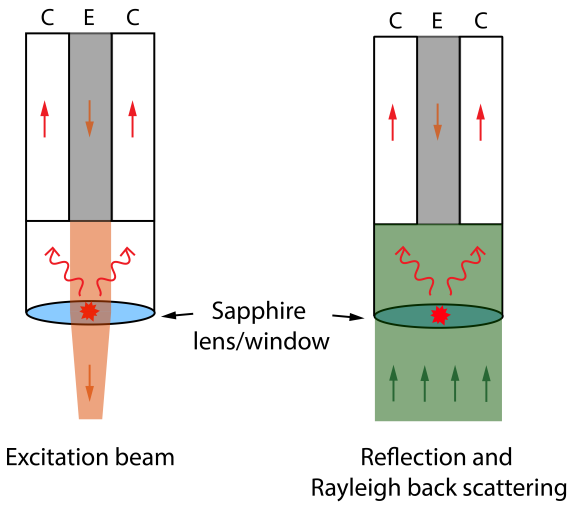

Figure 2.9: Schematic illustration of a Raman probe tip, employing a sapphire lens or window. The laser beam travels through the excitation fiber (E) and causes Raman scattering at the lens/window which is captured by the collection fibers (C). The laser beam hits the sample and may be reflected or Rayleigh scattered back at the same wavelength as the excitation. The back scattered radiation may again prompt Raman scattering as it travels through the lens/window.

The parameters a,b,..d_n are estimated and the correction is made according to

$$x_{corr}(\bar{\nu}) = \frac{x(\bar{\nu}) - a - d_1 \cdot \bar{\nu} - d_2 \cdot \bar{\nu}^2 - \cdots - d_n \bar{\nu}^n}{b}. \tag{2.13}$$

This model-based approach is a very versatile method which can be extended further in many ways, for example with additions of other constituent spectra [56, 58, 59]. In this case, contributions from unwanted constituents can be added in the model and be subtracted in Eq. 2.13. Wanted constituents can be added to the model without subtraction to stabilize parameter estimation when larger chemical variations are present.

Peak intensity normalization by the Raman sapphire band (750 cm^{-1}) was used for pre-processing in paper III. The sapphire band originates from the sapphire in the optics and may act as an internal standard. This is because the excitation laser beam and reflection or Rayleigh back scattering from the sample causes Raman scattering when passing through the sapphire (Figure 2.9). The amount of scattering from sapphire depends on laser fluctuations or variations in reflection and Rayleigh back scattering. Hence, this normalization strategy aims to better separate intensity differences caused by chemistry compared to other instrumental and physical effects. Indeed, using a sapphire or diamond window reference has previously been reported in the literature as a way to correct for laser fluctuations [60] and to make absolute intensity and concentration measurements feasible [61]. In contrast, multiplicative corrections based on the full spectral range may to some extent be affected by the chemistry, as intensities of several bands may be influenced by the concentration of effective Raman scatterers (see Eq. 2.5).

2.2 Multivariate modelling and validation

2.2.1 Calibration and Partial Least Squares Regression

The aim of a multivariate calibration model is to establish the relationship between a set of observations $\mathbf{X} \in \mathbb{R}^{nxm}$ and corresponding response variables $\mathbf{y} \in \mathbb{R}^n$. A linear model attempts to find a vector $\mathbf{b}$ to solve the linear equation by

$$\mathbf{Xb} = \mathbf{y}, \tag{2.14}$$

most frequently subject to the least squares approximation constraints below [62].

$$\min\|\mathbf{b}\| \qquad \text{subject to} \qquad \|\mathbf{Xb} - \mathbf{y}\| = \min \tag{2.15}$$

For this problem, we can establish the normal equations and obtain the following solution (regression vector)

$$\mathbf{b} = (\mathbf{X}^t\mathbf{X})^{-1}\mathbf{X}^t\mathbf{y}. \tag{2.16}$$

For calibration tasks involving wide data matrices with co-varying variables (e.g. spectroscopic data), employing this solution directly is not stable [63] and a variable reduction method is needed. Partial Least Squares Regression (PLSR) is a frequently used method for such data. It approximates a solution for the above problem by reducing the number of variables into k latent variables (PLS components). The components are constructed from $\mathbf{X}$ and $\mathbf{y}$ in a way that maximizes the covariance between the two. NIPALS is one possible algorithm for execution of PLS [64], and is often used as the default in available software applications. The algorithm is outlined in Table 2.3. However, there are a number of alternative algorithms which are considerably faster with similar numerical precision [62, 65]. Increased speed can be advantageous to make cross-validation more efficient for large $\mathbf{X}$ matrices or during testing and optimization of pre-processing parameters.

2.2.2 Validation

Validation of an obtained calibration model is important to assess its robustness and to avoid overfitting. Often, less than 100 samples are used for initial calibration development, since the required reference analyses can be very expensive. For samples sets with few samples, cross validation (CV) is usually considered an acceptable validation method. However, before implementing a model in the industry it is required to test the model on new independent samples (validation set). When doing this, one often encounters slope and bias errors. Slope and bias errors represent highly systematic errors. It is often helpful to separate slope, bias and variance errors as they may have different origins. If the origins are found, it

Assuming $\mathbf{X}_0$ and $\mathbf{y}_0$ are mean centered data,

for a = 1:k

1. $\mathbf{w}_a = \mathbf{X}_{a-1}^t \mathbf{y}_{a-1}$
2. $\mathbf{w}_a = \frac{\mathbf{w}_a}{\|\mathbf{w}_a\|}$
3. $\mathbf{t}_a = \mathbf{X}_{a-1}\mathbf{w}_a$
4. $\mathbf{t}_a = \frac{\mathbf{t}_a}{\|\mathbf{t}_a\|}$
5. $\mathbf{p}_a = \mathbf{X}_{a-1}^t \mathbf{t}_a$
6. $\mathbf{X}_a = \mathbf{X}_{a-1} - \mathbf{t}_a \mathbf{p}_a^t$ (deflation)
7. $q_a = \mathbf{t}_a^t \mathbf{y}_{a-1}$
8. $\mathbf{y}_a = \mathbf{y}_{a-1} - \mathbf{t}_a q_a$ (deflation)

end

The vectors and numbers are organized into matrices:

$\mathbf{T}_k = [\mathbf{t}_1\ \mathbf{t}_2 \dots \mathbf{t}_k]$ (orthonormal scores)
$\mathbf{W}_k = [\mathbf{w}_1\ \mathbf{w}_2 \dots \mathbf{w}_k]$ (orthonormal weights)
$\mathbf{P}_k = [\mathbf{p}_1\ \mathbf{p}_2 \dots \mathbf{p}_1]$ ($\mathbf{X}$ loadings)
$\mathbf{q}_k^t = [q_1\ q_2 \dots q_k]$ ($\mathbf{y}$ loadings)

The regression coefficients are computed for the original $\mathbf{X}$ data

$\boldsymbol{\beta}_k = \mathbf{W}_k(\mathbf{P}_k^t \mathbf{W}_k)^{-1}\mathbf{q}_k$
$\beta_{0,k} = \bar{y} - \bar{x}\boldsymbol{\beta}_k$,

where $\bar{y}$ and $\bar{x}$ are column means of $\mathbf{y}$ and $\mathbf{X}$, respectively.

Predictions for a new observation $\mathbf{x}$ (spectrum) can be made by

$\hat{y} = \beta_{0,k} + \mathbf{x}^t \boldsymbol{\beta}_k$

Table 2.3: The NIPALS algorithm for computing an k-component PLS1 regression model (one-column response variable). Adapted from Indahl [66].

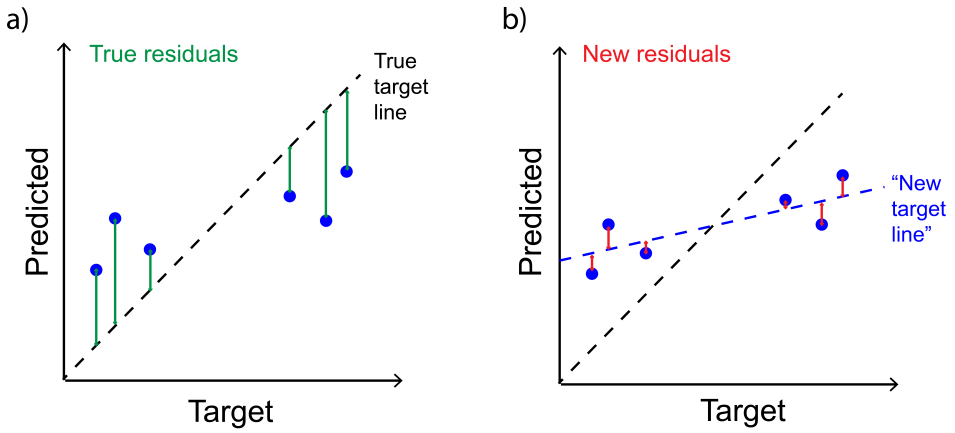

Figure 2.10: A conceptual illustration of the bias-and-slope correction employed for performance metrics. A set of predictions are made with slope and/or bias errors (a). Intuitively, the correction can be understood as defining a fitted line between target and prediction values as a "new target line" (b), which effectively removes all slope and bias errors. In reality, there is an actual correction of the predictions involved.

might be possible to correct them through further calibration development. In this thesis, we therefore report the classic validation metrics corrected for slope-and-bias errors ($\text{RMSE}_{\text{corr}}$ and R^2_{corr}). This is done by fitting a linear model between predicted and target values. From this, a regression vector is obtained, which we in turn can use to predict "new target values" from the predicted values, yielding a correction of the original predictions. Residuals are recalculated after correction, and metrics are calculated as usual. Alternatively, it can be seen as analogous to defining a fitted line between the target and predicted lines as a "new target line", as illustrated in Figure 2.10. It is important to note that in this thesis, we did not use this for correction of plotted predicted values, only as an alternative metric corrected for slope and offset errors. In general, slope and bias errors typically occur over time in most process applications. Therefore, a model employed in the industry needs careful supervision, i.e. regular calibration maintenance, during which models can be updated to correct for such errors.

Often, comparisons of models based on different versions of a data set, e.g. with different pre-processing or measurement methods, are made to suggest which method is best. Although one can compare the prediction errors directly, the conclusion is not always straight forward if the performance differences are only moderately improved by a given method. To test if the difference in performance is statistically significant, we can employ an analysis of variance (ANOVA). In such analysis we statistically determine if the means in a set of data differ with respect to levels of one or more factors. In the context of evaluating performance differences, the "data" are prediction residuals (e.g. on the form $(\hat{\mathbf{y}} - \mathbf{y})^2$). Indahl and Næs [67]

first introduced such an application of ANOVA. They used a two-way ANOVA model for cross-validated predictions residuals, where "method type" (here different spectral feature extraction methods) corresponded to one of the factors and "sample number" corresponded to the the other factor. The latter was considered a random effect. In this thesis, we use the same procedure for determining the the significance of performance differences. Generally, the scheme can be extended to n-way ANOVA if there are more factors to be accounted for.

2.3 Raman spectroscopy for food analysis

2.3.1 Food composition

The composition of food products is important for their functional, sensory and nutritional properties, and therefore the interest in quantifying these constituents is evident for quality monitoring and optimization. Foods and related by-products are complex sample matrices, consisting of a range of different tissue types of varying composition. Moreover, the composition can vary with livestock feed [22,68] and seasonal factors [69]. For meat products, muscle tissues and connective tissues such as adipose tissue are the main components. The major molecular constituents of such tissues are water, proteins and lipids. In terms of rest raw material from meat production, the amount of bone and cartilage tissue is also an important factor with respect to food quality [70,71]. Examples of other important constituents are minerals, pigments, vitamins and antioxidants.

Muscle tissue makes up different types of muscles in animals. The tissue consists of muscle cells which are specialized for contraction, mainly thanks to the proteins myosin and actin. Muscle tissue which is responsible for movement of the body is called skeletal muscle and is roughly composed of 75% water and 20% protein with the remaining 5% being fat and other components [72]. In skeletal muscle, cells are organized in bundles of muscle fibers, kept together by connective tissue.

Adipose tissue is a type of connective tissue consisting of fat cells which can store fat in lipid droplets [73]. The tissue contains roughly 80% fat with the remaining 20% being water, protein, and minerals [74]. Adipose tissue can be found around muscles, between muscle fibers and in the marrow [73]. Often fatty acids (FA) are of interest for quality measurements in foods, since specific FAs, such as eicosapentaenoic acid (EPA) and docosahexaenoic acid (DHA) are associated with e.g. health benefits [75–79]. FAs are stored in such tissue, mainly in the form of triacylglycerols (TAG). TAGs consist of a glycerol backbone and three FAs, as illustrated in Figure 2.11. FAs are mainly distinguished by the number of carbons in the chain, the number of double bonds and their position in the carbon chain, according to the IUPAC notation. For example, DHA (22:6n-3) has 22 carbons and 6 double bonds, with the first double bond positioned at the third carbon-carbon bond counted from the methyl (CH_3) end. A FA is referred to as *saturated* (SAT) when containing no double bonds, *monounsaturated* (MUFA) when containing one

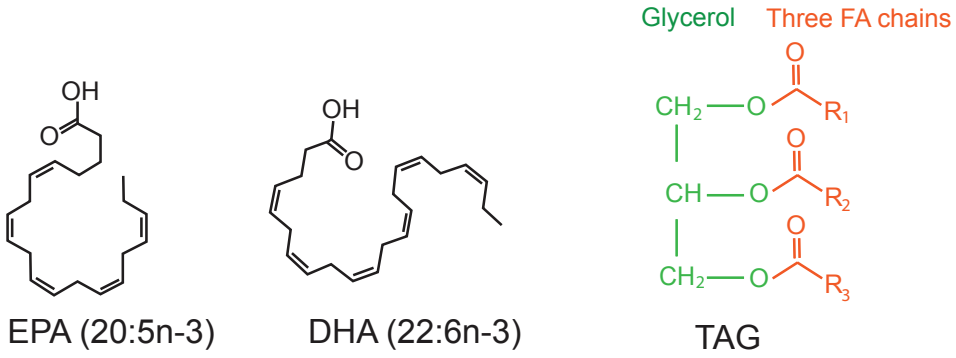

Figure 2.11: Simplified illustration of EPA and DHA as free fatty acids and the structure of a TAG. R denotes the rest of the fatty acid chains.

double bond or *polyunsaturated* (PUFA) when containing more than one double bond.

Bone tissue is a type of connective tissue which consist of bone cells surrounded by a matrix of fibers and ground substance, a gel-like extracellular matrix. The ground substance is calcified, and is found mainly in the form of hydroxyapatite and secondly in a smaller amount of calcium carbonate [73]. It consists roughly of 60% hydroxyapatite, 10% water and 30% proteins [80].

Other connective tissues include for example cartilage, blood and dense fibrous connective tissue. Such tissues consist of a variety of cells and ground substance containing protein fibers, glycoproteins and proteoglycans. Dense connective tissues support bones, muscles, and other tissues and organs. Examples are tendons and ligaments. Collagen is an important component of all connective tissues, but is particularly abundant in the dense tissues which contain little ground substance. Collagens are a group of proteins which have amino acids arranged in characteristic repeatable sequences which form a unique triple helix structure. The reapeatable sequences consist of Glycine-X-Y, where X and Y may be any amino acids, with Proline-Hydroxyproline-Glycine being the most common triplet [81, 82]. Moreover, hydroxyproline (HYP) is a signature amino acid for collagens, while few other proteins contribute with HYP in most tissues. Therefore, reference analyses for collagen are often based on HYP measurements [83].

2.3.2 Applications

Raman spectroscopy has been widely used as an analysis tool within the food processing domain. It has been used in a plethora of classification and quantification tasks, for analysis of adulteration, safety control, quality documentation and structural analysis in many types of foods, crops and beverages. This has been

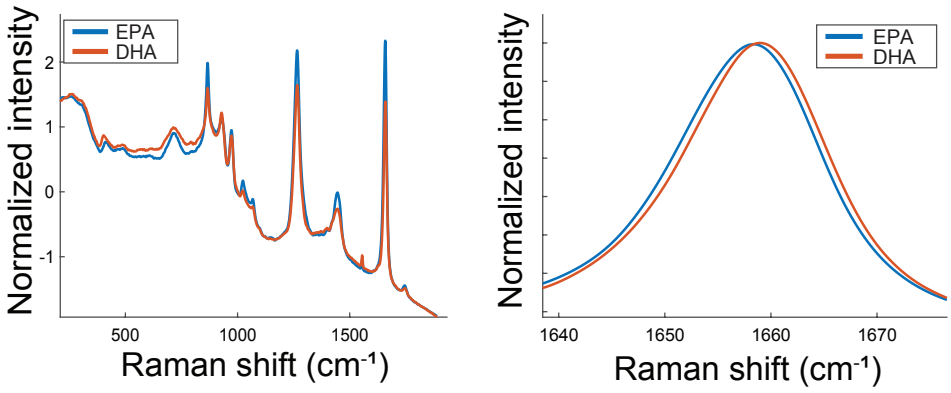

Figure 2.12: Pure EPA and DHA Raman spectra. They differ mainly in peak intensity ratios, but also by a small shift in the C=C stretch frequency (1658 cm^{-1}). Reproduced from Afseth et al. [9]

extensively reviewed elsewhere [37, 84–87]. Raman spectroscopy is a promising spectroscopic technique for compositional analysis of foods, with the advantage that the concentration of several compounds of interest can be measured at the same time. Recent feasibility studies also show how the various Raman techniques can be used for analysis of bulk composition [23] and to quantify complex food quality features like fatty acids in muscle foods [8,9], to describe protein structure related to water holding capacity in pork meat [10] and to quantify mineral, bone and collagen content [11,12] in meat slurries. Color is another example of an important quality factor in many food products, and several pigments are relatively effective Raman scatterers. Therefore, Raman spectroscopy has shown promising results for carotenoids based analysis, such as evaluation of redness (astaxhantin) in salmon fillets [88] and detection of adulteration with red Sudan I dye in paprika powders [89]. Using more specialized Raman methods such as Coherent Anti-Stokes Raman Spectroscopy (CARS) and Surface Enhanced Raman Spectroscopy (SERS), enables detection of low concentration contaminants, pesticides, fungicides and bacteria. [37, 90]. For example, Johnston et al. [91] applied CARS to detect presence of ionic titanium in the gut of rainbow trout.

Lipid analysis by Raman spectrocopy is particularly promising, since lipids are effective Raman scatterers. Corresponding signals often dominate in spectra of fatty foods, such as for salmon [92] and rest raw materials of pork and poultry [11, 15, 23]. Moreover, the Raman scattering cross section of the CH_2 bend (1440 cm^{-1}) has previously been estimated, showing up to a sixfold increase going from pure proteins to lipid components [13]. A distinction between analyses of complex foods with fat and analysis of pure oils should be made, because the latter contains less disturbance from overlapping signals from other constituents. For instance,

fat and protein bands are known to overlap in Raman spectra. Due to health effects [75–79, 93] and significance for functional properties [94], the degree of unsaturation and quantity of omega-3 fatty acids have gained particular interest. The use of Raman spectroscopy to measure such characteristics is promising for pure oils [95–97], for more complex mixtures [96] and tissues [9,98]. Afseth et al. [9] even found that separate calibration models for the two fatty acids EPA and DHA in homogenized salmon muscle contained signatures similar to the respective pure fatty acids and were distinguishable. The spectral signature difference of pure EPA and DHA can be seen in Figure 2.12. They completely overlap, but differ in peak intensity ratios and by a small shift in the C=C stretch frequency (1658 cm^{-1}). This shows that Raman spectroscopy has potential for analysis of specific fatty acids. Through-skin analysis of fatty acid composition in salmon has been attempted as well using Spatially Offset Raman Spectroscopy [92]. While it has been shown that this approach is in principle feasible, the skin absorbed laser light and reduced the lipid signals. In particular, spectrum quality was considerably reduced when measuring through dark skin compared to light skin, which could make through-skin quantification challenging.

2.4 In-line Raman spectroscopy

2.4.1 Definition of in-line measurements

In process analytical technology, it is often distinguished between different measurement setups according to how fast and directly the sample or sample stream is measured. An industrial measurement situation can be categorized as *in-line*, *on-line* or *at-line* (Figure 2.13). In-line measurements are automatically taken directly in the process and are usually continuous. Similarly, on-line measurements also refer to measurements that are continuous, but are done on a sub-sampled bypass stream. At-line measurements usually refer to measurements that are done in the industry facility, but require that the samples are taken manually to a nearby measurement station where the measurement conditions are optimal, which means that they are less continuous and involve a time lag between the sampling and the availability of the measurement result. Both in-line, at-line and on-line measurements could be relevant in the industry, depending on the application and the exact need for feedback speed. In contrast, measurements that are time-consuming and are done in an external laboratory are called *off-line*.

2.4.2 Reported in-line use

The relevance of Raman spectroscopy as an in-line process tool is based on its possibility for fast (< 30s), non-contact measurements and no need for sample preparation. The fact that water does not create strong signals in Raman spectroscopy, is a considerable advantage in many food analyses, where water could

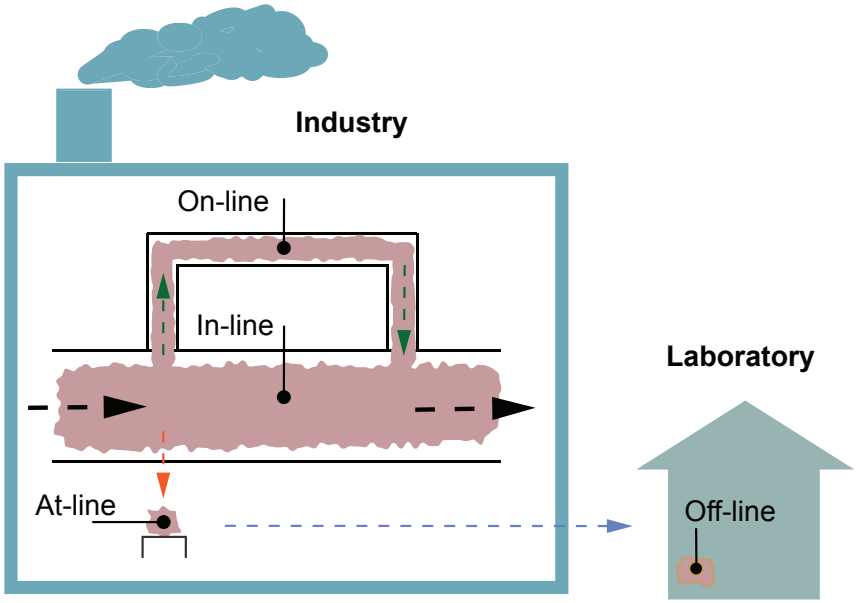

Figure 2.13: In-line, on-line, at-line and off-line measurements.

act as a disturbant. Due to an increased stability, affordability and versatility of Raman instruments in the last decades (See section 2.1.3), Raman spectroscopy has been investigated as an in-line PAT in several areas outside the food processing domain. The author refer to the thorough review by Esmonde-White et al. [33] for further details. Monitoring of continuous (flow) reactions has been particularly important in the chemical and petrochemical industries, where mixtures are often hazardous for humans. Raman spectroscopy has been reported as a monitoring tool for such reactions since 1993 [99]. One example within the production of active pharmaceutical ingredients, showed that Raman spectroscopy could be used to monitor a heterogeneous etherification reaction to determine reaction end-point at pilot scale [100]. This work also reported that the end-point was predicted 600 min before the process description stipulations, showing that the use of Raman spectroscopy could potentially reduce batch cycle time. Usage of in-line Raman spectroscopy has also been reported within the bio-processing domain, particularly since 2010 [33]. In 2014, Iversen et al. [27] inserted a Raman probe directly into a 1-L bioreactor and quantified glucose, ethanol and yeast concentration during a fermentation process. Craven et al. [101] demonstrated the use of a Raman-based control system for adjustment of the feed-rate of glucose into a bioreactor with Chinese hamster ovary cells. In this way, they were able to keep the glucose concentration in the bioreactor constant.

In the food processing domain, the potential of Raman spectroscopy as a tool for on-site and real-time measurements has been demonstrated for edible oil monitoring and control [102]. Recently, Castro et al. [28] reported successful in-situ real time monitoring of quality and safety parameters for frying oils. Frying oil quality deteriorates during cooking, and amounts of toxic compounds increase. Therefore, the main motivation of their work was to detect the critical discard point for the oils. They monitored acidity, total polar compounds (TPC) and peroxide values of different oils during a 16-h heating at 180 °C. Within this time frame, they were able to detect TPC values which were above common regulation limits. In-line Raman spectroscopy has, to the author's knowledge, not been reported in the literature for applications for more heterogeneous foods. This is likely due to the added complexity of overlapping bands from other compounds such as proteins, and the generally lower signal intensities for foods and related analytes. Due to the lower signals, SNR can be an issue in quantitative analyses of foods, particularly when the exposure time is limited due to the high in-line speeds of the food products. This holds particularly true for single products moving along a conveyor belt, such as for the application area A1 of this thesis (see section 1.2), considering single salmon fillets moving on a conveyor belt. For continuous streams, such as for the application area A2 of this thesis, considering measurement of poultry rest raw material streams, the exposure time is not limited in the same way which allows higher SNR measurements and it is easy to implement spectrum averaging as a way to help increase SNR further.

2.4.3 Robustness criteria

Due to the heterogeneity of the production volume of foods and the challenging measurement situation in the industry, the robustness of the employed measurement method is a key discussion point. What is meant by "robustness" in this context, is that the calibration obtained for a particular compound based on measurements under the relevant conditions works well for the material variations expected over time. More specifically, this requires that the predictions are

1. little affected by relevant physical changes of the food matrix (e.g. variations in absorption and scattering properties),
2. not strongly dependent on indirect measurements where correlations with concentrations of other components are required (unless these correlations are always present),
3. little affected by the relevant variations in the measurement condition (e.g. working distance).

2.4.4 Robustness of Raman and Near Infrared spectroscopy

Near Infrared spectroscopy (NIRS) have been applied for in-line measurements in the food industry for decades [103–105], and low cost systems are being con-

tinuously developed. Due to the affordability, relatively simple assembly directly in the process-line, and possibility for acquiring signals from the interior of thick samples, it is often preferred in the food industry.

In this thesis, a hypothesis is that Raman-based models might be more robust than NIRS-based models, particularly when more detailed chemical information is required from the analysis, such as specific FAs (e.g. EPA and DHA). We hypothesize that the first two robustness criteria above (section 2.4.3), i.e. degree of sensitivity to matrix effects and dependence on correlations with other compounds are the reason why Raman-based models might be more robust than NIRS-based models. NIRS is based on the measurement of overtones and combinations of vibrational modes. This means that the spectral bands of NIRS are generally broader compared to Raman bands, and consequently suffers more from overlapping information. This could be especially cumbersome in complex food matrices with signals from many constituents. In addition, it is well known that signals from water are strong and can be a challenge in calibration development for NIRS, while it is a very weak Raman scatterer. Consequently, chemical information is better resolved in Raman spectra. Afseth et al. [9] presented an example for this in the analysis of FAs in homogenized salmon samples. For Raman and NIR measurements of the same samples, they showed by PCA that the variation in the spectra were better resolved for Raman spectroscopy (Figure 2.14). Firstly, the

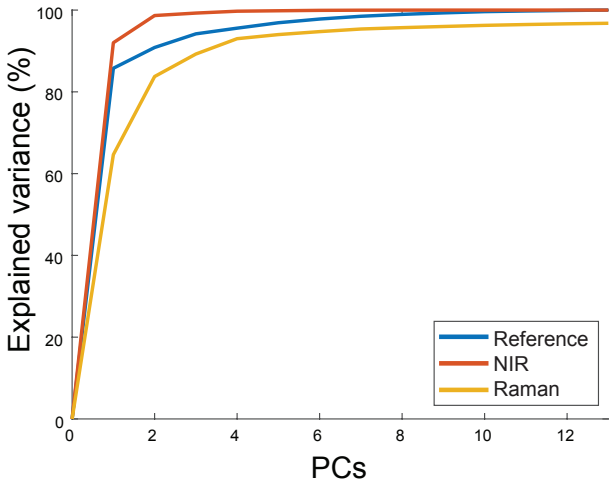

Figure 2.14: The explained variance of the reference data, NIR spectra, and Raman spectra of ground salmon samples. The figure shows 13 components because 13 FAs were included in the analyses. Reproduced from Afseth et al. [9].

variance explained by the first NIR components was considerably higher than for the references and Raman spectra. In correspondence with the above reasoning,

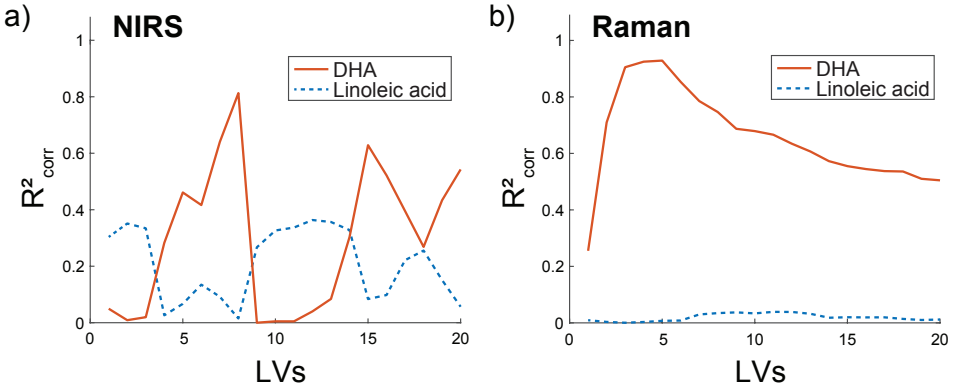

Figure 2.15: Performance of a PLSR model for DHA transferred from homogenized salmon samples (a previously collected data set) to intact salmon samples (from paper II). The performance for DHA as a function of number of included latent variables are shown for NIRS (a) and Raman spectroscopy (b). It is compared with the performance for prediction of Linoleic acid using the same DHA model. Presented at the Chemometrics in Analytical Chemistry Conference 2022, by Erik Tengstrand [107]. Acquired through personal communication.

this was because much of the variance in the NIR spectra originated from strong signals from water, proteins and from light scattering.Therefore a large part of the spectral information for NIRS was connected to the bulk composition and was explained by a few components. For Raman, more components were required to explain the variance, which means that there were more independent variations in the spectra. Furthermore, the fact that water and proteins are weak and moderate Raman scatterers, respectively, gives Raman an additional advantage over NIRS in context of lipid analysis. Corresponding signals are less pronounced in the spectra and disturb the FA signals less. Consequently, it is likely that NIRS is more susceptible to issues with dependence on conserved correlations (the so called cage of covariance [106]) and matrix effects, especially for samples which are heterogeneous and varying in composition.

As an extension of this reasoning, calibration maintenance as well as calibration transfer could possibly be less cumbersome for Raman spectroscopy. Figure 2.15 shows results from a calibration transfer of a PLSR model for DHA, based on homogenized salmon samples (from Afseth et al. [9]), to the intact salmon fillets from paper II in this thesis. For both sample sets, measurements were made by Raman spectroscopy and NIRS. The figure shows how the performance on the intact salmon set varies with the choice of number of latent variables (LV). For NIRS, a high variability in performance with the choice latent variables was seen. More interestingly, the performance dramatically drops when including 9-13 LVs. The reason for this is likely that these components introduce indirect modelling on other FAs, and that the covariance between DHA and these other FAs are

strongly reduced in the intact salmon sample set. The figure shows indications that linoleic acid is one such FA. The performance for prediction of linoleic acid, using the model for DHA, is shown. It can be seen that the very same LVs (9-13) that caused a dramatic performance drop for DHA, results in a considerable performance lift for linoleic acid. This shows that the NIRS-based DHA model was very sensitive to variation in the covariance structure in the sample sets. In contrast, such behaviour is much less pronounced for the calibration transfer of the Raman-based DHA model, and performance is fairly high for any chosen number of LVs. This is again a testimony to the higher chemical resolution in Raman spectra. Therefore, the hypothesis of Raman spectroscopy being more robust than NIRS is well motivated for specific fatty acids, and should be expected to extend to other detailed chemical analysis for heterogeneous foods as well.

Chapter 3

Results and discussions

3.1 Paper I

Feasibility of In-line Raman Spectroscopy for Quality Assessment in Food Industry - How Fast Can We Go?

For the first time, a Wide Area Illumination (WAI) Raman probe was tested for stand-off measurements on a conveyor of raw material relevant for the two defined application areas in this thesis, i.e. A1) salmon fillets and A2) a poultry rest raw material stream. Concentration of the fatty acids EPA + DHA in ground salmon samples ($n = 63$) and residual bone concentration in samples of mechanically recovered ground chicken ($n = 66$) were estimated. The paper was specifically focused on measurements of single samples on a conveyor belt, and not a continuous stream. We prepared samples of defined sizes, and showed how spectrum quality (SNR) and prediction errors were affected by decreasing exposure time from 10 s down to 1 s (Figure 3.1). The exposure time was adjusted by the speed of the belt. We found that high belt speeds reduced spectrum quality and increased prediction errors, an effect that was stronger when reducing the exposure time below 4 s. Comparatively, an exposure time of around 1 s corresponded to belt speeds (0.3 m/s) currently employed in-line in the industry. This confirmed that the higher belt speeds limited the performance and that SNR is a critical parameter. The obtained spectrum quality and estimation accuracy were still acceptable for industrial use showing that the applications are feasible. This emphasizes that strategies for SNR optimization in an in-line system are important with respect to robustness.

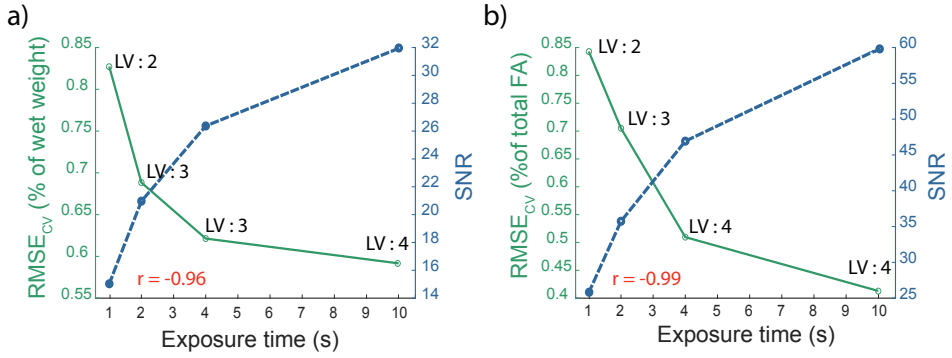

Figure 3.1: The prediction error and average spectrum SNR as a function of exposure time for estimation of residual bone concentration in mechanically recovered ground chicken (a) and concentration of fatty acids EPA+DHA in ground salmon (b). The correlation between SNR and RMSE$_{CV}$ is indicated

We further compared simple strategies for noise reduction, including in-line replicate averaging and variable selection, for which prediction errors are shown in Figure 3.2. Replicate averaging was considered an analogy to installing two Ra-

man instruments in series, and this strategy lead to the most pronounced positive effect on the performance. However, this represents a high cost solution, while only providing a moderate performance lift. In addition to the strategies indicated in Figure 3.2, we showed that, with the given normalization strategy (EMSC), a calibration based on 10 s exposure time could be used at shorter exposure times without compromising performance. This demonstrated a practical versatility with respect to handling samples of different sizes and potentially for employing adjustable exposure times to optimize SNR for individual samples.

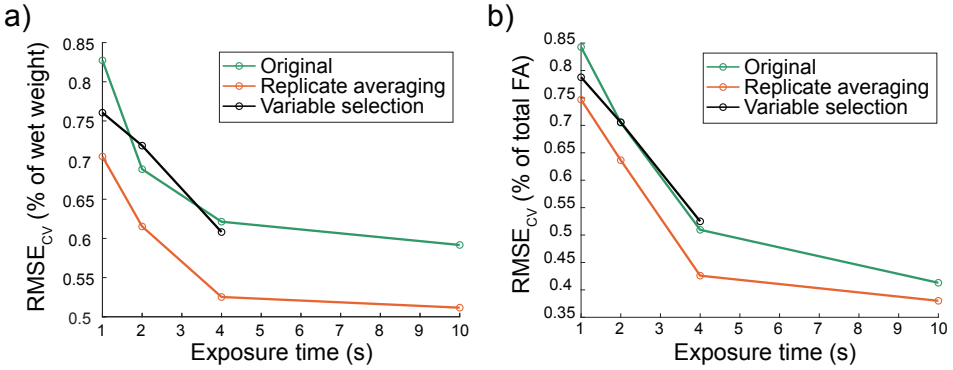

Figure 3.2: The prediction error as a function of exposure time for the different noise reduction strategies tested, compared to the original data. Performance is shown for estimation of residual bone concentration in mechanically recovered ground chicken (a) and concentration of fatty acids EPA+DHA in ground salmon (b).

The possibility for instrumental improvements was mentioned in paper I, but not thoroughly discussed. One way to increase signal recovery is to tailor the laser excitation wavelength to the application. By employing shorter wavelengths, Raman signal intensities (Eq. 2.5) could be greatly enhanced, but may also greatly enhance fluorescence signals and the risk of detector saturation. Therefore, the spectrum noise component would also be increased, and the SNR gain is uncertain. However, when the aim is to minimize exposure time while maintaining high SNR, it is possible that the increased Raman signal at shorter laser wavelengths could allow lower exposure times, without sacrificing SNR to the same extent. In this approach, there is clearly a need to characterize the SNR as a function of laser wavelength at short exposure times (below 4 s). Another potential way to increase SNR is to add reflective mirrors or similar to the back scattering configuration, which allows reflected or Rayleigh-scattered photons to be reflected back into the sample and potentially be Raman scattered. Thus, the Raman signal may be increased at shorter exposure times. Such approaches have have led to improvement in SNR and performance in other applications [108], and could possibly be adapted for in-line use on moving samples. However, also in this case, fluorescence would be increased and further investigation of the impact of such strategies on SNR

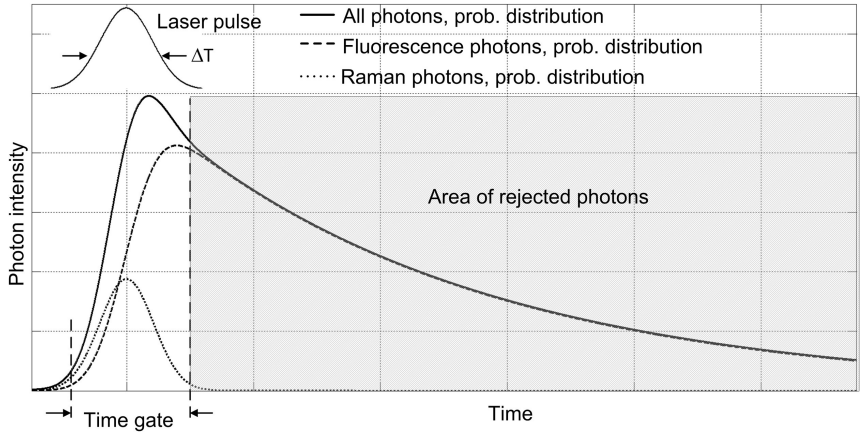

Figure 3.3: The time-gated Raman spectroscopy principle. Reproduced from Nissinen et al. [109]

at short exposure times (below 2 s) is needed. Yet another interesting possibility which could be investigated is the use of time-gated Raman. In this approach, fluorescence is physically avoided by employing a pulsed laser and a detector with programmable shutter. The concept exploits the fact that Raman scattering is a faster process than fluorescence. By collecting the signal at the detector in a limited period, many fluorescence photons are not collected, as illustrated in Figure 3.3. This reduces the shot noise component associated with fluorescence and may lead to higher SNR at short exposure times, and at the same time act as a safeguard against detector saturation by fluorescence.

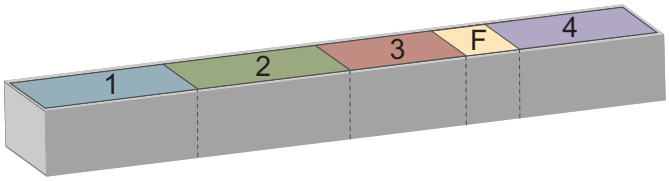

Figure 3.4: The heterogeneous poultry sample composition, consisting of different poultry rest raw materials placed in slots 1-4. A fat rich material F of varying size was placed at a random position.

Paper I considered single samples. For the salmon application (A1), this addressed the final goal to measure single salmon fillets on a conveyor belt. With respect to the poultry rest raw material measurements, the final goal was to perform measurements on large volumes in a continuous stream. However, as a proof of concept it was decided to start with single poultry raw material samples to investigate the impact of lower SNR and to study a different food matrix in addition

to the salmon. Furthermore, it allowed a controlled check of how the performance was impacted by measuring the same samples in heterogeneous state versus homogenized state.This was motivated by the potential differences in absorption and scattering properties within heterogeneous material, which could possibly disturb spectrum intensities. The heterogeneous samples were made by combining different base species of poultry material in a sample holder, without mixing (Figure 3.4). Samples were scanned at the conveyor and then homogenized and scanned again. We found that the difference in performance between these two measurement sets were not significant, which was promising with respect to measurements on heterogeneous samples, and suggested that differences in material properties did not critically disturb the acquired sample spectra.

3.2 Paper II

Raman Spectroscopy and NIR Hyperspectral Imaging for In-line Estimation of Fatty Acid Features in salmon fillets

In paper II, we looked more thoroughly into application A1) in-line determination of fat composition in salmon fillets at short exposure times, concentrating on %EPA+DHA. In contrast to paper I, the particular focus was on strategies for tackling the spatial heterogeneity of intact fillets, i.e. the fat distribution over the fillet. This was done by testing different scanning paths for signal accumulation, including one path over the low fat loin area and two scanning paths over the high fat belly area (sinusoid and line scan), as shown in Figure 3.5a. Additionally, we considered measurements on trimmed versus untrimmed fillets. In trimmed fillets, the high fat deposition layer in the belly is removed. Such trimming is often employed industrially, and it was of interest to check if trimming impacted the performance. From cross validation on a calibration set ($n = 51$) with salmon fillets from different locations and feeding regimes acquired in the spring, we found again that SNR of the spectrum was the limiting factor for the choice of scanning strategy. Figure 3.5 shows the prediction error as a function of SNR for the different

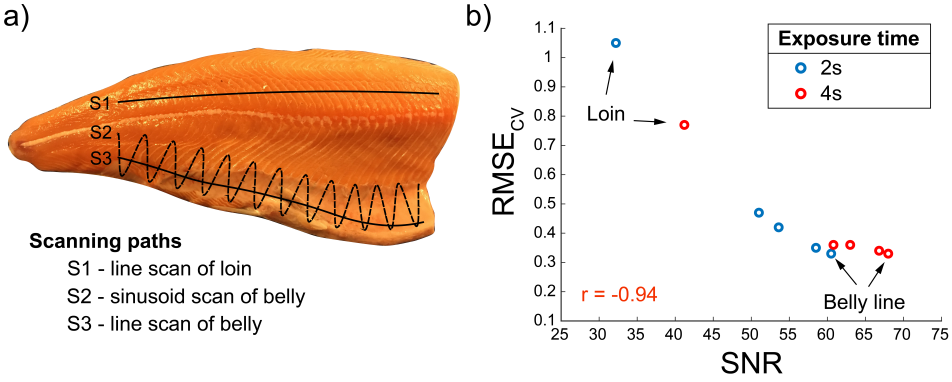

Figure 3.5: The scanning strategies employed for Raman signal accumulation (a) and prediction errors (CV) for the calibration set, as a function of SNR of the different Raman scanning strategies. The overall correlation between SNR and RMSE_{CV} is indicated.

Raman scanning strategies. Clearly, the loin scans exhibited considerably lower SNR and performance. The performance would be even lower at higher speeds, e.g. 1 s exposure, which is closer to industrial conveyor belt speeds. The belly line scan on untrimmed fillets gave the highest SNR and performance. Furthermore it could be seen that there was a moderate decrease in performance for SNRs between 50-60 (i.e. different belly scanning strategies at 2 s exposure time), while there was little increase in performance above 60 (i.e. different belly scanning strategies at 4 s exposure time). This showed that the choice of scanning strategy is more

important at lower exposure times. Consequently, for industrial employment of Raman measurements on a conveyor belt, a robotic solution might be needed in order to target the high fat belly region of the fillets, and so far Raman might be better suited for fast at-line measurements. Integration of Raman spectroscopy with robotics is a topic that is being investigated in other areas such as in nuclear waste operation decision making [110] and tissue characterization in surgical robotics [111, 112]. To the author's knowledge, it has not yet been investigated for use on a conveyor belt for measurements of single samples, where high-speed operation and exact laser trigger timing is important.

Currently, it is uncertain whether the choice of scanning strategy can be influenced by potential variation in fat composition across the fillet. Although it is well known that the fat level varies over the fillet, there is a lack of larger studies mapping the fat composition over the fillet, most likely due to the high costs associated with the FA analyses. Further work is needed to understand how representative measurements in the belly are for the rest of the fillet.

The choice of measuring EPA+DHA as percent of total fat was made in order to reduce indirect modelling on total fat level. Such a situation would not be considered robust, for instance since fat levels typically vary seasonally [69]. Correspondingly, one must be aware that the estimation does not give any information on total fat level and therefore no absolute values for amount of EPA+DHA. This limits the interpretation and conclusions that can be made based on the measurements. In that sense there is still a missing link with respect to informative value on a total nutritional level.

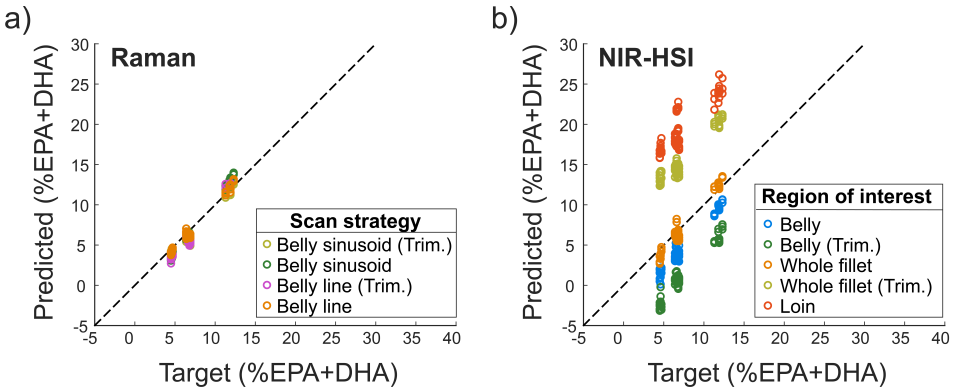

Figure 3.6: Predicted versus measured %EPA+DHA values for the test set, based on various Raman scanning strategies (a) and various NIR-HSI regions of interest (b). For Raman, the loin scan was not considered for the test set, as the calibration set had revealed critically low SNR values.

Further, we compared the Raman measurements with NIR hyperspectral imaging (HSI), to elucidate the hypothesis motivated in section 2.4.4, i.e. that Raman might be more robust than NIR. Prediction on a test set ($n = 20$) acquired in a different season (i.e. autumn where fat deposition is higher than in spring) supported this hypothesis. Figure 3.6 shows the predictions based on Raman spectroscopy and NIR-HSI. For Raman spectroscopy, the predictions based on belly measurements had very low bias and slope errors. For NIRS, models based on different fillet regions of interest exhibited large and varied biases, indicating sensitivity to matrix effects or dependence on conserved correlations. Notwithstanding, the NIRS-based models did give low variance and slope errors, indicating that, with careful calibration maintenance, NIR-HSI is also a viable method.

3.3 Paper III

In-line Raman Spectroscopy for Characterization of an Industrial Poultry Raw Material Stream

In paper III, we studied more thoroughly A2) in-line characterization of a poultry rest raw material stream. We established calibrations ($n = 59$) for fat, protein, ash (proxy for bone) and hydroxyproline (proxy for collagen) in ground poultry rest raw material. Calibrations were established in the laboratory using samples with high compositional variation. To mimic expected in-line variations in the measurement situation, samples were measured using a Wide Area Illumination (WAI) Raman probe at varying working distance (6 cm, 9 cm, 12 cm) and probe tilt angle (0°, 30°).

Firstly, the average spectrum intensities were little affected by working distance, as shown in Figure 3.7a., although there was a trend that spectra acquired at non-optimal working distances had slightly lower intensities. This showed that the

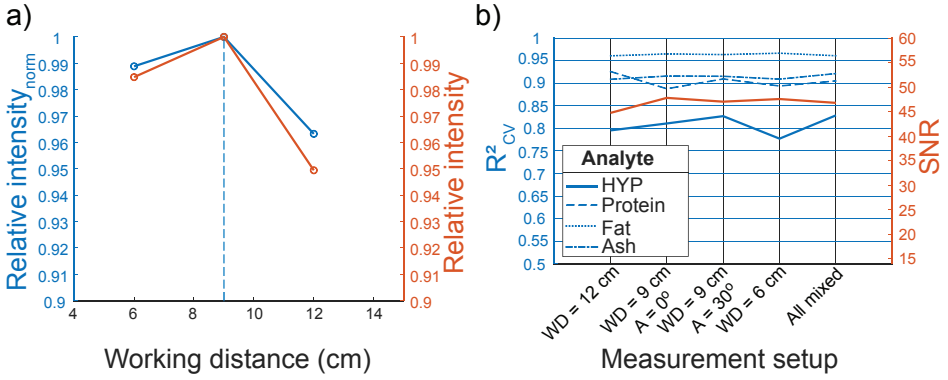

Figure 3.7: Results from the poultry rest raw material calibration set, illustrating how working distance moderately impacted the average spectrum intensity, relative to the intensity at the optimal working distance at 9 cm (a). The figure compares how the intensity changes for spectra that are normalized by the sapphire peak intensity (blue) and spectra that are only baseline corrected (red). The moderate impact of the different measurement setups (WD = working distance and A = probe tilt angle) on model performance and SNR is shown (b).

WAI probe handled these moderate variations in working distances well. One hypothesis in this paper was that normalization by the sapphire peak intensity could correct for variations in working distance. This was based on the assumption that the intensity of the reflected or back scattered laser beam from the sample (see section 2.1.5) is dependent on the working distance due to the back scattering geometry (e.g. spherical). Although the calibration set did not contain large enough variations in working distance to properly elucidate this assumption, there was a trend that intensities were less reduced when applying this normalization strategy

compared to applying baseline correction only (Figure 3.7a). Furthermore, the spectrum SNR was little affected by the variations in working distance and probe tilt, and predictive performances were not significantly affected for any analytes ($\alpha = 10\%$), as shown in Figure 3.7b.

We further tested the obtained calibrations in-line with continuous measurements of the ground poultry rest raw material stream at a commercial hydrolysis facility over the course of two days. Measurements were acquired under demanding conditions, including large variations in working distance and angle, moderate variations in exposure time and presence of light pollution from an LCD screen and ambient LED light. The models needed modifications compared to the suggested cross-validated models for the calibration set. These modifications were larger for the HYP and protein models. In particular, reducing the number of PLS components considerably, improved the model performance for in-line predictions. However, this was with the result that the protein model relied more on signals from fat and that the HYP model relied more on general protein signals. There were also indications that more custom pre-processing for different analytes may be advantageous. However, given the above listed challenges, we were still able to obtain

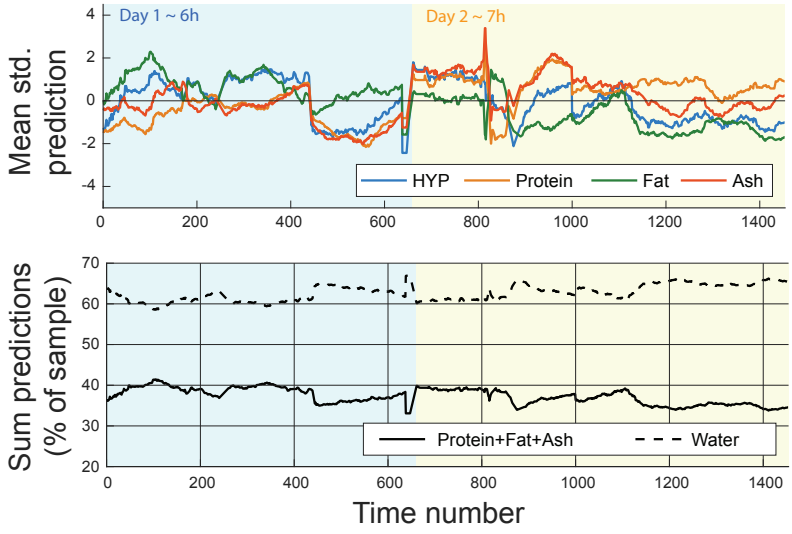

Figure 3.8: Prediction trends (15 minute moving average) for analytes during in-line testing of obtained models from laboratory calibration. The mean standardized trend for each analyte is shown (a), for easy comparison of qualitative trends. The sum ($\sum$) of predictions of protein, fat and ash concentrations is shown (b). As the remaining component is assumed to be water, the residual, i.e. 100% - $\sum$, is plotted as an indication of variation in water level.

reasonable estimates of compositional trends, as shown in Figure 3.8. For instance, higher fat concentrations were often accompanied by lower concentrations in other

analytes, as expected. The sum of prediction trends for protein, fat, and ash concentrations in the sample stream varied approximately by 30-40 %, suggesting a water concentration between 60-70 %, which also corresponds well with previous experience.

The variations in working distance during in-line testing was much larger compared to the laboratory calibration measurements. An unknown factor for these measurements was to what extent the variation in working distance impacted predictions. The effect of the working distance on the predictions depends on two main factors: i) how large working distances the pre-processing can effectively correct for and ii) whether the spectra which are not effectively corrected are filtered out. In this paper, we employed a simple criterion for filtering out low quality spectra, based on the SNR. Since measurements of working distance were not available for these in-line measurements, we could not properly evaluate whether the pre-processing and filtering method together tackled the larger variations in working distance. Therefore it is of interest to elucidate the effect of larger working distances in a more systematic study in the laboratory. However, Figure 3.9 shows an example of

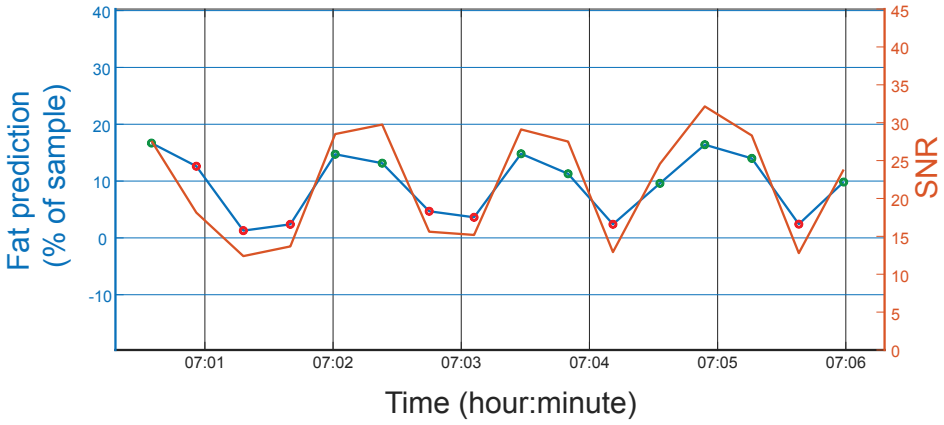

Figure 3.9: Fat predictions in a small time span, showing periodic variations in predictions and SNR, corresponding with the alternating output volume (i.e. working distance) at the grinder. Spectra with SNR below 23 were filtered out, and corresponding predictions are marked (red), while predictions based on spectra with accepted quality are marked (green).

how predictions and SNR varied periodically in correspondence with the alternating output volume (i.e. working distance) at the grinder. This clearly indicated that SNR does indeed vary with working distance, and that filtering based on SNR is justified. However, SNR will also be affected by other phenomena that changes either the average Raman signal intensity (chemistry) or the noise level (e.g. shot noise from fluorescence). Filtering methods that are more directly related to working distance might be more robust. If working distance cannot be diagnosed from the spectra, an option is to integrate a laser distance sensor with the instrument.

Alternatively, another way to eliminate errors introduced by varying working distances is to use contact probes coupled directly into the stream. In this case, this was not practically feasible and would require more invasive installments such as bypass tubes. Moreover, this is often inconvenient during feasibility trials in the food industry. Therefore the WAI Raman standoff probe is a good compromise in many cases. Establishing the operational limits of such a measurement method with respect to working distance, together with development of diagnosis tools for measurements outside of these limits, will be important to take Raman WAI stand-off probes towards industrial application development for food raw material streams.

In case of Raman deployment, another important factor to consider is the heterogeneity of the stream. Raman introduces a considerable subsampling of the output stream from the grinder. In order to ensure that Raman measurements provide representative measurements for the stream on average, the degree of heterogeneity of the cross section of the stream should be correlated to temporal variation. If the main variation is temporal, Raman measurements may still be a good solution.

Chapter 4

Conclusion and further research

The overall goal of this thesis was to elucidate the feasibility of Raman spectroscopy as a tool for detailed quality evaluation of heterogeneous food raw materials under in-line industrial conditions. To this end, two main application areas were chosen, including A1) in-line measurements of fatty acid features in salmon fillets and A2) in-line characterization of a poultry rest raw material stream. Table 4.1 summarizes in detail the subgoals, main findings and suggestions for further actions within these two application areas. The main findings are summarized below.

Paper I was a first confirmation of feasibility for the two applications, where we showed that spectra obtained by using a WAI stand-off Raman probe for surface scanning of chicken and salmon samples on a conveyor belt have sufficiently high quality at industrially relevant conveyor belt speeds, down to 2-1 s exposure time. This motivated further investigation of the two applications in paper II and III.

In paper II, we developed scanning strategies to tackle the heterogeneity of the salmon fillets, and at the same time optimize SNR. The salmon belly was identified as the optimal scanning region, while loin scans gave low performance in comparison, due to low SNR. This illustrates the importance of considering the heterogeneity of the food product in a given application, and of optimizing measurement strategies accordingly. One way to ensure optimal in-line measurements in case of spatial heterogeneity in the food product, is to implement robotic scanning solutions. In the salmon fillet application, our finding suggested the need for a robotic Raman system which can guide the Raman probe over the belly during signal accumulation. It remains to test measurements of salmon fillets in an actual industry environment, for which a robotic demo would be needed. In further work, more focused application development could be advantageous, for example to investigate the possibility for employment as a fast phenotyping tool in genetics trials. Before this, extension of the calibration to salmon in different sizes and life stages is needed, to elucidate the robustness of the method further. In addition, it would be preferable to combine the Raman measurements of fat composition with total fat analysis, for better representation of nutritional value and broader phenotyping. If an in-line measurement system is successfully realized, Raman spectroscopy could prove itself a valuable tool for the salmon industry, by monitoring product quality with frequent feedback over the seasons and years. This

would provide a unique basis for analysis and quality optimization by measuring effects of feeding strategies, breeding and possibly other farming parameters.

In paper III, we found that measuring detailed chemistry in a heterogeneous poultry raw material stream is feasible when using a WAI Raman probe. Variations in working distance can be a critical factor in such a process. Such variations may be handled by efficient normalization and filtering algorithms for spectra and novel probes with enhanced focusing depth. In further work, it is important to elucidate the limitations of such hardware and pre-processing to handle larger variations in working distance. Establishing the corresponding operational limits and developing diagnosis tools for measurements outside of these limits will be important to take Raman WAI probes towards industrial implementation for food raw material streams. If an in-line measurement system is successfully realized, WAI Raman spectroscopy could be a valuable tool for monitoring and controlling the mechanical deboning process or the hydrolysis process. This provides the opportunity for real-time optimization of yield and quality.

Overall, the work of this thesis illustrates that measurements of detailed chemistry in single samples on a conveyor belt can have good performances at exposure times of around 2-1 s. Nevertheless, it was evident that these low exposure times reduced SNR and performance and that SNR was a critical parameter. This indicates that such fast Raman measurements might be less robust with respect to tackling samples of varying sizes or lower analyte concentrations. Therefore, it is critical to monitor spectrum quality in a practical implementation, and further work on SNR optimization strategies will be important. For such types of measurements, Raman is therefore so far better suited for fast at-line/on-line measurements. Nevertheless, the Raman-based measurement approach presented in this thesis, represents a considerably faster and cheaper method compared to corresponding off-line laboratory methods.

Further efforts on calibration development, SNR optimization and practical measurement setup is needed to unlock the full potential for in-line measurements in the two application areas. Still, this thesis has shown that it is feasible to use a WAI Raman probe for detailed characterization of very heterogeneous streams of raw material, at industrially relevant speeds and in presence of moderate variations in working distance and probe tilt. It was shown that WAI Raman spectroscopy is promising, both for measurements of continuous raw material streams and single food products on a conveyor belt. This introduces many new application opportunities for Raman spectroscopy within quality documentation, sorting, process analysis and real-time process control in the food industry. Although this was demonstrated through measurements of poultry rest raw material and salmon fillets in this thesis, it could clearly be relevant also for other raw material streams in other meat production.

NIRS methodologies are well established for measurement of many quality parameters in the food industry. This method has considerable advantages with respect

to affordability, relatively simple assembly directly in the process-line, easier compatibility with ambient light, much better sampling capabilities and consequently more representative sampling. In contrast, Raman spectroscopy will require more careful development of practical measurement setup. However, this thesis indicates that Raman spectroscopy might be more robust with respect to variations in absorption and scattering properties within a sample or between samples and dependence on conserved correlations with other compounds. This suggests that once practical measurement setups are developed, Raman-based calibrations could be more easily maintained in the industry and reduce associated costs. In addition, NIRS is not suitable for measuring all relevant quality parameters, such as bone and collagen for which Raman is promising. Moreover, the inherent sensitivity of Raman to ambient light need not be an issue with the appropriate shielding development or employment of suitable light sources at the measurement location. Overall, WAI Raman spectroscopy may be a good alternative to NIRS for industrial food quality monitoring, particularly in applications where more detailed chemical analysis is desired.

	G1 Develop effective Raman sampling regimes for heterogeneous foods, suitable for industrial in-line conditions		**G2** Develop analysis strategies for in-line evaluation of food quality parameters based on Raman measurements		**G3** Evaluate performance of developed strategies in a real in-line industry setting	
	Finding	Further action	Finding	Further action	Finding	Further action
A1 In-line measurements of fatty acid features in salmon fillets	Using a WAI Raman probe for surface scanning of salmon fillets on a conveyor belt is feasible for %EPA+DHA estimation Belly identified as optimal scanning region with respect to SNR	Mapping fat composition across fillet Investigate SNR optimization of belly measurements below 2 s exposure time	Good PLSR performances for %EPA+DHA at short exposure times (ca 2 s)	Investigate combination with total fat analysis Extension of calibration to salmon in various life stages	Good performance under mimicked industry conditions (in motion and in presence of ambient light)	Development of robotic Raman demo system
A2 In-line characterization of a poultry rest raw material stream	Using a WAI Raman probe for surface scanning of very heterogeneous poultry material is feasible for %HYP, %protein, %fat and %ash estimation Moderate variation in WD[a] (6 - 12 cm) and probe tilt (0 - 30°) impacted spectra and performance minimally	Investigate if main compositional variations of sample stream at hydrolysis facility is temporal	Good performances for %HYP, %protein, %fat and %ash Indications that normalization by sapphire peak intensity in combination with SNR filtering may be used to tackle variations in WD	Optimize separate pre-processing for different analytes Laboratory study for proper testing of suggested pre-processing and filtering in presence of larger WD (e.g 4 - 30 cm)	In-line testing at a real hydrolysis plant provided predictions with reasonable average trends Further robustification of HYP and protein models needed	After further robustification of calibrations, re-evaluate at hydrolysis facility

[a] WD - working distance

Table 4.1: Goals (G1 - G3), main findings and suggestions for further actions in the two application areas (A1 - A2).

References

[1] Tiril Aurora Lintvedt, Petter Vejle Andersen, Nils Kristian Afseth, Brian Marquardt, Lars Gidskehaug, and Jens Petter Wold. Feasibility of In-line Raman Spectroscopy for Quality Assessment in Food Industry - How Fast Can We Go? *Applied Spectroscopy*, 76(5):559–568, 2022.

[2] Tiril Aurora Lintvedt, Petter Vejle Andersen, Nils Kristian Afseth, Karsten Heia, Stein-Kato Lindberg, and Jens Petter Wold. Raman Spectroscopy and NIR Hyperspectral Imaging for In-line Estimation of Fatty Acid Features in Salmon Fillets. *Talanta*, 254:124113, 2023.

[3] Tiril Aurora Lintvedt, Petter Vejle Andersen, Nils Kristian Afseth, and Jens Petter Wold. In-line Raman Spectroscopy for Characterization of an Industrial Poultry Raw Material Stream. *Submitted to Talanta.*

[4] Tiril Aurora Lintvedt, Petter Vejle Andersen, Nils Kristian Afseth, Karsten Heia, Stein-Kato Lindberg, and Jens Petter Wold. Raman Spectroscopy for In-line Food Quality Sensing on a Conveyor Belt. In *SciX Conference*, Providence, RI, 2021.

[5] Tiril Aurora Lintvedt, Petter Vejle Andersen, Nils Kristian Afseth, Brian Marquardt, Lars Gidskehaug, and Jens Petter Wold. Feasibility of In-line Raman Spectroscopy for Quality Assessment in the Food Industry. In *European Biosensor Symposium*, 2021.

[6] Tiril Aurora Lintvedt, Petter Vejle Andersen, Nils Kristian Afseth, Karsten Heia, Stein-Kato Lindberg, and Jens Petter Wold. Raman Spectroscopy for In-line Estimation of Fatty Acid Features in Salmon Fillets. In *The International SensorFINT Conference*, Izola, Slovenia, 2022.

[7] Bjørn Inge Bendiksen. Driftsundersøkelsen i Fiskeindustrien 2021, in press, 2023.

[8] Feifei Tao and Michael Ngadi. Recent Advances in Rapid and Nondestructive Determination of Fat Content and Fatty Acids Composition of Muscle Foods. *Critical Reviews in Food Science and Nutrition*, 58(9):1565–1593, 2018.

[9] Nils Kristian Afseth, Katinka Dankel, Petter Vejle Andersen, Gareth Frank Difford, Siri Storteig Horn, Anna Sonesson, Borghild Hillestad, Jens Petter Wold, and Erik Tengstrand. Raman and Near Infrared Spectroscopy for Quantification of Fatty Acids in Muscle Tissue: A Salmon Case Study. *Foods*, 11(7):962, 2022.

[10] Petter Vejle Andersen, Jens Petter Wold, Eli Gjerlaug-Enger, and Eva Veiseth-Kent. Predicting Post-mortem Meat Quality in Porcine Longissimus Lumborum using Raman, Near Infrared and Fluorescence Spectroscopy. *Meat Science*, 145:94–100, 2018.

[11] Sileshi Gizachew Wubshet, Jens Petter Wold, Ulrike Böcker, Karen Wahlstrøm Sanden, and Nils Kristian Afseth. Raman Spectroscopy for Quantification of Residual Calcium and Total Ash in Mechanically Deboned Chicken Meat. *Food Control*, 95:267–273, 2019.

[12] Olga Monago-Maraña, Jens Petter Wold, Rune Rødbotten, Katinka Riiser Dankel, and Nils Kristian Afseth. Raman, Near-Infrared and Fluorescence Spectroscopy for Determination of Collagen Content in Ground Meat and Poultry By-Products. *Food Science and Technology*, 95:267–273, 2019.

[13] Ramasamy Manoharan, Joseph J. Baraga, Michael S. Feld, and Richard P. Rava. Quantitative Histochemical Analysis of Human Artery using Raman Spectroscopy. *Journal of Photochemistry and Photobiology B: Biology*, 16(2):211–233, 1992.

[14] Olga Monago-Maraña, Nils Kristian Afseth, Svein Halvor Knutsen, Sileshi Gizachew Wubshet, and Jens Petter Wold. Quantification of Soluble Solids and Individual Sugars in Apples by Raman Spectroscopy: A Feasibility Study. *Postharvest Biology and Technology*, 180:111620, 2021.

[15] Sileshi Gizachew Wubshet, Jens Petter Wold, Nils Kristian Afseth, Ulrike Böcker, Diana Lindberg, Felicia Nkem Ihunegbo, and Ingrid Måge. Feed-Forward Prediction of Product Qualities in Enzymatic Protein Hydrolysis of Poultry By-products: a Spectroscopic Approach. *Food and Bioprocess Technology*, 11:2032–2043, 2018.

[16] Holly J. Butler, Lorna Ashton, Benjamin Bird, Gianfelice Cinque, Kelly Curtis, Jennifer Dorney, Karen Esmonde-White, Nigel J. Fullwood, Benjamin Gardner, Pierre L. Martin-Hirsch, Michael J. Walsh, Martin R. McAinsh, Nicholas Stone, and Francis L. Martin. Using Raman Spectroscopy to Characterize Biological Materials. *Nature Protocols*, 11(4):664–687, 2016.

[17] Fran Nekvapil, Ioana Brezestean, Daniel Barchewitz, Branko Glamuzina, Vasile Chiş, and Simona Cintă Pinzaru. Citrus Fruits Freshness Assessment using Raman Spectroscopy. *Food Chemistry*, 242:560–567, 2018.

[18] Laser Institute of America. ANSI Z136.1: American National Standard for Safe Use of Lasers. *SPIE Medical Imaging*, 2007.

[19] Jakob Christensen, Lars Nørgaard, Rasmus Bro, and Søren Balling Engelsen. Multivariate Autofluorescence of Intact Food Systems, 2006.

[20] Chad A. Lieber and Anita Mahadevan-Jansen. Automated Method for Subtraction of Fluorescence from Biological Raman Spectra. *Applied Spectroscopy*, 57(11):1363–1367, 2003.

[21] Alexey N. Semenov, Boris P. Yakimov, Anna A. Rubekina, Dmitry A. Gorin, Vladimir P. Drachev, Mikhail P. Zarubin, Alexander N. Velikanov, Juergen Lademann, Victor V. Fadeev, Alexander V. Priezzhev, Maxim E. Darvin, and Evgeny A. Shirshin. The Oxidation-Induced Autofluorescence Hypothesis: Red Edge Excitation and Implications for Metabolic Imaging. *Molecules*, 25(8):1863, 2020.

[22] Dominic A. Nanton, Anne Vegusdal, Anna Maria Bencze Rørå, Bente Ruyter, Grete Baeverfjord, and Bente E. Torstensen. Muscle Lipid Storage Pattern, Composition, and Adipocyte Distribution in Different Parts of Atlantic Salmon (Salmo Salar) Fed Fish Oil and Vegetable Oil. *Aquaculture*, 265(1-4):230–243, 2007.

[23] Petter Vejle Andersen, Jens Petter Wold, and Nils Kristian Afseth. Assessment of Bulk Composition of Heterogeneous Food Matrices Using Raman Spectroscopy. *Applied Spectroscopy*, 75(10):1278–1287, 2021.

[24] Håkan Wikström, Ian R. Lewis, and Lynne S. Taylor. Comparison of Sampling Techniques for In-line Monitoring using Raman Spectroscopy. *Applied Spectroscopy*, 59(7):934–941, 2005.

[25] Matthew V. Schulmerich, William F. Finney, Richard A. Fredricks, and Michael D. Morris. Subsurface Raman Spectroscopy and Mapping Using a Globally Illuminated Non-Confocal Fiber-Optic Array Probe in the Presence of Raman Photon Migration. *Applied Spectroscopy*, 60(2):109–114, 2006.

[26] Kayeong Shin and Hoeil Chung. Wide Area Coverage Raman Spectroscopy for Reliable Quantitative Analysis and its Applications, 2013.

[27] Jens A. Iversen, Rolf W. Berg, and Birgitte K. Ahring. Quantitative Monitoring of Yeast Fermentation using Raman Spectroscopy. *Analytical and Bioanalytical Chemistry*, 406(20):4911–4919, 2014.

[28] Rafael C. Castro, David S.M. Ribeiro, João L.M. Santos, and Ricardo N.M.J. Páscoa. The use of In-situ Raman Spectroscopy to Monitor at Real Time the Quality of Different Types of Edible Oils Under Frying Conditions. *Food Control*, 136, 2022.

[29] C. V. Raman and K. S. Krishnan. A New Type of Secondary Radiation. *Nature*, 121(3048):501–502, 1928.

[30] John R. Ferraro, Kazuo Nakamoto, and Chris W. Brown. *Introductory Raman Spectroscopy*. Elsevier, 2003.

[31] Norman B. Colthup, Lawrence H. Daly, and Stephen E. Wiberley. Vibrational and Rotational Spectra. In *Introduction to Infrared and Raman Spectroscopy*, chapter 1, pages 1–73. Elsevier, San Diego, 3 edition, 1990.

[32] Peter Vandenabeele. Theoretical Aspects. In *Practical Raman Spectroscopy: an introduction*, chapter 1, pages 1–38. Wiley, Chichester, UK, 1 edition, 2013.

[33] Karen A. Esmonde-White, Maryann Cuellar, Carsten Uerpmann, Bruno Lenain, and Ian R. Lewis. Raman Spectroscopy as a Process Analytical Technology for Pharmaceutical Manufacturing and Bioprocessing. *Analytical and Bioanalytical Chemistry*, 409(3):637–649, 2017.

[34] Howard Peng Sin Heng, Chi Shu, Wei Zheng, Kan Lin, and Zhiwei Huang. Advances in Real-time Fiber-optic Raman Spectroscopy for Early Cancer Diagnosis: Pushing the Frontier into Clinical Endoscopic Applications. *Translational Biophotonics*, 3(1), 2021.

[35] Harry Owen. The Impact of Volume Phase Holographic Filters and Gratings on the Development of Raman Instrumentation. *Journal of Chemical Education*, 84(1):61, 2007.

[36] M. L. Myrick and S. M. Angel. Elimination of Background in Fiber-Optic Raman Measurements. *Applied Spectroscopy*, 44(4):565–570, 1990.

[37] Ying-Sing Li and Jeffrey S. Church. Raman Spectroscopy in the Analysis of Food and Pharmaceutical Nanomaterials. *Journal of Food and Drug Analysis*, 22(1):29–48, 2014.

[38] Eliana Cordero. In-vivo Raman Spectroscopy: From Basics to Applications. *Journal of Biomedical Optics*, 23(7):1, 2018.

[39] Ines Latka, Sebastian Dochow, Christoph Krafft, Benjamin Dietzek, and Jürgen Popp. Fiber Optic Probes for Linear and Nonlinear Raman Applications - Current Trends and Future Development. *Laser and Photonics Reviews*, 7(5):698–731, 2013.

[40] Catharina Latz, Thomas Asshauer, Christian Rathjen, and Alireza Mirshahi. Femtosecond-Laser Assisted Surgery of the Eye: Overview and Impact of the Low-Energy Concept. *Micromachines*, 12(2):122, 2021.

[41] Peter Vandenabeele. Raman Instrumentation. In *Practical Raman Spectroscopy: an introduction*, chapter 4, pages 61–100. Wiley, Chichester, UK, 1 edition, 2013.

[42] Minjung Kim, Hoeil Chung, Youngah Woo, and Mark Kemper. New Reliable Raman Collection System using the Wide Area Illumination (WAI) Scheme combined with the Synchronous Intensity Correction Standard for the Analysis of Pharmaceutical Tablets. *Analytica Chimica Acta*, 579(2):209–216, 2006.

[43] Cheng Qu, Yuzhu Li, Shanshan Du, Yuchuang Geng, Mengke Su, and Honglin Liu. Raman Spectroscopy for Rapid Fingerprint Analysis of Meat Quality and Security: Principles, Progress and Prospects. *Food Research International*, 161:111805, 2022.

[44] Darren A. Whitaker and Kevin Hayes. A Simple Algorithm for Despiking Raman Spectra. *Chemometrics and Intelligent Laboratory Systems*, 179:82–84, 2018.

[45] Abraham Savitzky and Marcel J.E. Golay. Smoothing and Differentiation of Data by Simplified Least Squares Procedures. *Analytical Chemistry*, 36(8):1627–1639, 1964.

[46] Paul H.C. Eilers and Hans F.M. Boelens. A Perfect Smoother. *Life Sciences*, 75(14):3631–3636, 2003.

[47] Lin Zhang and Mark J. Henson. A Practical Algorithm to Remove Cosmic Spikes in Raman Imaging Data for Pharmaceutical Applications. *Applied Spectroscopy*, 61(9):1015–1020, 2007.

[48] Sheng Li and Liankui Dai. An Improved Algorithm to Remove Cosmic Spikes in Raman Spectra for Online Monitoring. *Applied Spectroscopy*, 65(11):1300–1306, 2011.

[49] Oleg Ryabchykov, Thomas Bocklitz, Anuradha Ramoji, Ute Neugebauer, Martin Foerster, Claus Kroegel, Michael Bauer, Michael Kiehntopf, and Juergen Popp. Automatization of Spike Correction in Raman Spectra of Biological Samples. *Chemometrics and Intelligent Laboratory Systems*, 155:1–6, 2016.

[50] Yao Tian and Kenneth S. Burch. Automatic Spike Removal Algorithm for Raman Spectra. *Applied Spectroscopy*, 70(11):1861–1871, 2016.

[51] Boris Iglewicz and David C. Hoaglin. Outlier Labeling. In Edward F. Mykytka, editor, *Volume 16: How to Detect and Handle Outliers*, pages 9–13, Milwaukee, Wisconsin, 1993. ASQC Quality Press.

[52] Sergey Mozharov, Alison Nordon, David Littlejohn, and Brian Marquardt. Automated Cosmic Spike Filter Optimized for Process Raman Spectroscopy. *Applied Spectroscopy*, 66(11):1326–1333, 2012.

[53] Sinead J. Barton, Tomas E. Ward, and Bryan M. Hennelly. Algorithm for Optimal Denoising of Raman Spectra. *Analytical Methods*, 10(30):3759–3769, 2018.

[54] W.J. Tompkins and J.G. Webster. Design of Microcomputer-based Medical Instrumentation. Englewood Cliffs, NJ, 1981. Prentice Hall.

[55] R.J. Barnes, M.S. Dhanoa, and Susan J. Lister. Standard Normal Variate Transformation and De-Trending of Near-Infrared Diffuse Reflectance Spectra. *Applied Spectroscopy*, 43(5):772–777, 1989.

[56] Harald Martens and Edward Stark. Extended Multiplicative Signal Correction and Spectral Interference Subtraction: New Preprocessing Methods for Near Infrared Spectroscopy. *Journal of Pharmaceutical and Biomedical Analysis*, 9(8):625–635, 1991.

[57] Kristian Hovde Liland, Achim Kohler, and Nils Kristian Afseth. Model-based Pre-processing in Raman Spectroscopy of Biological Samples. *Journal of Raman Spectroscopy*, 47(6):643–650, 2016.

[58] Johanne Heitmann Solheim, Boris Zimmermann, Valeria Tafintseva, Simona Dzurendová, Volha Shapaval, and Achim Kohler. The Use of Constituent Spectra and Weighting in Extended Multiplicative Signal Correction in Infrared Spectroscopy. *Molecules*, 27(6):1900, 2022.

[59] Sabrina Diehn, Boris Zimmermann, Valeria Tafintseva, Murat Bağcıoğlu, Achim Kohler, Mikael Ohlson, Siri Fjellheim, and Janina Kneipp. Discrimination of Grass Pollen of Different Species by FTIR Spectroscopy of Individual Pollen Grains. *Analytical and Bioanalytical Chemistry*, 412(24):6459–6474, sep 2020.

[60] Mads Sylvest Bergholt, Shiyamala Duraipandian, Wei Zheng, and Zhiwei Huang. Multivariate Reference Technique for Quantitative Analysis of Fiber-Optic Tissue Raman Spectroscopy. *Analytical Chemistry*, 85(23):11297–11303, 2013.

[61] Ryan N. Favors, Yanan Jiang, Yvette L. Loethen, and Dor Ben-Amotz. External Raman standard for Absolute Intensity and Concentration Measurements. *Review of Scientific Instruments*, 76(3), 2005.

[62] Åke Björck and Ulf G. Indahl. Fast and Stable Partial Least Squares Modelling: A Benchmark Study with Theoretical Comments. *Journal of Chemometrics*, 31(8), 2017.

[63] Tormod Næs, Tomas Isaksson, Tom Fearn, and Tony Davies. Multicollinearity and the Need for Data Compression. In *Multivariate Calibration and Classification*, chapter 4, pages 19–25. NIR Publications, Chichester, UK, 2004.

[64] S. Wold, A. Ruhe, H. Wold, and W. J. Dunn, III. The Collinearity Problem in Linear Regression. The Partial Least Squares (PLS) Approach to Generalized Inverses. *SIAM Journal on Scientific and Statistical Computing*, 5(3):735–743, 1984.

[65] Martin Andersson. A Comparison of Nine PLS1 Algorithms. *Journal of Chemometrics*, 23(10):518–529, 2009.

[66] Ulf G. Indahl. The Geometry of PLS1 Explained Properly: 10 Key Notes on Mathematical Properties of and Some Alternative Algorithmic Approaches to PLS1 Modelling. *Journal of Chemometrics*, 28(3):168–180, 2014.

[67] Ulf G. Indahl and Tormod Næs. Evaluation of Alternative Spectral Feature Extraction Methods of Textural Images for Multivariate Modelling. *Journal of Chemometrics*, 12(4):261–278, 1998.

[68] Paula Manuela de Castro Cardoso Pereira and Ana Filipa dos Reis Baltazar Vicente. Meat nutritional composition and nutritive role in the human diet. *Meat Science*, 93(3):586–592, 2013.

[69] Turid Mørkøre and Kjell-Arne Rørvik. Seasonal Variations in Growth, Feed Utilisation and Product Quality of Farmed Atlantic Salmon (Salmo Salar) Transferred to Seawater as 0+Smolts or 1+Smolts. *Aquaculture*, 199(1-2):145–157, 2001.

[70] R.A. Field. Ash and Calcium as Measures of Bone in Meat and Bone Mixtures. *Meat Science*, 55(3):255–264, 2000.

[71] EFSA. Scientific Opinion on the Public Health Risks Related to Mechanically Separated Meat (MSM) derived from Poultry and Swine. *EFSA Journal*, 11(3), 2013.

[72] Ralston A. Lawrie. *Lawrie's Meat Science*. Woodhead Publishing, Cambridge, England, 1998.

[73] Zi Mian Wang, Richard N. Pierson, and Steven B. Heymsfield. The Five-level Model: A New Approach to Organizing Body-Composition Research. *The American Journal of Clinical Nutrition*, 56(1):19–28, 1992.

[74] W.S. Snyder, M.J. Cook, E.S. Nasset, L.R. Karhausen, G.P. Howells, and I.H. Tipton. Report of the Task Group on Reference Man ICRP Publication 23 (1975). *Annals of the ICRP*, 4(3-4), 1980.

[75] Philip Calder. Marine Omega-3 Fatty Acids and Inflammatory Processes: Effects, Mechanisms and Clinical Relevance, 2015.

[76] A. Eilander, D.C. Hundscheid, S.J. Osendarp, C. Transler, and P.L. Zock. Effects of n-3 Long Chain Polyunsaturated Fatty Acid Supplementation on Visual and Cognitive Development Throughout Childhood: A Review of Human Studies. *Prostaglandins Leukotrienes and Essential Fatty Acids*, 76(4):189–203, 2007.

[77] Marcelo Rogero and Philip Calder. Obesity, Inflammation, Toll-Like Receptor 4 and Fatty Acids, 2018.

[78] C.H.S. Ruxton, S.C. Reed, M.J.A. Simpson, and K.J. Millington. The Health Benefits of Omega-3 Polyunsaturated Fatty Acids: A Review of the Evidence. *Journal of Human Nutrition and Dietetics*, 17(5):449–459, 2004.

[79] Rohith N. Thota, Jessica J.A. Ferguson, Kylie A. Abbott, Cintia B. Dias, and Manohar L. Garg. Science Behind the Cardio-Metabolic Benefits of Omega-3 Polyunsaturated Fatty Acids: Biochemical Effects vs . Clinical Outcomes, 2018.

[80] Xu Feng. Chemical and Biochemical Basis of Cell-Bone Matrix Interaction in Health and Disease. *Current Chemical Biology*, 3(2):189–196, 2009.

[81] Matthew D. Shoulders and Ronald T. Raines. Collagen Structure and Stability. *Annual Review of Biochemistry*, 78(1):929–958, 2009.

[82] A. Rygula, K. Majzner, K.M. Marzec, A. Kaczor, M. Pilarczyk, and M. Baranska. Raman Spectroscopy of Proteins: A Review. *Journal of Raman Spectroscopy*, 44(8):1061–1076, 2013.

[83] Ivan Stoilov, Barry C. Starcher, Robert P. Mecham, and Thomas J. Broekelmann. Measurement of Elastin, Collagen, and Total Protein Levels in Tissues. In Robert P Mecham, editor, *Methods in Extracellular Matrix Biology*, volume 143 of *Methods in Cell Biology*, chapter 7, pages 133–146. Academic Press, 2018.

[84] Ana M. Herrero. Raman Spectroscopy a Promising Technique for Quality Assessment of Meat and Fish: A Review. *Food Chemistry*, 107(4):1642–1651, 2008.

[85] Danting Yang and Yibin Ying. Applications of Raman Spectroscopy in Agricultural Products and Food Analysis: A Review. *Applied Spectroscopy Reviews*, 46(7):539–560, 2011.

[86] Huaizhou Jin, Qipeng Lu, Xingdan Chen, Haiquan Ding, Hongzhi Gao, and Shangzhong Jin. The Use of Raman Spectroscopy in Food Processes: A Review. *Applied Spectroscopy Reviews*, 51(1):12–22, 2016.

[87] Marlen Petersen, Zhilong Yu, and Xiaonan Lu. Application of Raman Spectroscopic Methods in Food Safety: A Review. *Biosensors*, 11(6):187, 2021.

[88] Jun-ichi Hikima, Masahiro Ando, Hiro-o Hamaguchi, Masahiro Sakai, Masashi Maita, Kazunaga Yazawa, Haruko Takeyama, and Takashi Aoki. On-site Direct Detection of Astaxanthin from Salmon Fillet Using Raman Spectroscopy. *Marine Biotechnology*, 19(2):157–163, 2017.

[89] Olga Monago-Maraña, Carl Emil Eskildsen, Nils Kristian Afseth, Teresa Galeano-Díaz, Arsenio Muñoz de la Peña, and Jens Petter Wold. Non-destructive Raman Spectroscopy as a Tool for Measuring ASTA Color Values and Sudan I Content in Paprika Powder. *Food Chemistry*, 274:187–193, 2019.

[90] Roger M. Jarvis and Royston Goodacre. Characterisation and Identification of Bacteria using SERS. *Chemical Society Reviews*, 37(5):931, 2008.

[91] Blair D. Johnston, Tessa M. Scown, Julian Moger, Susan A. Cumberland, Mohamed Baalousha, Kathryn Linge, Ronny van Aerle, Kym Jarvis, Jamie R. Lead, and Charles R. Tyler. Bioavailability of Nanoscale Metal Oxides TiO2 , CeO2 , and ZnO to Fish. *Environmental Science Technology*, 44(3):1144–1151, 2010.

[92] Nils Kristian Afseth, Matthew Bloomfield, Jens Petter Wold, and Pavel Matousek. A Novel Approach for Subsurface Through-Skin Analysis of Salmon using Spatially Offset Raman Spectroscopy (SORS). *Applied Spectroscopy*, 68(2):255–262, 2014.

[93] Marijana Todorčević and Leanne Hodson. The Effect of Marine Derived n-3 Fatty Acids on Adipose Tissue Metabolism and Function, 2015.

[94] Amita Devi and B.S. Khatkar. Physicochemical, Rheological and Functional Properties of Fats and Oils in Relation to Cookie Quality: A Review. *Journal of Food Science and Technology*, 53(10):3633–3641, 2016.

[95] Michael Yemane Bekhit, Bjørn Grung, and Svein Are Mjøs. Determination of Omega-3 Fatty Acids in Fish Oil Supplements using Vibrational Spectroscopy and Chemometric Methods. *Applied Spectroscopy*, 68(10):1190–1200, 2014.

[96] N. K. Afseth, V. H. Segtnan, B. J. Marquardt, and J. P. Wold. Raman and Near-Infrared Spectroscopy for Quantification of Fat Composition in a Complex Food Model System. *Applied Spectroscopy*, 59(11):1324–1332, 2005.

[97] Daniel P. Killeen, Susan N. Marshall, Elaine J. Burgess, Keith C. Gordon, and Nigel B. Perry. Raman Spectroscopy of Fish Oil Capsules: Polyunsaturated Fatty Acid Quantitation Plus Detection of Ethyl Esters and Oxidation. *Journal of Agricultural and Food Chemistry*, 65(17):3551–3558, 2017.

[98] J. Renwick Beattie, Steven E.J. Bell, Claus Borgaard, Ann Fearon, and Bruce W. Moss. Prediction of Adipose Tissue Composition using Raman Spectroscopy: Average Properties and Individual Fatty Acids. *Lipids*, 41(3):287–294, 2006.

[99] John J. Freeman, David O. Fisher, and Gregory J. Gervasio. FT-Raman On-Line Analysis of PCI3 Reactor Material. *Applied Spectroscopy*, 47(8):1115–1122, 1993.

[100] Richard J. Hart, Nicholas I. Pedge, Alan R. Steven, and Kevin Sutcliffe. In Situ Monitoring of a Heterogeneous Etherification Reaction using Quantitative Raman Spectroscopy. *Organic Process Research Development*, 19(1):196–202, 2015.

[101] Stephen Craven, Jessica Whelan, and Brian Glennon. Glucose Concentration Control of a Fed-batch Mammalian Cell Bioprocess using a Nonlinear Model Predictive Controller. *Journal of Process Control*, 24(4):344–357, 2014.

[102] Rui Hu, Ting He, Zhaowei Zhang, Yunhuang Yang, and Maili Liu. Safety Analysis of Edible Oil Products via Raman Spectroscopy. *Talanta*, 191:324–332, 2019.

[103] Haibo Huang, Haiyan Yu, Huirong Xu, and Yibin Ying. Near Infrared Spectroscopy for On/In-line Monitoring of Quality in Foods and Beverages: A Review. *Journal of Food Engineering*, 87(3):303–313, 2008.

[104] Jan U. Porep, Dietmar R. Kammerer, and Reinhold Carle. On-line Application of Near Infrared (NIR) Spectroscopy in Food Production. *Trends in Food Science Technology*, 46(2):211–230, 2015.

[105] Jens Petter Wold, Eva Veiseth-Kent, Vibeke Høst, and Atle Løvland. Rapid On-line Detection and Grading of Wooden Breast Myopathy in Chicken Fillets by Near-Infrared Spectroscopy. *PLOS ONE*, 12(3), 2017.

[106] Carl Emil Eskildsen, Tormod Næs, Peter B. Skou, Lars Erik Solberg, Katinka R. Dankel, Silje A. Basmoen, Jens Petter Wold, Siri S. Horn, Borghild Hillestad, Nina A. Poulsen, Mette Christensen, Theo Pieper, Nils Kristian Afseth, and Søren B. Engelsen. Cage of Covariance in Calibration Modeling: Regressing Multiple and Strongly Correlated Response Variables onto a Low Rank Subspace of Explanatory Variables. *Chemometrics and Intelligent Laboratory Systems*, 213, 2021.

[107] Erik Tengstrand, Tiril Aurora Lintvedt, Petter Vejle Andersen, Lars Erik Solberg, Jens Petter Wold, and Nils Kristian Afseth. Calibration Transfer of Near-Infrared and Raman Models Without using Transfer Samples. In *Chemometrics in Analytical Chemistry Conference*, Rome, 2022.

[108] Peter J. Larkin, Matthew Santangelo, and Slobodan Šašič. Internal Multiple-Scattering Hole-Enhanced Raman Spectroscopy: Improved Backscattering Fourier Transform Raman Sampling in Pharmaceutical Tablets Utilizing Cylindrical–Conical Holes. *Applied Spectroscopy*, 66(8):892–902, 2012.

[109] Ilkka Nissinen, Jan Nissinen, Pekka Keränen, and Juha Kostamovaara. On the Effects of the Time Gate Position and Width on the Signal-to-Noise Ratio for Detection of Raman Spectrum in a Time-gated CMOS Single-Photon Avalanche Diode Based Sensor. *Sensors and Actuators B: Chemical*, 241:1145–1152, 2017.

[110] Paul Coffey, Nick Smith, Barry Lennox, Gerben Kijne, Bob Bowen, Adrian Davis-Johnston, and Philip A. Martin. Robotic Arm Material Characterisation using LIBS and Raman in a Nuclear Hot Cell Decommissioning Environment. *Journal of Hazardous Materials*, 412, 2021.

[111] Praveen C. Ashok, Mario E. Giardini, Kishan Dholakia, and Wilson Sibbett. A Raman Spectroscopy Bio-Sensor for Tissue Discrimination in Surgical Robotics. *Journal of Biophotonics*, 7(1-2):103–109, 2014.

[112] Michael Pinto, Kevin C. Zorn, Jean-Philippe Tremblay, Joannie Desroches, Frédérick Dallaire, Kelly Aubertin, Eric Marple, Chris Kent, Frederic Leblond, Dominique Trudel, and Frederic Lesage. Integration of a Raman Spectroscopy System to a Robotic-Assisted Surgical System for Real-Time Tissue Characterization during Radical Prostatectomy Procedures. *Journal of Biomedical Optics*, 24(2):1, 2019.

Appendix A

Paper I

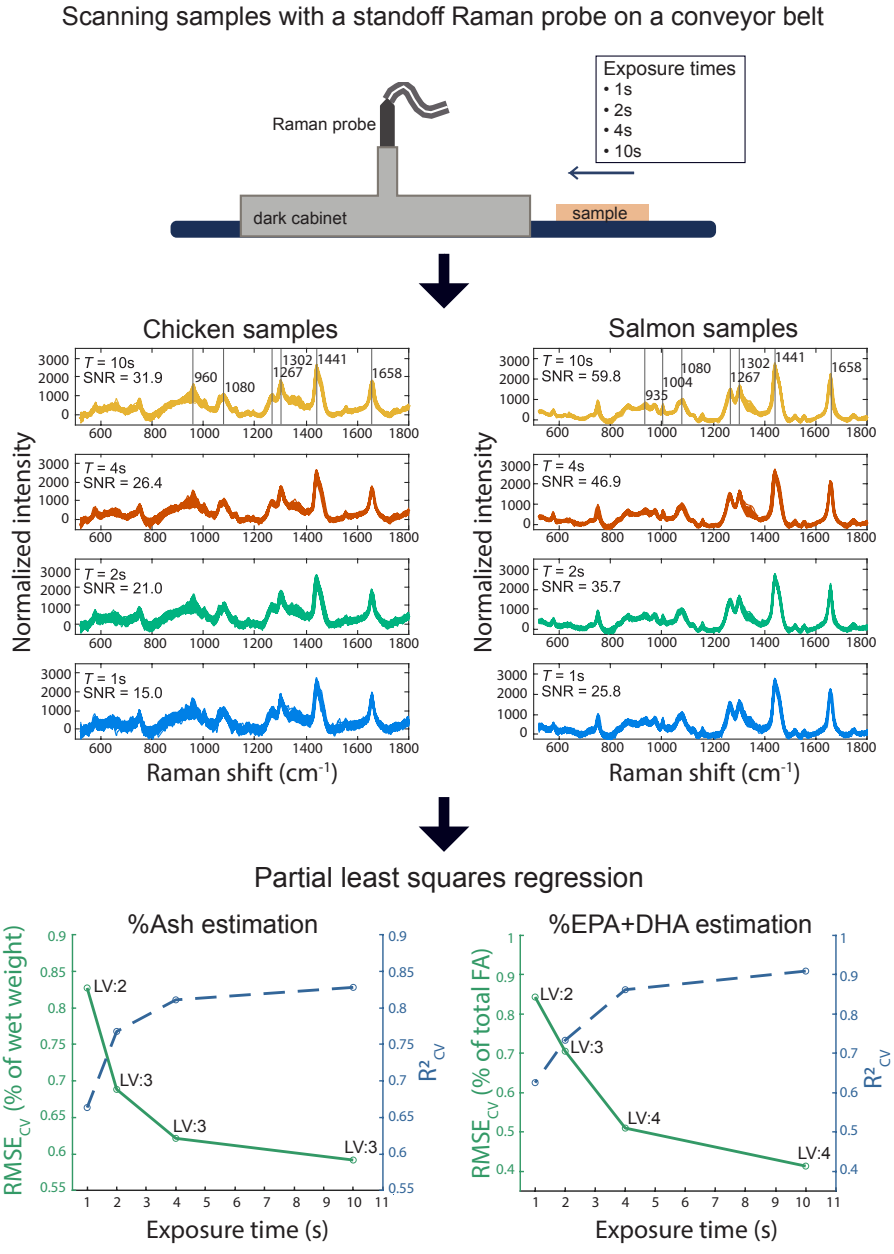

Submitted Paper

Applied Spectroscopy

Applied Spectroscopy
2022, Vol. 76(5) 559–568

DOI: 10.1177/00037028211056931
journals.sagepub.com/home/asp
SAGE

Feasibility of In-Line Raman Spectroscopy for Quality Assessment in Food Industry: How Fast Can We Go?

Tiril Aurora Lintvedt[1], Petter V. Andersen[1], Nils Kristian Afseth[1], Brian Marquardt[2], Lars Gidskehaug[3], and Jens Petter Wold[1]

Abstract

Raman spectroscopy is a viable tool within process analytical technologies due to recent technological advances. In this article, we evaluate the feasibility of Raman spectroscopy for in-line applications in the food industry by estimating the concentration of the fatty acids EPA + DHA in ground salmon samples (n = 63) and residual bone concentration in samples of mechanically recovered ground chicken (n = 66). The samples were measured under industry like conditions: They moved on a conveyor belt through a dark cabinet where they were scanned with a wide area illumination standoff Raman probe. Such a setup should be able to handle relevant industrial conveyor belt speeds, and it was studied how different speeds (i.e., exposure times) influenced the signal-to-noise ratio (SNR) of the Raman spectra as well as the corresponding model performance. For all samples we applied speeds that resulted in 1 s, 2 s, 4 s, and 10 s exposure times. Samples were scanned in both heterogenous and homogenous state. The slowest speed (10 s exposure) yielded prediction errors (RMSECV) of 0.41%EPA + DHA and 0.59% ash for the salmon and chicken data sets, respectively. The more in-line relevant exposure time of 1 s resulted in increased RMSECV values, 0.84% EPA + DHA and 0.84% ash, respectively. The increase in prediction error correlated closely with the decrease in SNR. Further improvements of model performance were possible through different noise reduction strategies. Model performance for homogenous and heterogenous samples was similar, suggesting that the presented Raman scanning approach has the potential to work well also on intact heterogenous foods. The estimation errors obtained at these high speeds are likely acceptable for industrial use, but successful strategies to increase SNR will be key for widespread in-line use in the food industry.

Keywords

Raman spectroscopy, process analytical technology, PAT, in-line food evaluation, representative sampling, omega-3 fatty acids, bone content

Date received: 20 July 2021; revised: 10 September 2021; accepted: 26 September 2022

Introduction

According to the United Nations, the percentage of food lost after harvesting and during transport, storage and processing is estimated to be 13.8% globally.[1] It is suggested that the production costs could be lowered and the efficiency of food systems increased if targeted interventions at critical stages of the value chain are implemented. Detailed in-line spectroscopic measurements of food raw materials can provide means for increased raw material utilization and ensuring stable product quality. Previously, several applications of near-infrared spectroscopy (NIRS) for evaluation of food products in the industry have been successfully realized, for example, rapid determination of edible meat content in crabs,[2] in-line fat distribution analysis of salmon fillets[3] and detection of woody breast syndrome in chicken fillets.[4] However, NIRS has limitations in chemical resolution because absorptions originate from overtones and combination modes which overlap intricately.[5] In situations where higher chemical specificity is needed, one option is to use Raman spectroscopy, which is based on

[1]Nofima AS, TromsØ, Norway
[2]MarqMetrix Inc, Seattle, WA, USA
[3]Aspen Technology Inc, Oslo, Norway

Corresponding author:
Tiril Aurora Lintvedt, Faculty of Science and Technology, NMBU, Nofima—Norwegian Institute for Food, Fisheries, and Aquaculture Research, Muninbakken 9-13, Breivika, Tromsø 9291, Norway.
Email: tiril.lintvedt@nofima.no

fundamental transitions and do not suffer from overlapping bands to the same extent. This can for instance be seen in spectra of fish oil as shown by Bekhit et al.[6] Raman spectroscopy is becoming a viable tool within process analytics due to recent technological advances. Low-cost Raman instruments are available and instrumental advances provide a new degree of versatility. The potential of in-line Raman applications have been demonstrated in several areas, such as in the pharmaceutical and bioprocessing domain, as reviewed by Esmonde-White et al.[7] However, the literature on Raman spectroscopy for in-line food evaluation is scarce, although the possibilities within the food industry are undoubtedly many. In addition, the existing studies on Raman-based strategies for reaction monitoring and control is often based on analysis of continuous and homogenous sample streams, while reported studies on in-line evaluation of single products moving along a conveyor belt is to a huge part lacking. The latter situation is frequently encountered in the food industry.

A prerequisite for in-line Raman applications is proper and representative optical sampling tools, and a development of particular interest in this respect is wide area illumination probes. This approach utilizes a defocused laser combined with multiple collection fibers, resulting in larger measurement areas and insensitivity to smaller variations in working distance.[8] This optical setup is suitable for measurements of food samples in a surface scanning mode. Recent work[9–12] demonstrates the potential for a surface scanning setup for food evaluation. Andersen et al. showed the applicability of Raman spectroscopy for bulk composition analysis of heterogenous foods. However, they used rather long exposure times ranging from 60 s to 80 s and pointed out that sampling speed could be a limitation for applications where single samples need to be analyzed in real-time. In other applications, Raman spectroscopy may give satisfactory measurements within milliseconds given the adequate laser power. In contrast, foods often have low Raman signals and may be damaged by exposure to higher laser powers, making in-line food applications more challenging.

One potential in-line application in the food industry is the evaluation of ground meat from the mechanical deboning process of rest-raw material of chicken, where remaining meat on the carcasses after filleting is separated from the bones. Perfect separation of bone and meat is not achieved, and the content of finely ground bone in the meat fraction is regulated.[13] In-line monitoring and control of the bone concentration is yet to be implemented, but Wubshet et al.[10] recently showed that Raman spectroscopy potentially could be used to quantify bone contents in these samples. Another relevant application is in-line determination of omega-3 fatty acids in salmon. Due to reported health effects, fatty acid composition is an important quality parameter in the market. NIRS has been successfully used for determination of total fat content in whole salmon fillets[14] and estimation of omega-3 fatty acids in pure fish oils is promising.[15,6] Brown et al.[16] reported that eicosapentaenoic acid (EPA) and docosahexaenoic acid (DHA) could be determined in salmon by NIR spectroscopy, but their calibration were less successful for intact salmon cutlets than for minced salmon and they suggest that the obtained performances are acceptable for rough approximation only. In addition, it is not clear whether the calibrations relied on measurements of the actual fatty acids or just a covariation with total fat as discussed by Eskildsen et al.[17] Raman spectroscopy is a promising tool for compositional analysis of fatty acids,[18–21] and in-line determination of omega-3 fatty acids in fillets can expand the opportunities for product differentiation. Furthermore, the implementation of such a spectroscopic sorting system on an industrial basis can provide the means for a rapid and affordable mapping of how feeding regimes affect the final fatty acid composition in the fish.

The main aim of this work was to evaluate the feasibility of Raman spectroscopy for in-line evaluation of complex foods, and to elucidate how fast a product can pass by on the conveyor belt while still obtaining a spectrum of sufficient signal-to-noise ratio (SNR) and acceptable modeling errors. This was investigated for sample sets based on (i) chicken rest-raw material from the mechanical deboning process and (ii) ground salmon belly trims. We used an industry relevant setup, applying the surface scanning strategy on samples moving along a conveyor belt. As food samples in general are heterogenous, we also aimed to confirm that the heterogeneity of the sample surface is not necessarily a limitation for a Raman scanning system. We did this by comparing prediction performance on heterogenous and homogenous versions of the same samples.

Material and methods

Raw Materials

Chicken Samples. Chicken samples came from a mechanical deboning process of rest-raw material of chicken. In this process, the remaining meat on the carcasses after filleting is separated from the bone fragments, resulting in two fractions: The mechanically deboned meat (MDM), containing mostly meat, and the mechanical deboning residues (MDR) containing mostly bone. Batches of MDM and MDR were provided by a poultry processing plant (Bioco, Nortura Hrland, Norway) and subsequently frozen. The batches were then ground in frozen state and used to make five different base blends with different bone concentrations. These blends were made by mixing ground MDM and MDR in different ratios, according to the following shares

A : 100%MDR
B : 20%MDM + 80%MDR
C : 50%MDM + 50%MDR
D : 80%MDM + 20%MDR
E : 100%MDM

Each sample was then made by combining four sub-samples of the available base blends A–E into the positions 1–4 in different arrangements in a rectangular sample holder (30 cm × 3 cm) as indicated in Fig. 1. This sample arrangement

was scanned with the Raman system. The aim of the arrangements was to create samples with different bone concentrations and varying heterogeneity. The bone content typically covaries with fat content in this kind of material. To reduce this correlation and to avoid overoptimistic modeling results, a fat-rich sub-sample (ground chicken skin) of varying size was added randomly to each sample (Fig. 1). A total of 66 different samples were made, spanning a realistic range of bone content. The samples were first measured as heterogenous compositions of base blends, then homogenized (Retsch Knife Mill Grindomix GM 200, 7000 rpm for 6 s twice with a stir in between) and measured again in the same sample holder. Five samples which consisted of only one base blend were not homogenized. The samples were made consecutively and the base blends were kept in a cold room (−1 °C–0 °C) throughout the whole experiment. Smaller portions of the blends were taken out to the experiment room (room temperature) at a time, to reduce possible temperature effects.

Salmon Samples. The samples were based on homogenized belly trims from 52 salmons acquired from three farming locations. Different feeding regimes were used on the different farming locations. Before homogenization (Retsch Knife Mill Grindomix GM 200, 7000 rpm for 3 s), the bellies were stored at (−1 °C–0 °C) to prevent liquid loss and lipid oxidation. The target for these samples was the concentration of omega-3 fatty acids EPA and DHA. To obtain an even distribution of fatty acid concentration in the sample set, 11 additional samples were made of 50/50 combination of two samples of the original set of 52. Those two sub-samples were placed side by side in the sample holder (Fig. 1). The total number of samples was then 63.

Reference Measurements

Reference analyses of the chicken samples were carried out by an external laboratory (ALS Laboratory Group, Oslo, Norway). Measurements for ash concentration (percent of wet weight) were carried out by gravimetric analysis (BS 4401 Part 1 1998 Commision Regulation (EC) 152/2009 MU 6,5%), and reference measurements for fat concentration (percent of wet weight) were carried out using pulsed nuclear magnetic resonance (NMR) analysis (MU 6.5%). Analyses of the salmon samples were carried out by BioLab (Bergen, Norway). Measurements of EPA and DHA concentration applied the reference standard AOCS Ce 1b-89 (methyl esterification capillary gas chromatography with a flame ionization detector or GC-FID), and was expressed as a percentage of the total amount of fatty acids (FA) in the analyzed sample. For all reference analyses the mean of two parallel sample measurements was reported.

Measurements and Data Analysis

Raman Measurements. For spectral acquisition, we employed a MarqMetrix all-in-one (AIO) Raman system equipped with a 785 nm laser operating at 450 mW power. The sampling optic used with the AIO was a wide area illumination (D = 3 mm), Proximal BallProbe HV standoff Raman probe with optimal working distance 8–10 cm (MarqMetrix Inc., Seattle, WA, USA). The probe was placed inside a tube structure in a dark cabinet on a conveyor belt, as shown in Fig. 2. The tube structure was perfectly fitted around the probe. The dark cabinet, designed for reducing ambient light, was a steel cabinet of 100 cm length and 5.2 cm height with black coating inside. For each measurement the Raman laser and signal acquisition were activated by a trigger system which relied on a laser sensor (CMOS laser sensor LR-ZB90CB from Keyence) for detection of a block placed beside the sample on the belt.

Each sample was placed on a plate covered with aluminum foil. The foil was used to prevent disturbing signals from the plastic conveyor belt upon potential imperfect sample triggering. Samples were passed through the dark cabinet and scanned at belt speeds 0.3 m/s, 0.15 m/s, 0.075 m/s, and 0.03 m/s. Corresponding exposure times were 1 s, 2 s, 4 s, and 10 s, respectively. The belt speed was tuned and controlled by using a contact tachometer (Tachometer PCE-DT 65 from PCE Instruments). Two technical replicates were measured for all samples and exposure times. Homogenized chicken samples were measured only for 2 s and 10 s exposures, for comparison with measurements on the corresponding heterogenous samples. Salmon samples were measured only in homogenized version, except for the 11 additional combination samples which were measured only in heterogenous state.

Pre-Processing.Chicken and salmon spectra were pre-processed using Savitzky–Golay (SG) smoothing (polynomial

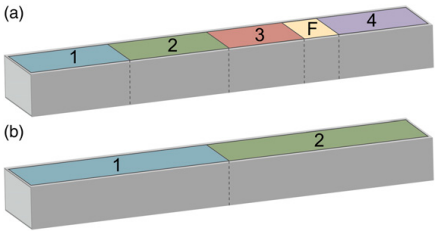

Figure 1. Sample composition scheme for chicken (a) and the 11 salmon combination samples (b). A fat-rich species F of varying size was placed at a random position in the chicken samples.

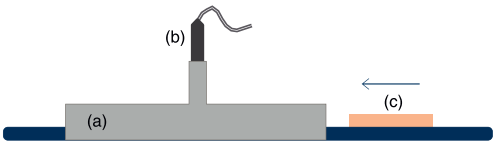

Figure 2. Spectrum acquisition setup consisting of a dark cabinet (a), wide area illumination standoff Raman probe (b) and a moving sample (c) on a conveyor belt.

order 2 and window size 9)[22] followed by extended multiplicative signal correction (EMSC)[23,24] employing up to the sixth order polynomial and the asymmetric least squares (ALS) algorithm[25,26] for baseline correction of the EMSC reference spectrum. The ALS reference spectrum correction employed a smoothing parameter of 5.8 (λ) and an asymmetric weighting parameter (of the residuals) of 0.01 (p). Pre-processing was applied on the full data sets, including all exposure times. Subsequently, the data sets were organized into separate exposure time subsets for data modeling.

Data Modeling. The Raman shift range 520 cm^{-1}–1800 cm^{-1} was utilized in the data modeling for both data sets. Partial least squares regression (PLSR)[27,28] was used for calibration development. We established models for ash concentration in chicken samples (proxy for bone content) and EPA + DHA concentration for salmon samples. Note that EPA and DHA concentrations were not estimated separately, but as a joint concentration value. The PLSR models were validated by cross-validation (CV) where replicate measurements were held out in the same segment to avoid overfitting. The reason for not averaging the replicates was to keep the prediction conditions as close to an in-line situation as possible. The choice of number of latent variables for the PLS modeling was based on a simple criterion using a 3% punish factor, as described by Westad and Martens.[29] Noise reduction and improvement in the model performance was attempted for the shorter exposure time subsets (4 s, 2 s, and 1 s) through variable selection employing the significance multivariate correlation (sMC) method.[30] For selection of variables in the 1 s exposure data, we applied sMC on the 2 s exposure data, and for selection of variables in the 2 s exposure data, sMC on the 4 s exposure data was used, and so on. This was to avoid overfitting. The results were compared with the corresponding calibrations based on the full spectrum (642 channels). Another method we investigated for noise reduction was averaging of in-line replicates. To evaluate this strategy, cross-validated PLSR models were obtained for three versions of the exposure time subsets; one version where the two spectrum replicates were averaged, one where replicate number 1 was selected as a representative for each sample and one where replicate number 2 was selected as a representative for each sample. We report the average performance of the two single-replicate versions as a representative for a single-measurement system.

The chicken samples were used to compare the performance of regression models on heterogenous samples versus homogenous samples. This comparison was conducted with CVANOVA,[31–33] a two-way analysis of variance (ANOVA) of cross-validation errors. In total five samples which consisted of only one base blend were excluded from this analysis, since these were not homogenized. The ANOVA was carried out in Python version 3.7, Anaconda3 distribution (Anaconda, Austin, TX). All other data analysis was carried out in Matlab version R2020a (The MathWorks, Natick, MA). The data that support the findings of this study are available from the corresponding author, upon reasonable request.

Signal-to-Noise Ratio. Calculation of SNR was based on the ratio between the average spectrum intensity and the standard deviation of the estimated noise, similar to Guo et al.[34] An SNR value was calculated for each spectrum using Eq. 1.

$$\mathrm{SNR} = \frac{mean(I)}{sd(I_n)} \quad (1)$$

where I is the spectrum intensity and I_n is the estimated noise intensity. Noise was estimated as the difference between the spectrum and the smoothed version of the same spectrum, using SG with polynomial order 2 and window size 9. The SNR was compared across exposure times and data sets, and we have reported the average SNR of each exposure time subset (pre-processed versions).

Results and Discussion

Spectral Data

Figure 3 shows that there was a more prominent fluorescence background in the chicken spectra compared to the salmon spectra. This was expected since bone matrices are prone to fluoresce.[10] The fluorescence naturally increased with higher exposure times. From the pre-processed spectra (Fig. 4), the chemical bands are more easily distinguished. The chicken spectra consist mainly of bands associated with fatty acids (e.g., 1080, 1267, 1302, and 1441 cm^{-1}).[19,20] The peak at 1658 cm^{-1} may be associated with both the Amide I band related to proteins and the olefinic stretch related to fatty acids,[19,20] which overlap. More importantly, another prominent peak at 960 cm^{-1} is associated with phosphate ($\nu_1 PO_4^{3-}$), a well known bone mineral.[10,35] The salmon spectra are dominated by bands associated with fatty acids, similar to the chicken spectra. The most pronounced peaks are located in the region above 1200 cm^{-1}. This includes the bands at 1267 cm^{-1} and 1658 cm^{-1} which may be assigned to the Olefinic hydrogen bend and the Olefinic stretch, respectively, of which both can be related with unsaturated modes.[19,20] Peaks related to saturated modes, that is, at 1302 cm^{-1} and 1441 cm^{-1}, can be assigned to the methylene twisting deformations and the Methylene scissor deformations, respectively.[19,20] In the region below 1200 cm^{-1}, two noticeable peaks are located at 1004 cm^{-1} and 1080 cm^{-1}, which originate from the aromatic ring breathing of phenylalanine, and the liquid aliphatic C–C stretch in gauche, respectively.[19,20] Another important peak at 935 cm^{-1} is most likely related to the alkene C–H deformation in polyunsaturated fatty acid moieties.[36,37]

Implication of Conveyor Belt Speed

Figure 4 shows pre-processed spectra at different exposure times for both sample sets. As indicated, the SNR clearly decreased with higher scanning speed. Note also that the

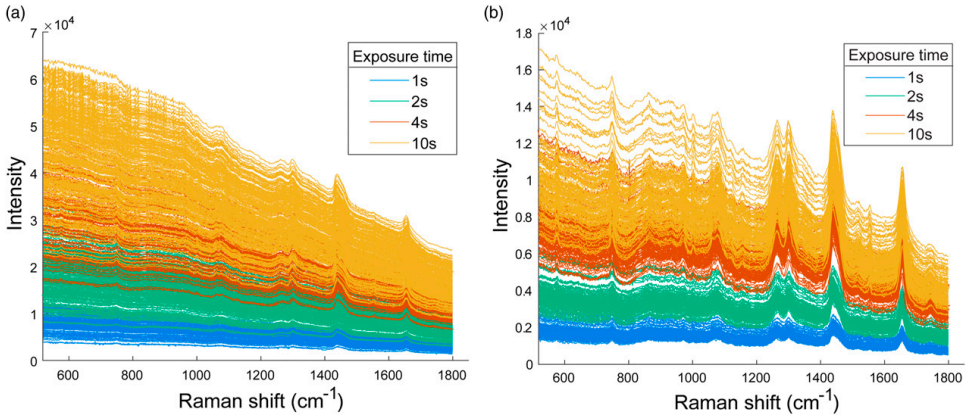

Figure 3. Raw spectra from chicken (a) and salmon samples (b), colored according to exposure time.

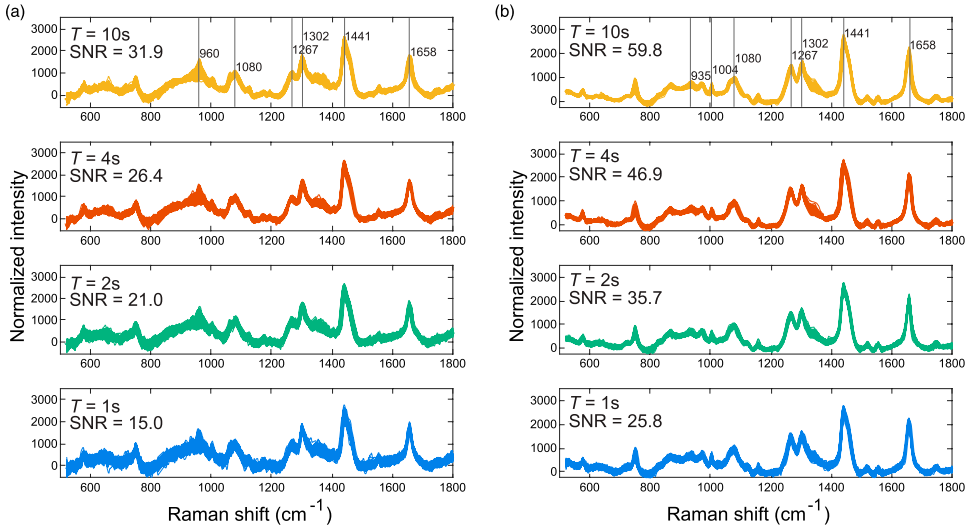

Figure 4. Pre-processed sample spectra from chicken (a) and salmon (b) for all exposure times *T*.

spectra from chicken had considerably lower SNR than those from salmon. Hence, in this context the chicken measurements represent low SNR spectra, while the salmon measurements represent high SNR spectra. The regression results for both sample sets and all exposure times are summarized in Fig. 5 (see additional results in the Supplemental Material). There was a clear trend in performance as function of exposure time for both sample sets, and as expected we obtained higher root mean square errors (RMSECV) for shorter exposure times. This was in essence due to lower SNR, as apparent from the strong negative correlations between these two ($r = -0.96$ for chicken and $r = -0.99$ for salmon). Nevertheless, the models based on different exposure times overall showed the same chemical signatures in the regression vectors (Fig. 6), which was encouraging. Note, however, that as the exposure time decreased, the most pronounced regions in the regression vectors became less weighted.

The exposure time of 10 s was regarded a best case reference and represented a rather slow conveyor belt speed, while the 1–2 s exposure times represented highly relevant conveyor belt speeds. With respect to model performance, there seemed to be a critical exposure time limit around

3 s–4 s. The graphs (Fig. 5) indicate that higher exposure times gave only a marginal increase in performance, while decreasing the exposure time below this limit had a more detrimental effect. Such critical limits will vary depending on the food properties related to Raman scattering cross sections and for different target compounds. For instance, measurements on low fat salmon muscle might increase the critical exposure time limit due to weaker signals and lower SNR. Although the estimation errors obtained at the lower exposure times in these particular cases are close to acceptable for industrial use, the rapid decrease in performance below 3 s–4 s illustrates that it would be a definitive advantage with developments on instrument sensitivity and other efforts on SNR optimization. In spite of the overall higher SNR levels and the same relative decrease in SNR from 4 s to 2 s, there was a more dramatic effect on the model performance for salmon than chicken (Fig. 5). This may be because the %ash model relies mainly on a single peak while the %EPA + DHA model relies on more subtle spectroscopic changes in several peaks, as can be seen from the regression coefficients in Fig. 6. This emphasizes that the critical SNR level in a predictive might system depend on the complexity of the model.

In the closely related work by Wubshet et al.,[10] where a Raman system (standoff probe, 785 nm, spot size 6 mm) was utilized for %ash estimation in similar chicken samples, an RMSECV of 0.63% (of wet weight) was obtained with an accumulation time of 15 s × 4. We obtained a corresponding RMSECV with 4 s exposure, which emphasize that the sampling strategy employed in this study performs very well. Considering that the exposure time was significantly decreased from 10 s to 1 s, the resulting error increase of only 0.2% is promising, also taken into account that the error in the reference measurements of ash concentration was 6.5% of measured value, similar to the modeling error. The reference uncertainty gives a limit for how well our model can perform. However, one should consider in more detail the implication of the exposure time reduction on the model itself. The main observation (Fig. 5) was a decrease in number of latent variables (LVs) going from 2 s to 1 s exposure time, indicating that we lose some information by employing an exposure time of 1 s. The regression vectors in Fig. 6 clearly show that predictions are mainly based on the mineral band at 960 cm^{-1}. Moreover, it can be noted that fat associated peaks are not prominent in the chicken model regression vectors, and the correlation between %fat and %ash reference values ($r = -0.65$) is not critical.

The regression coefficients for the %EPA + DHA models (Fig. 6) show that the main positively correlated peaks are at 935 cm^{-1}, 1264 cm^{-1}, and 1663 cm^{-1}. The first is most likely related to the alkene C–H deformation in polyunsaturated fatty acid moieties.[36,37] The two latter can be associated with other unsaturated modes.[20,19] The main negatively correlated peaks are at 1004 cm^{-1}, 1081 cm^{-1}, 1305 cm^{-1}, and 1443 cm^{-1}, of which the two latter can both be associated with saturated fatty acids.[20,19] In such PLSR models there will always be some uncertainty with respect to indirect modeling on other constituents which co-vary with the analyte, as discussed thoroughly by Eskildsen et al.[17] In this sample set, reference values for %EPA + DHA did not correlate strongly with total polyunsaturated fatty acids ($r = 0.40$), but correlations were more evident with total monounsaturated fatty acids ($r = -0.77$) and total saturated fatty acids ($r = 0.88$). However, peaks associated with unsaturated modes are clearly important for the model. All peaks mentioned above are visible in models based on different exposure times. However, the more subtle details visible in the 10 s exposure model are gradually more compromised with decreasing exposure time. Additionally, the models of exposure times below 4s have a decreasing complexity with respect to number of LVs (Fig. 5). This reinforces the impression that we lose information by decreasing exposure time below the critical exposure time around 3 s–4 s.

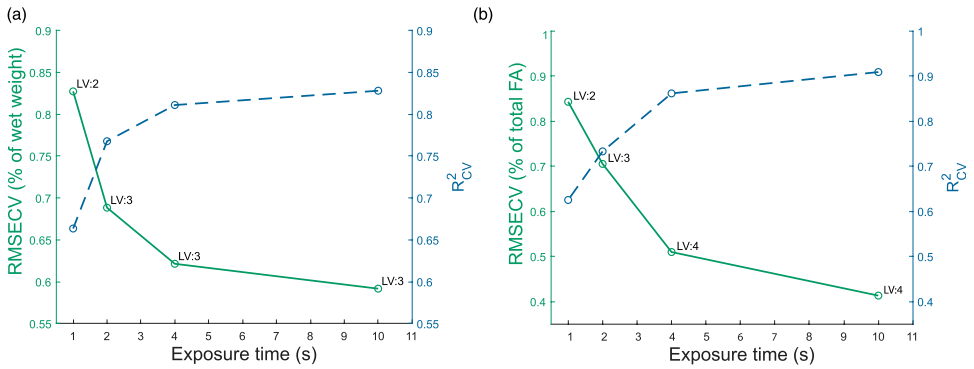

Figure 5. Model performance metrics across different exposure times for ash estimation in chicken (a) and EPA+DHA estimation in salmon (b). We show the RMSECV (solid line) and the coefficient of determination (R^2_{CV} in dashed line). The number of latent variables (LV) employed for each calibration is indicated.

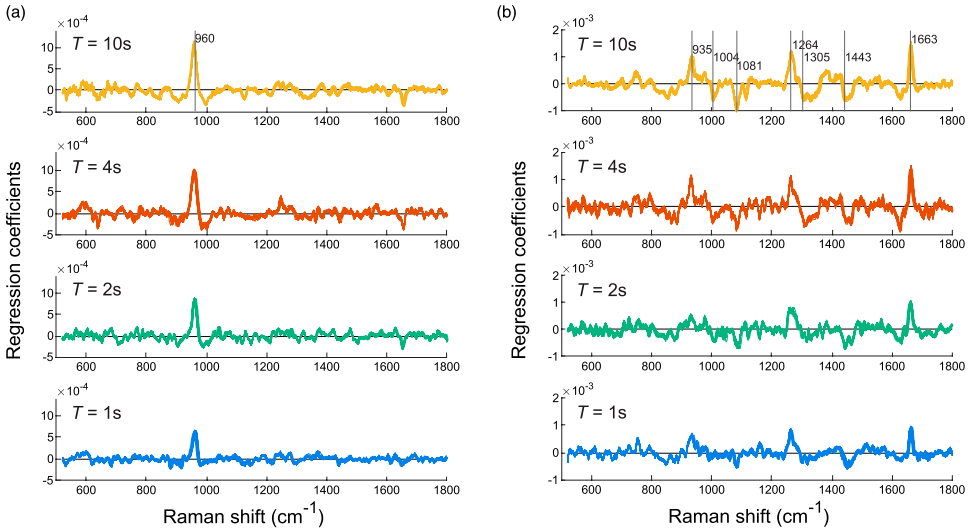

Figure 6. Regression vectors for PLSR models for ash in chicken (a) and EPA+DHA in salmon (b) for all exposure times *T*.

Reduction of Noise

Since SNR is the main limiting factor for model performance, three different strategies for noise reduction were investigated for potential improvement. Variable selection was motivated by the apparently uninformative regions in the regression vectors (Fig. 6) which could possibly contribute with noise. Cross-validated results with applied sMC variable selection are summarized in Table I. The effect on the performance was moderate for 4 s and 2 s exposure times for both chicken and salmon, but resulted in a reduction in number of LVs in the models, which indicate more robust models. For 1 s exposure time, the effect of variable selection on the performance was slightly more pronounced in both chicken and salmon data.

Another possible strategy to increase SNR is to place two instruments in series on the conveyor belt and make predictions based on average spectra. In Table II we compare the average performance based on the two single-replicate versions of the data sets to the replicate-average versions. For both chicken and salmon, the effect of replicate averaging was evident. For chicken, the effect was particularly apparent for 1s exposure time, where the RMSECV decreased by 0.18 %ash. For salmon, the effect was more evenly pronounced across exposure times, with an RMSECV decrease around 0.1 %EPA + DHA for the 1 s–4 s exposures, while the impact for the 10 s exposure was less discernible. Note that in most cases, the effect of replicate averaging was approximately the same as doubling the exposure time for the single-replicate set.

Table I. PLSR results for ash in chicken (% of wet weight) and EPA+DHA in salmon (% of total FA) before and after variable selection.

	Full spectrum		Selected variables		
Exp. time	RMSECV	LV[a]	RMSECV	LV	No. variables[b]
Chicken					
1 s	0.84	2	0.76	2	199
2 s	0.70	3	0.68	2	204
4 s	0.63	3	0.61	2	211
Salmon					
1 s	0.84	2	0.78	2	217
2 s	0.71	3	0.70	2	192
4 s	0.51	4	0.53	2	217

[a]Latent variables.
[b]Number of selected variables.

From another practical perspective, products on the conveyor belt may vary in size and it might be desirable to adjust exposure time according to product size in order to optimize the SNR for each product. To investigate if measurements from different exposure times can be used in the same calibration, we applied the 10 s exposure model on the shorter exposure data (4 s, 2 s, and 1 s) in a cross-validation scheme. Two replicates were held out of all exposure time subsets for each validation segment, where a model was built on the 10 s exposure data and applied on the held out samples of the shorter exposure data. The number of LVs included in the models were predefined as three for %ash

and four for %EPA + DHA estimation. Results are summarized in Table III. The two data sets showed very similar results when basing predictions on the 10 s exposure model as when applying the original cross-validation scheme for the separate exposure time subsets. Thus, it indicates that a model built on 10 s exposure time measurements works just as well for the spectra of 1 s exposure. This demonstrates that smaller variations in exposure time between samples are not critical to the performance of the system. A preprocessing step involving spectral normalization is essential for this approach to work. One practical instrument issue when varying exposure times may be the occurrence of mismatch between acquired spectra and dark spectra.

Table II. PLSR results for ash in chicken (% of wet weight) and EPA+DHA in salmon (% of total FA), using (i) only one of the replicates for each sample and (ii) the mean of two replicates.

	One selected replicate		Replicate average	
Exp. time	$RMSECV_{avg}$	LV[a]	RMSECV	LV
Chicken				
1 s	0.88	2	0.70	3
2 s	0.68	3	0.62	3
4 s	0.62	3	0.53	3
10 s	0.58	3	0.51	3
Salmon				
1 s	0.85	2,3	0.75	2
2 s	0.74	3	0.64	3
4 s	0.54	3,4	0.43	4
10 s	0.43	4,3	0.38	4

[a]Latent variables.

Table III. PLSR results for ash in chicken (% of wet weight) and EPA+DHA in salmon (% of total FA), using a calibration based on 10 s exposure spectra on the shorter exposure data sets. Results from the original cross-validation scheme is included.

	Original	10 s calibration	
Exp. time	RMSECV	RMSECV	LV[a]
Chicken			
1 s	0.84	0.83	3
2 s	0.70	0.70	3
4 s	0.63	0.62	3
Salmon			
1 s	0.84	0.82	4
2 s	0.71	0.74	4
4 s	0.51	0.49	4

[a]Latent variables.

Strategies to tackle this, either through pre-processing or practical solutions, should be considered.

Impact of Heterogeneity on the Raman Scanning Measurements

The results from CVANOVA showed that the differences in cross-validation errors for homogenized and heterogenous chicken samples were not significantly different for either the 2 s or 10 s exposure times (p-values of 0.47 and 0.36, respectively). This indicates that the heterogeneity itself is not a major challenge for the scanning strategy. However, it should be noted that the sample surfaces in this experiment were representative for the sample bulk composition and that the heterogeneity of certain intact foods such as fish fillets is more complex. Due to the still limited sampling volume of a Raman scan, it is important to consider appropriate sampling strategies in more detail when we encounter heterogeneity in several dimensions of a product (e.g., in depth and transverse to the scanning direction). An important step for suggesting a robust sampling regime in such situations is to map the composition profile of the product. In this work, we used chicken samples with carefully designed heterogeneity and salmon samples which were homogenous. Nevertheless, the results provide a useful insight towards determining the feasibility of a Raman surface scanning strategy, also for intact and more heterogenous products like salmon fillets.

Conclusion

We have shown that spectra obtained from in-line Raman scanning of single chicken and salmon samples have sufficiently high quality for exposure times ranging from 10 s to 1 s. With appropriate strategy developments, it is viable to use a wide area illumination standoff Raman probe for fast in-line evaluation of % ash and %EPA + DHA in complex foods. The SNR clearly decreases with higher scanning speeds, and it was evident from model performances that SNR is a critical parameter. Efforts to optimize SNR in a given system is therefore important. This can be achieved through instrument improvements, variable selection and also by strategies based on flexible exposure times or using Raman instruments in series. Furthermore, we confirmed that the heterogeneity of the sample surface is not necessarily a limitation for the scanning strategy, but for food products where heterogeneity is more complex, it is likely important to consider individual sampling strategies.

Acknowledgments

We would like to express our gratitude to Katinka Dankel and Karen Wahlstrøm Sanden at Nofima for assistance during sample preparation and data acquisition.

Declaration of Conflicting Interests

The author(s) declared no potential conflicts of interest with respect to the research, authorship, and/or publication of this article.

Funding

The author(s) disclosed receipt of the following financial support for the research, authorship, and/or publication of this article: This work was partially funded by the Research Council of Norway through the projects SFI Digital Food Quality [grant number 309259] and the Food Pilot Plant [grant number 296083], along with the Norwegian Agricultural Food Research Foundation through the project Precision Food Production [grant number 314111].

ORCID iDs

Tiril Aurora Lintvedt https://orcid.org/0000-0001-8527-0138
Petter V. Andersen https://orcid.org/0000-0002-8241-1051

Supplemental Material

The supplemental material mentioned in the text, consisting of Figures S1, is available in the online version of the journal

References

1. United Nations Department of Economic and Social Affairs. "Responsible consumption and production". In: The Sustainable Development Goals Report. 2020. Pp. 48–49. doi: 10.18356/214e6642-en.
2. J.P. Wold, M. Kermit, A. Woll. "Rapid Nondestructive Determination of Edible Meat Content in Crabs (*Cancer Pagurus*) by Near-Infrared Imaging Spectroscopy". Appl. Spectrosc. 2010. 64(7): 691–699. doi: 10.1366/000370210791666273.
3. V.H. Segtnan, M. Høy, F. Lundby, B. Narum, J.P. Wold. "Fat Distribution Analysis in Salmon Fillets Using Non-Contact Near Infrared Interactance Imaging: A Sampling and Calibration Strategy". J. Near Infrared Spectrosc. 2009. 17(5): 247–253. doi: 10.1255/jnirs.851.
4. J.P. Wold, I. Måge, A. Løvland, K.W. Sanden, R. Ofstad. "Near-infrared Spectroscopy Detects Woody Breast Syndrome in Chicken Fillets by the Markers Protein Content and Degree of Water Binding". Poult. Sci. 2019. 98(1): 480–490. doi: 10.3382/ps/pey351.
5. Y. Ozaki, C.W. Huck, K.B. Beć. "Near-IR Spectroscopy and its Applications". In: V.P. Gupta, editor. Molecular and Laser Spectroscopy: Advances and Applications. Amsterdam, Netherlands: Elsevier, 2017. Pp 11–38.
6. M.Y. Bekhit, B. Grung, S.A. Mjøs. "Determination of Omega-3 Fatty Acids in Fish Oil Supplements Using Vibrational Spectroscopy and Chemometric Methods". Appl. Spectrosc. 2014. 68(10): 1190–1200. doi: 10.1366/13-07210.
7. K.A. Esmonde-White, M. Cuellar, C. Uerpmann, L. Bruno, I.R. Lewis. "Raman Spectroscopy as a Process Analytical Technology for Pharmaceutical Manufacturing and Bioprocessing". Anal. Bioanal. Chem. 2017. 409: 637–649. doi:10.1007/s00216-016-9824-1.
8. H. Wikström, I.R. Lewis, L.S. Taylor. "Comparison of Sampling Techniques for In-Line Monitoring Using Raman Spectroscopy". Appl. Spectrosc. 2005. 59(7): 934–941. doi: 10.1366/0003702054411553.
9. S.G. Wubshet, J.P. Wold, N.K. Afseth, U. Böcker, D. Lindberg. "Feed-Forward Prediction of Product Qualities in Enzymatic Protein Hydrolysis of Poultry By-products: A Spectroscopic Approach". Food Bioprocess. Technol. 2018. 11: 2032–2043. doi: 10.1007/s11947-018-2161-y.
10. S.G. Wubshet, J.P. Wold, U. Böcker. "Raman Spectroscopy for Quantification of Residual Calcium and Total Ash in Mechanically Deboned Chicken Meat". Food Control. 2019. 95: 267–273. doi: 10.1016/j.foodcont.2018.08.017.
11. O. Monago-Maraña, J.P. Wold, R. Rødbotten, K.R. Dankel, N.K. Afseth. "Raman, Near-infrared and Fluorescence Spectroscopy for Determination of Collagen Content in Ground Meat and Poultry By-products". Food Sci. Technol. 2021. 140: 110592. doi: 10.1016/j.lwt.2020.110592.
12. P.V. Andersen, J.P. Wold, N.K. Afseth. "Assessment of Bulk Composition of Heterogeneous Food Matrices Using Raman Spectroscopy". Appl. Spectrosc. 2021. 75(10): 1278–1287. doi: 10.1177/0003702821006150.
13. EFSA. "Scientific Opinion on the Public Health Risks Related to Mechanically Separated Meat (MSM) Derived from Poultry and Swine". EFSA J. 2013. 11(3): 3137. doi: 10.2903/j.efsa.2013.3137.
14. J.P. Wold, M. Kermit, V.H. Segtnan. "Chemical Imaging of Heterogeneous Muscle Foods Using Near-Infrared Hyperspectral Imaging in Transmission Mode". Appl. Spectrosc. 2016. 70(6): 953–961. doi: 10.1177/0003702816641260.
15. M. M Cascant, C. Breil, A.S. Fabiano-Tixier, F. Chemat, S. Garrigues. "Determination of Fatty Acids and Lipid Classes in Salmon Oil by Near Infrared Spectroscopy". Food Chem. 2018. 239: 865–871. doi: 10.1016/j.foodchem.2017.06.158.
16. M.R. Brown, P.D. Kube, R.S. Taylor, N.G. Elliott. "Rapid Compositional Analysis of Atlantic Salmon (*Salmo Salar*) Using Visible-Near Infrared Reflectance Spectroscopy". Aquacult. Res. 2014. 45(5): 798–811. doi: 10.1111/are.12021.
17. C.E. Eskildsen, T. Næs, P.B. Skou, L.E. Solberg, K.R. Dankel. "Cage of Covariance in Calibration Modeling: Regressing Multiple and Strongly Correlated Response Variables onto a Low Rank Subspace of Explanatory Variables". Chemom. Intell. Lab. Syst. 2021. 213: 104311. doi: 10.1016/j.chemolab.2021.104311.
18. N.K. Afseth, V.H. Segtnan, B.J. Marquardt, J.P. Wold. "Raman and Near-Infrared Spectroscopy for Quantification of Fat Composition in a Complex Food Model System". Appl. Spectrosc. 2005. 59(11): 1324–1332. doi: 10.1366/000370205774783304.
19. N.K. Afseth, J.P. Wold, V.H. Segtnan. "The Potential of Raman Spectroscopy for Characterisation of the Fatty Acid Unsaturation of Salmon". Anal. Chim. Acta. 2006. 572(1): 85–92. doi: 10.1016/j.aca.2006.05.013.
20. J.R. Beattie, S.E. Bell, C. Borgaard, A. Fearon, B.W. Moss. "Prediction of Adipose Tissue Composition Using Raman Spectroscopy: Average Properties and Individual Fatty Acids". Lipids. 2006. 41(3): 287–294. doi: 10.1007/s11745-006-5099-1.

21. D.P. Killeen, S.N. Marshall, E.J. Burgess, K.C. Gordon, N.B. Perry. "Raman Spectroscopy of Fish Oil Capsules: Polyunsaturated Fatty Acid Quantitation Plus Detection of Ethyl Esters and Oxidation". J. Agric. Food Chem. 2017. 65(17): 3551–3558. doi: 10.1021/acs.jafc.7b00099.
22. A. Savitzky, M.J. Golay. "Smoothing and Differentiation of Data by Simplified Least Squares Procedures". Anal. Chem. 1964. 36(8): 1627–1639. doi: 10.1021/ac60214a047.
23. H. Martens, E. Stark. "Extended Multiplicative Signal Correction and Spectral Interference Subtraction: New Preprocessing Methods for Near Infrared Spectroscopy". J. Pharm. Biomed. Anal. 1991. 9(8): 625–635. doi: 10.1016/0731-7085(91)80188-F.
24. K.H. Liland, A. Kohler, N.K. Afseth. "Model-Based Pre-Processing in Raman Spectroscopy of Biological Samples". J. Raman Spectrosc. 2016. 47(6): 643–650. doi: 10.1002/jrs.4886.
25. P.H.C. Eilers, H.F.M. Boelens. "A Perfect Smoother". Life Sci. 2003. 75(14): 3631–3636. doi: 10.1021/ac034173t.
26. K.H. Liland, T. Almøy, B.H. Mevik. "Optimal Choice of Baseline Correction for Multivariate Calibration of Spectra". Appl. Spectrosc. 2010. 64(9): 1007–1016. doi: 10.1366/000370210792434350.
27. H. Martens, T. Næs. Multivariate Calibration. Chichester, UK: John Wiley and Sons, 1989. Pp. 116–165.
28. Å. Björck, U.G. Indahl. "Fast and Stable Partial Least Squares Modelling: A Benchmark Study with Theoretical Comments". J. Chemom. 2017. 31(8). doi: 10.1002/cem.2898.
29. F. Westad, H. Martens. "Variable Selection in Near Infrared Spectroscopy Based on Significance Testing in Partial Least Squares Regression". J. Near Infrared Spectrosc. 2000. 8(2): 117–124. doi: 10.1255/jnirs.271.
30. T.N. Tran, N.L. Afanador, L.M. Buydens, L. Blanchet. "Interpretation of Variable Importance in Partial Least Squares with Significance Multivariate Correlation (sMC)". Chemom. Intell. Lab. Syst. 2014. 138: 153–160. doi: 10.1016/j.chemolab.2014.08.005.
31. L. Eriksson, J. Trygg, S. Wold. "CV-ANOVA for Significance Testing of PLS and OPLS Models". J. Chemom. 2008. 22(11–12): 594–600. doi: 10.1002/cem.1187.
32. U.G. Indahl, T. Næs. "Evaluation of Alternative Spectral Feature Extraction Methods of Textural Images for Multivariate Modeling". J. Chemom. 1998. 12(4): 261–278. doi: 10.1002/(sici)1099-128x(199807/08)12:4{\textless}261::aid-cem513{\textgreater}3.3.co;2-q.
33. J.P. Wold, K. Kvaal, B. Egelandsdal. "Quantification of Intramuscular Fat Content in Beef by Combining Autofluorescence Spectra and Autofluorescence Images". Appl. Spectrosc. 1999. 53(4): 448–456. doi: 10.1366/0003702991946730.
34. S. Guo, C. Beleites, U. Neugebauer, S. Abalde-Cela, N.K. Afseth. "Comparability of Raman Spectroscopic Configurations: A Large Scale Cross-Laboratory Study". Anal. Chem. 2020. 92(24): 15745–15756. doi: 10.1021/acs.analchem.0c02696.
35. M.D. Morris, G.S. Mandair. "Raman Assessment of Bone Quality". Clin. Orthop. Relat. Res. 2011. 469(8): 2160–2169. doi: 10.1007/s11999-010-1692-y.
36. K. Czamara, K. Majzner, M.Z. Pacia, K. Kochan, A. Kaczor. "Raman Spectroscopy of Lipids: A Review". J. Raman Spectrosc. 2015. 46(1): 4–20. doi: 10.1002/jrs.4607.
37. G. Socrates. "Alkenes, Oximes, Imines, Amidines, Azo compounds: C=C, C=N, N=N Groups". In: G. Socrates, editor. Infrared and Raman Characteristic Group Frequencies: Tables and Charts. Chichester, UK: John Wiley and Sons, 2004. p. 74.

Supplemental material – Additional results from PLS regression

Feasibility of in-line Raman spectroscopy for quality assessment in food industry - how fast can we go?

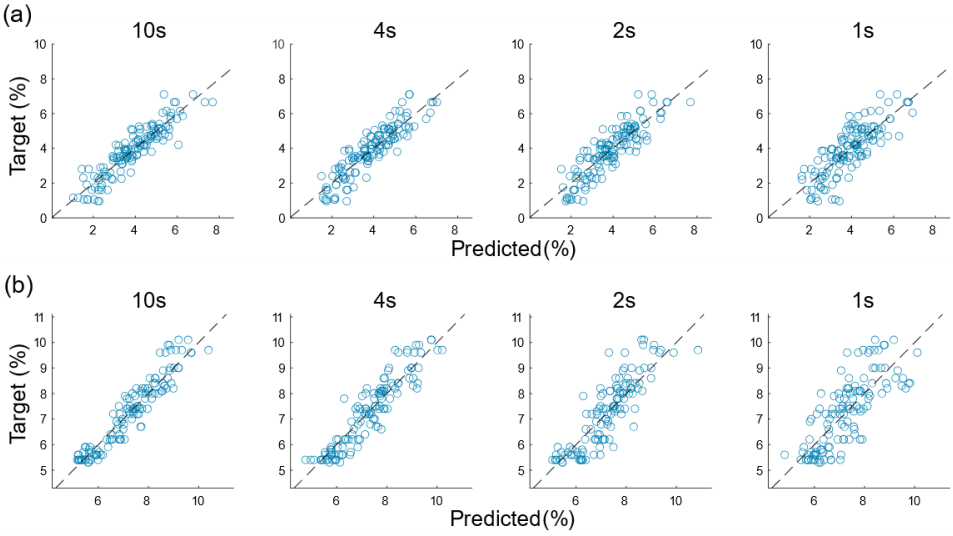

Figure S1: Predicted versus measured values for estimation of ash (% of wet weight) in chicken (a) and predicted versus measured values for EPA+DHA (% of total FA) in salmon (b) for all exposure times.

Appendix B

Paper II

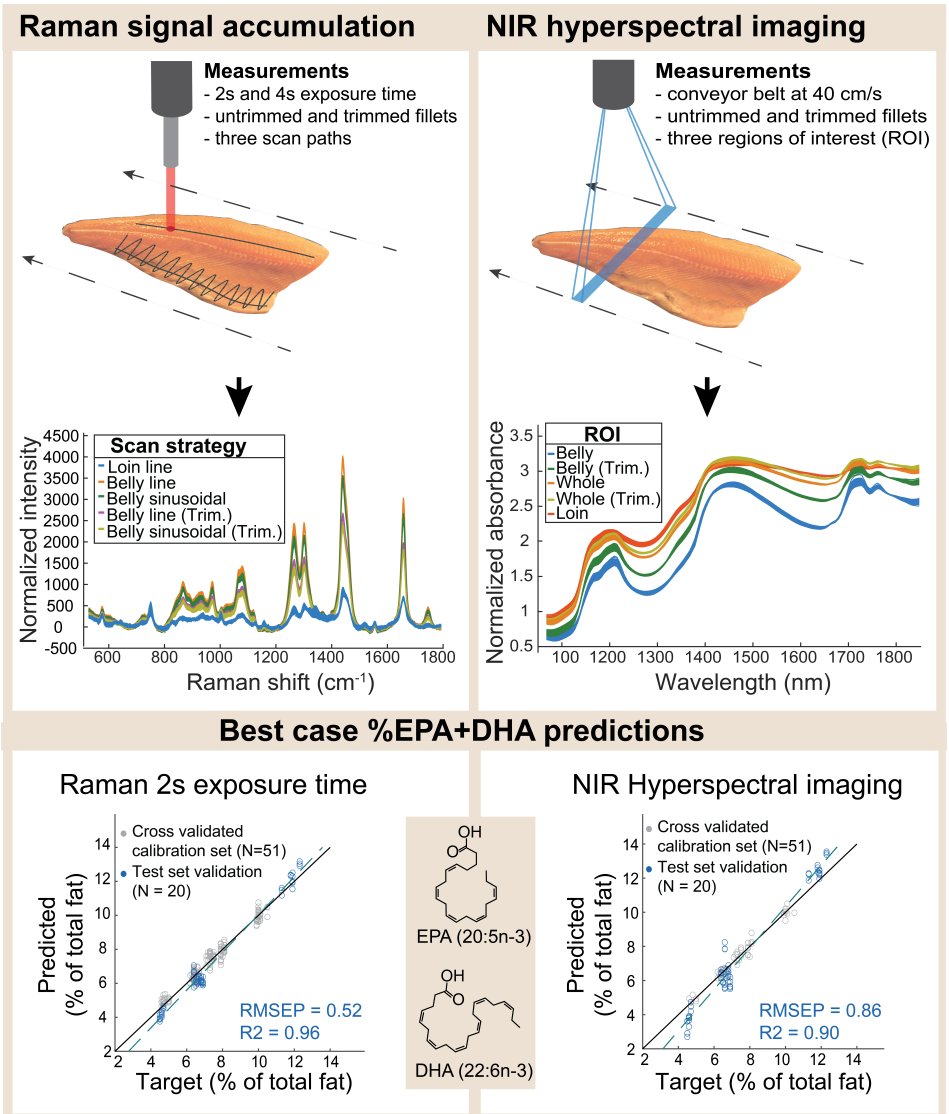

Talanta 254 (2023) 124113

Contents lists available at ScienceDirect

Talanta

journal homepage: www.elsevier.com/locate/talanta

Raman spectroscopy and NIR hyperspectral imaging for in-line estimation of fatty acid features in salmon fillets

Tiril Aurora Lintvedt [a,b,*], Petter Vejle Andersen [a], Nils Kristian Afseth [a], Karsten Heia [a], Stein-Kato Lindberg [a], Jens Petter Wold [a]

[a] Norwegian Institute for Food, Fisheries and Aquaculture Research, Muninbakken 9-13, Breivika, Tromsø, 9291, Norway
[b] Faculty of Science and Technology, Norwegian University of Life Sciences, Ås, 1432, Norway

ARTICLE INFO

Keywords:
Raman Spectroscopy
NIR hyperspectral Imaging
In-line food evaluation
Representative sampling
Salmon quality
Omega-3 fatty acids

ABSTRACT

Raman spectroscopy was compared with near infrared (NIR) hyperspectral imaging for determination of fat composition (%EPA + DHA) in salmon fillets at short exposure times. Fillets were measured in movement for both methods. Salmon were acquired from several different farming locations in Norway with different feeding regimes, representing a realistic variation of salmon in the market. For Raman, we investigated three manual scanning strategies; i) line scan of loin, ii) line scan of belly and iii) sinusoidal scan of belly at exposure times of 2s and 4s. NIR images were acquired while the fillets moved on a conveyor belt at 40 cm/s, which corresponds to an acquisition time of 1s for a 40 cm long fillet. For NIR images, three different regions of interest (ROI) were investigated including the i) whole fillet, ii) belly segment, and iii) loin segment. For both Raman and NIR measurements, we investigated an untrimmed and trimmed version of the fillets, both relevant for industrial in-line evaluation. For the trimmed fillets, a fat rich deposition layer in the belly was removed. The %EPA + DHA models were validated by cross validation (N = 51) and using an independent test set (N = 20) which was acquired in a different season. Both Raman and NIR showed promising results and high performances in the cross validation, with $R2_{CV}$ = 0.96 for Raman at 2s exposure and $R2_{CV}$ = 0.97 for NIR. High performances were obtained also for the test set, but while Raman had low and stable biases for the test set, the biases were high and varied for the NIR measurements. Analysis of variance on the squared test set residuals showed that performance for Raman measurements were significantly higher than NIR at 1% significance level (p = 0.000013) when slope-and-bias errors were not corrected, but not significant when residuals were slope-and-bias corrected (p = 0.28). This indicated that NIR was more sensitive to matrix effects. For Raman, signal-to-noise ratio was the main limitation and there were indications that Raman was close to a critical sample exposure time at the 2s signal accumulation.

1. Introduction

For many years, the health effects of the omega-3 fatty acids eicosapentaenoic acid (EPA) and docosahexaenoic acid (DHA) have gained much attention [1–6]. Fat rich fish, such as Atlantic salmon, is a major source of EPA and DHA in the human diet and therefore, the abundance of these fatty acids can be considered an important quality parameter in the aquaculture industry. Today most of the salmon found in the stores are farmed, and studies have shown that feed is the main factor determining fatty acid composition of the muscle of Atlantic salmon [7–9]. It is also known that other factors such as genetics can influence [10–12]. In later years, there has been a trend to replace marine ingredients in feed with vegetable oils, resulting in lower abundance of EPA and DHA [13–15]. A challenge is that low levels of EPA and DHA have been connected to low fish welfare in sea cages and low fillet quality [16,17]. This emphasizes the motivation to monitor fatty acid features in salmon more closely. Continuous monitoring of EPA and DHA in salmon fillets could provide opportunities for salmon farms to obtain continuous knowledge on impact of different feeding regimes and potentially other farming parameters. It could also provide the opportunity to report specific quality features to consumers, resulting in increased consumer trust and more targeted quality differentiation. Preferably, measurement stations should be integrated on the conveyor belt, scanning each single fillet. For this to be realized, a robust and rapid in-line

* Corresponding author. Norwegian Institute for Food, Fisheries and Aquaculture Research, Muninbakken 9-13, Breivika, Tromsø, 9291, Norway.
E-mail address: tiril.lintvedt@nofima.no (T.A. Lintvedt).

https://doi.org/10.1016/j.talanta.2022.124113
Received 29 June 2022; Received in revised form 14 November 2022; Accepted 16 November 2022
Available online 1 December 2022

measurement technique is needed. Two of the practically relevant methods in this respect are Raman spectroscopy and near infrared spectroscopy (NIRS).

The reported use of NIRS for estimation of omega-3 fatty acids in pure fish oils is promising [18,19]. However, estimation of specific fatty acids in intact salmon fillets is more challenging due to lower concentrations and more interferants, such as water and protein. Brown et al. [20] utilized NIR spectra in the range 800–1850 nm and reported moderate performances for prediction of EPA and DHA in intact salmon cutlets, which indicated compatibility with rough screening applications only. In addition, it was unclear if these models relied on indirect modelling on total fat, as discussed by Eskildsen et al. [21] An advantage of NIRS (400–2500 nm) is that hyperspectral imaging instruments are available and reasonably affordable. NIR hyperspectral imaging has been successfully used for determination of total fat content and fat distribution in whole salmon fillets [22–24]. These instruments already allow very fast measurements of whole fillets on the conveyor belt. In an in-line situation, imaging ensures representative measurements of whole salmon fillets and provides the opportunity for distributional analysis. To the authors knowledge there are no studies concerning EPA and DHA measurements in salmon fillets using NIR hyperspectral imaging which include the spectral region above 1700 nm. This region is likely important for more robust modelling of unsaturated fatty acids since it is associated with the CH=CH vibration [25].

Raman spectroscopy is a promising tool for compositional analysis of fatty acids [26–29]. In a recent work, Lintvedt et al. [30] demonstrated the potential use of in-line Raman spectroscopy for samples of ground salmon which were passing by on the conveyor belt. Here it was shown that the spectra had sufficient quality at high speeds and could be used for estimation of the fatty acids %EPA + DHA. However, fast non-contact Raman measurements of intact salmon fillets have not been investigated, and the challenge that is posed by the heterogeneity of the fillets should be addressed. Raman spectroscopy is practically challenging due to sensitivity to ambient light signals in the production hall, the limited focal volume and the need for timing the signal accumulation. Since the Raman focal volume is small, the collection of representative measurements from a heterogeneous fillet is not self-evident. By using a so called wide area illumination probe one can obtain larger measurement areas (spot size diameter 3–6 mm) than with traditional Raman instrumentation which in addition provides insensitivity to smaller variations in working distance [31]. The latter is important when measuring samples varying in thickness. The signal-to-noise ratio (SNR) is a limiting factor for Raman when exposure time is reduced to only a few seconds [30]. Fat is a relatively strong Raman scatterer, so stronger Raman signals will be obtained on fat rich tissue. The fat deposition in salmon gradually increases from loin to belly and from tail to head, and as much as 49% of the belly flap wet weight can be lipids. This means that it is important to determine the optimal sampling region on the fillets, and for in-line Raman measurements, robotics can be used to implement this critical sampling. This motivates an investigation of different strategies for robotic control of the Raman probe, i. e to determine what is the optimal scanning path.

Although Raman spectroscopy is practically more challenging to employ in the industry, the method could have considerable advantages with respect to robustness of the %EPA + DHA predictions. Firstly, Raman scattering originate from fundamental vibrational transitions yielding a lower degree of overlapping spectral bands (e.g. between protein and fat) compared to NIR spectra [19]. This is because NIR absorptions are based on overtones and combination modes, in contrast [32]. In addition, water signals can dominate NIR spectra, while it is well known that water is a very weak Raman scatterer and is usually not a challenge. Robust methods can potentially reduce the needed frequency of re-calibrations. Although relevant Raman instrumentation is currently about twice the cost of NIR hyperspectral cameras, the potential gain from less effort on model maintenance represents a considerable cost reduction, which should be considered. Afseth et al. [33] compared Raman and NIR laboratory measurements of homogenized salmon samples (N = 668) and found that chemical information on fatty acids in Raman measurements are much better resolved than in NIR measurements. This study also showed that Raman had significantly higher cross validated performances for estimation of EPA and DHA, indicating that Raman might be the more robust solution. However, at higher speeds, signal-to-noise ratio (SNR) can be a limitation for Raman as pointed out above. Therefore it is of interest to compare the two methods in a relevant in-line setup employing short exposure times.

In this work, the main aim was to investigate the feasibility of in-line Raman measurements of %EPA + DHA in single intact salmon fillets employing a wide area Raman probe and to compare the robustness of this method with measurements with an NIR hyperspectral camera (930–2500 nm). The model generalization ability to new samples was mainly demonstrated through predictions on an independent test set. For Raman spectroscopy, in-line measurements were manually mimicked by employing short exposure times of several different scanning paths over the fillet. For the same samples, NIR images were acquired while the fillets moved on a conveyor belt at 40 cm/s, investigating different regions of interest (ROI). For both Raman and NIR measurements, we investigated a fat trimmed and an untrimmed version of the fillets, which are both relevant for industrial in-line evaluation. To the best of our knowledge, this is the first time the feasibility for in-line Raman measurements of %EPA + DHA prediction in intact salmon fillets is investigated and compared with NIR hyperspectral imaging (930–2500 nm).

2. Material and methods

2.1. Salmon fillets

A calibration set of 51 salmon fillets was acquired from five different farming locations with varying feeding regimes from three different Norwegian suppliers (SalMar ASA, Norway Royal Salmon ASA and Lerøy Seafood Group ASA). Salmon were supplied as whole gutted fish stored on ice in which state they were kept for about 5 days in a cold room at 1–2 °C before filleting. Subsequently the right fillet was vacuum packed and frozen (−30 °C) and used for the NIR measurements which were carried out in a different location. The left fillet was immediately used for the Raman measurements. Thawing of the salmon fillets before the NIR experiment was done on racks in a room with air circulation for about 2 h, then they were kept in a cold room (1–2 °C) over night. Approximately half a year later, an independent test set consisting of 20 salmon fillets was acquired from three different farming suppliers with different feeding regimes. The test set was treated the same way as the calibration set.

Two fillet versions were measured in both Raman and NIR experiments. First, each fillet was measured untrimmed, with a surface layer of deposited fat and bones covering the muscle fibers in the belly. Afterwards, the surface layer of deposited fat and bones were trimmed away while keeping as much intact belly muscle as possible. Fillets were stored in a cold room at 1–2 °C during the experiment time.

2.2. Measurements and data analysis

2.2.1. Raman measurements

We employed a MarqMetrix All-in-One (AIO) Raman system covering a Raman shift range of 100–3250 cm^{-1}. The system was equipped with a 785 nm laser operating at 450 mW power and the sampling optic was a wide area illumination (D = 3 mm), Proximal BallProbe HV standoff Raman probe (MarqMetrix Inc., Seattle, WA, USA) with working distance at approximately 9 cm. Each salmon fillet was placed on a PE plastic plate covered with aluminium foil. The foil was used to prevent potentially disturbing signals from the plate plastic. We mimicked in-line scans manually in a dark room, with the help of a movable instrument rack for the probe. One person pushed the fillet

forward while another handled the rack which allowed the probe to be moved transversely to the speed direction, resulting in the three different scanning strategies illustrated in Fig. 1 and denoted as S1) line scan of loin, S2) sinusoidal scan of belly and S3) line scan of belly. The result was one accumulated spectrum for each of the illustrated paths. The different scans were chosen to elucidate the effect of varying fat deposition across the salmon fillet on spectra and performance. Two different accumulation times were applied: 4s and 2s, where 4s represented fast at-line measurements and 2s was regarded short enough to be relevant in the process line. Three replicate measurements were acquired for each combination of scanning path and accumulation time.

2.2.2. NIR measurements

We employed a hyperspectral camera (HySpex SWIR-384) from Norsk Elektro Optikk (NEO) with spectral range 930–2500 nm that employs an MCT detector cooled down to 150 K. Diffuse halogen lighting was used for illumination, and measurements were done in reflectance mode. The fillets moved on a conveyor belt at a speed of 40 cm/s, which correspond to an acquisition time of 1s for a 40 cm long fillet. The images were collected from a working distance of approximately 1 m with an acquisition speed of 200 frames per second. The focus plane was about 4 cm over the conveyor belt. For the 51 calibration fillets, one image scan was collected per fillet. For the test set fillets, 3 replicate measurements were acquired.

2.2.3. Reference measurements

Since the right fillet was frozen and sent to a different location for NIR imaging, the reference samples were prepared from the belly of the trimmed left-side fillets as indicated in Fig. 2b. The variation between the left and right fillet was assumed to be negligible. The bellies were homogenized (Retsch Knife Mill GRINDOMIX GM 200, 7000 rpm for 3s), vacuum packed and frozen at −30 °C. Analyses of the samples were carried out by BioLab (Bergen, Norway). Fatty acid concentrations were determined by gas chromatography (capillary GC-FID) on fatty acid methyl esters (AOCS Official Method Ce 1b-89), and were expressed as a percentage of the total fat in the analyzed sample. The total fat of the belly samples was determined by the Bligh and Dyer method [34].

2.2.4. Estimation of iodine value

As a measure of total unsaturation in the salmon, the iodine value (IV) was estimated from the full fatty acids (FA) profile in accordance with the AOCS recommended practice Cd 1c-85, and same as reported by Berhe et al. [35] and Afseth et al. [33].

$$IV = M_w(I_2)\sum_{i=1}^{n}\frac{DB_{(i)}V_{FAMe(i)}}{M_w(FAMe_{(i)})} \quad (1)$$

where M_w is molecular weight, I_2 is iodine, $FAMe(i)$ is the fatty acid methyl ester number i, DB is the number of double bonds and $V_{FAMe(i)}$ is percentage of fatty acid number i.

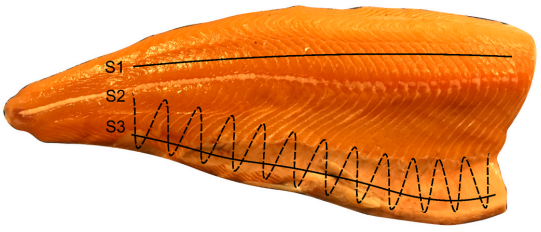

Fig. 1. Scanning strategies for Raman signal accumulation, including S1) line scan of loin, S2) sinusoidal scan of belly, and S3) line scan of belly.

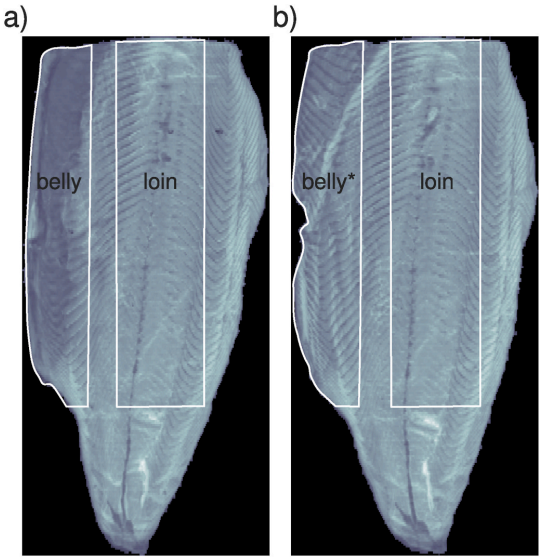

Fig. 2. Example of hyperspectral NIR images (1210 nm shown) for one salmon fillet in untrimmed (a) and trimmed (b) version, with the belly and loin ROIs indicated by the white outlines. References were prepared from the corresponding belly area (*) of the fillet used for the Raman experiment.

2.2.5. Pre-processing of spectral data

For Raman spectra, the Raman shift range 520–1800 cm^{-1} was used in analyses. Cosmic ray spikes were removed manually by a simple spike detection algorithm based on derivatives. Subsequently Savitsky-Golay (SG) smoothing (polynomial order 2 and window size 9) [36] was applied, followed by Extended Multiplicative Signal Correction (EMSC) [37,38] employing up to the sixth order polynomial and the Asymmetric Least Squares (ALS) algorithm [39,40] for baseline correction of the EMSC reference spectrum. The ALS reference spectrum correction employed a smoothing parameter of 5.8 and an asymmetric weighting parameter (of the residuals) of 0.01. For the test set spectra, pre-processing by EMSC employed the mean spectrum of the calibration samples as the reference spectrum. Pre-processing was applied separately on subsets which were defined by the combinations of fillet version, scanning paths and exposure time.

The NIR hyperspectral images were radiance calibrated in the Hyspex Rad V2.5 software (NEO, Oslo, Norway) and reflectance values were calculated through division by a spectralon white reference. Each reflectance spectrum was then transformed to the pseudo-absorbance ($A = \log_e(1/R)$). An average spectrum across all pixels was used for further analysis. For each image, three different regions of interest (ROI) were investigated, where we used the i) whole fillet, ii) belly region and iii) loin region, as indicated in Fig. 2. The average spectra were pre-processed by regular EMSC employing linear and quadratic polynomials for baseline correction and the spectral region 1170–1850 nm was selected and used for further analysis to avoid the noisy region above 2000 nm. Similar to the Raman spectra, pre-processing on NIR spectra was applied on the separate subsets which were defined by the combinations of fillet version and ROIs. Between the two periods of acquisition of calibration data and test set data, the camera was repaired and a small wavelength shift occurred. This required an additional wavelength interpolation for the test set sample spectra.

2.2.6. Data modelling

Partial least squares regression (PLSR) [41,42] was used for

calibration development. We established models for EPA + DHA concentration in salmon fillets. Note that EPA and DHA concentrations were not estimated separately, but as a joint concentration value. PLSR models were built on the 51 calibration fillets. For selection of optimal number of latent variables for the models, we employed cross-validation (CV), where replicate measurements were held out in the same CV segment to avoid overfitting. The reason for not averaging the replicates was to keep the prediction conditions as close to an in-line situation as possible. The choice of number of latent variables for the PLS modelling was based on a simple criterion using a 3% punish factor, as described by Westad and Martens [43]. The model was then rebuilt on the full calibration set with the optimum number of components and applied on the pre-processed test set spectra. We report performance through the coefficient of determination (R2) and the root mean squared error (RMSE). For the test set validation, we also report these metrics when corrected for slope and bias errors, together with the bias and slope. To establish whether the estimation errors of the test set using Raman spectra were significantly different from those using NIR hyperspectral images, we applied a two-way analysis of variance (ANOVA) of the squared residuals. In addition, the confidence intervals of the coefficient of determination (R2) were reported in some figures. These were calculated from the Fisher Z-transformation [44,45].

2.3. Signal to noise ratio

In this work, we compared the SNR of sets of spectra obtained by different Raman measurement strategies. First, the spectra in the given set were pre-processed as described in section 2.2.5. Then, the SNR of each spectrum was calculated as the ratio between the average spectrum and the standard deviation of the estimated noise, according to Eq. (2). The reported value for one set was the average SNR of all individual spectra in the respective set.

$$SNR = \frac{mean(I)}{sd(I_n)} \tag{2}$$

where I is the spectrum intensity and I_n is the estimated noise intensity. The noise component of the spectrum was estimated by subtracting a smoothed version of the spectrum from the original spectrum I. This resulted in a residual spectrum I_n containing mainly noise. For smoothing we used SG with polynomial order 2 and window size 9. This is similar to Guo et al. [46] and same as in our previous work [30].

2.3.1. Repeatability of predictions

For the test set, 3 replicates were acquired for both Raman and NIR. The repeatability of the measurements by each method was calculated as the pooled standard deviation of the predictions within the replicate groups

$$STD_{pooled} = \sqrt{\sum_{j=1}^{M}\sum_{i=1}^{N}\frac{(\hat{y}_{ij} - \overline{Y}_j)}{M(N-1))}} \tag{3}$$

where M is the number of salmon fillets, N is the number of replicate measurements and $\hat{y}_{ij}$ is the predicted value of replicate number i in replicate group number j. The average prediction within the replicate group number j is denoted by $\overline{Y}_j$.

3. Results and discussion

3.1. Sample variation in fat composition

The calibration samples spanned a range of %EPA + DHA levels (4.6–10.5%) and DHA/EPA ratios (1.1–2.4) representing typical effects of different feeds. The test set samples spanned a similar %EPA + DHA range (4.5–12.3%), but had a less even distribution due to the lower number of samples. Moreover, there was a shorter span in DHA/EPA ratio (1.1–1.6) and higher overall fat level than in the calibration samples. The higher fat level in the test set corresponded well with expected seasonal variations in fat deposition. Note also that the test set represented some extrapolation in %EPA + DHA levels in comparison to the calibration set. See supplementary for distributions in FA properties (Fig.A.7).

3.2. Spectral features

The Raman spectra (Fig. 3a) were dominated by bands associated with fatty acids. The main absorption bands related to fatty acid unsaturation are the C═C stretch (1657 cm^{-1}) and the alkene C–H bend (1266 cm^{-1}) [27,28]. The peak around 930 cm^{-1} is most likely related to the alkene C–H deformation in polyunsaturated fatty acid moieties [47,48]. The main bands related to fatty acid saturation are the methylene scissor deformation (1440 cm^{-1}) and the methylene twisting deformation (1302 cm^{-1}). Other bands of interest originate from the aromatic ring breathing of phenylalanine (1004 cm^{-1}) and the liquid aliphatic C–C stretch in gauche (1080 cm^{-1}) [27,28].

The NIR spectra (Fig. 3b) had broader bands which overlapped and a baseline related to e.g. scattering effects was apparent. The main absorption bands are associated with the second overtone of the CH stretch (1210 nm [49]), the CH stretch first overtone (1723, 1761 nm [25,50]) and OH stretch first overtone (1400 nm [49]). The shoulder around 1164 nm is related to the degree of unsaturation and is an important peak for estimation of iodine value [25,51]. Furthermore, the CH band at 1761 nm has been primarily related to saturated fatty acids, while literature indicate that a shift of the band around 1723 nm towards shorter wavelengths is related to the degree of unsaturation [25,49]. The spectral region above 2000 nm was noisy and detrimental for model performance, and therefore discarded from the further analyses. It should be noted that some bands of interest are located in this region [49,50].

3.3. Implication of Raman sampling strategies

Regression results from employing the different Raman sampling methods, i.e. different fillet versions and scan paths, are shown in Table 1. Differences in Raman signal level as a consequence of the different sampling strategies were clearly visible in the spectra (Fig. 3), and were reflected in the SNR levels (Table 1). Scans of typical high fat regions had higher intensity, with highest signals from measurements of the untrimmed belly, followed by the scans of the trimmed belly. The sinusoidal belly scans had slightly lower signals compared to the corresponding line scans. The loin scans exhibited considerably weaker signals. From the cross validation on the designated calibration set, it was evident that the loin scan stood out with the poorest model errors ($R2_{CV} = 0.77$ at 4s exposure and $R2_{CV} = 0.56$ at 2s exposure) as well. All belly scan variations gave high performances at both 4s and 2s exposure. Part of the reason for the low performances from loin measurements can also be that the reference sample was taken from belly, and moderate variations in FA composition across the fillet is possible [52]. However, in previous work [30], we found that %EPA + DHA estimation based on Raman spectra was limited by the SNR level. Together, these results indicate that pointing the Raman probe toward areas with high fat deposition is important to acquire spectra with sufficient quality at short exposure times.

Measurements on untrimmed fillets gave the overall highest performances across the two exposure times. While the fillet trimming did not seem to greatly affect the estimations at 4s exposure, there was a moderate impact at 2s, with lower $R2_{CV}$ (Table 1). The impact of scan path was less discernible. The differences seen between the measurement strategies are at least partly connected to the SNR. The $R2_{CV}$ correlated closely with SNR at 2s exposure ($r_{2s} = 0.99$), but not at 4s exposure ($r_{4s} = 0.67$). This indicated that the signal strength gained from measuring on the untrimmed fillets and from choosing the optimal scan

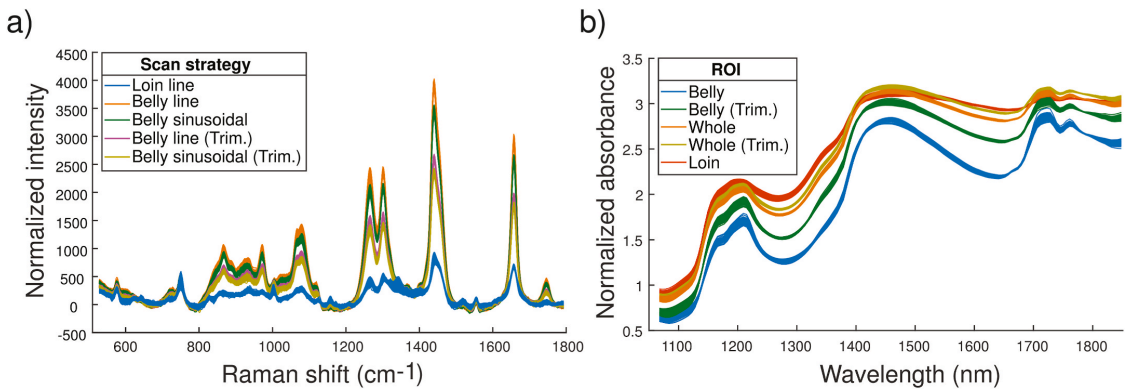

Fig. 3. Calibration sample spectra from Raman (a) and NIR (b) measurements compared across the respective investigated subset versions, i.e. combinations of exposure time, scanning paths and fillet versions for Raman spectra and combinations of ROIs and fillet versions for NIR spectra. The Raman spectra shown are the 2s exposure time measurements.

Table 1
PLS regression results for EPA + DHA in salmon fillets (% of total fat), using Raman spectra. Cross validated results for the calibration set (CV) and test set validation results are shown. For the test set validation, metrics corrected for bias and slope errors are indicated as well (corr).

Sampling method			Calibration set				Test set					Corrected test set	
Exp.	Fillet version	Scan	LV[a]	$R2_{CV}$	$RMSE_{CV}$	SNR[b]	R2	RMSEP	Bias	Slope	STD_{pooled}[c]	$R2_{corr}$	$RMSE_{corr}$
4s	–	S1	3	0.77	0.77	41.2	–	–	–	–	–	–	–
4s	untrimmed	S2	3	0.95	0.34	66.8	0.94	0.66	−0.14	1.20	0.20	0.99	0.31
4s	untrimmed	S3	3	0.96	0.33	68.0	0.95	0.60	−0.21	1.17	0.14	0.99	0.29
4s	trimmed	S2	3	0.95	0.36	60.8	0.91	0.79	−0.44	1.18	0.23	0.98	0.37
4s	trimmed	S3	3	0.95	0.36	63.0	0.95	0.60	−0.29	1.11	0.25	0.98	0.38
2s	–	S1	2	0.56	1.05	32.2	–	–	–	–	–	–	–
2s	untrimmed	S2	2	0.95	0.35	58.5	0.87	0.98	−0.33	1.31	0.18	0.99	0.29
2s	untrimmed	S3	3	0.96	0.33	60.5	0.96	0.52	−0.24	1.11	0.18	0.99	0.32
2s	trimmed	S2	1	0.91	0.47	51.0	0.93	0.71	−0.35	1.14	0.40	0.98	0.41
2s	trimmed	S3	3	0.93	0.42	53.6	0.88	0.95	−0.54	1.24	0.27	0.98	0.36

[a] Latent variables.
[b] Signal to noise ratio for calibration set.
[c] Pooled standard deviation (repeatability).

path is more important when the scan speed is increased further. Correspondingly, it might indicate that at 2s signal accumulation, we are approaching a critical limit for spectrum quality, while at 4s signal accumulation the Raman scanning approach will likely be more robust towards lower fat levels in fillets. One should bear in mind that there are more information about pigments and other bulk properties in scans of trimmed fillets (e.g. peaks at 1004, 1158, 1342 and 1519 cm^{-1}). See Fig B.9 for easier distinction of Raman peaks between the different measurement strategies. If an in-line system should be coupled with other analyses, it is a greater chance of accomplishing this with trimmed fillets.

With respect to exposure time, we overall saw more uniform results with respect to $R2_{CV}$ and the number of latent variables included in the models at 4s exposure. However, the performances seen at 2s exposure time was very encouraging, as they were considerably improved compared to what was obtained for homogenized salmon samples in previous work [30]. Notably, the SNR in this work was overall comparable to 10s exposure time in the previous work, most likely because the fat content of the measured regions were higher in the current work.

3.4. Implication of sampling strategies for NIR hyperspectral imaging

For NIR spectral data, it was evident (Fig. 3) that spectra from the belly region, particularly for the untrimmed fillets, had less prominent baselines than the spectra from regions which included the loin. This was seen also in the test set data (Fig.B.8b). The differences in baselines were most likely a combination of different tissue structures, which can lead to differences in scattering effects, and that high fat areas are dominated by fat absorbance. This consequently allows less absorption by other interferants such as water, which has broader absorption peaks. Additionally, measurements of the belly and whole untrimmed fillets had relatively stronger fat signals than the measurements of loin and the whole trimmed fillets. Cross validation on the calibration set showed that the effect was that measurements of the separate loin region had considerably lower performance than the measurements from other regions, similar as for Raman. Differences in $R2_{CV}$ between the rest of the ROIs were small, but $R2_{CV}$ increased with fat level of the regions, with measurements of untrimmed belly yielding highest performance. SNR was naturally not the reason (above 2000), and it might rather be because the higher fat signals decreased the relative disturbance from interferants.

3.5. Regression models

EPA (20:5 n-3) and DHA (22:6 n-3) have 5 and 6 double bonds, respectively, and are among the FAs with highest unsaturation. In addition they have long carbon chains. Prediction models are expected to emphasize spectral features related to these characteristics. Typical

Raman regression coefficients (Fig. 4) showed that the main positively correlated peaks were at 926, 1261 and 1666 cm^{-1}, which can all be associated with unsaturated modes, as discussed in section 3.2. The main negatively correlated peaks were at 1012, 1084 and 1442 cm^{-1}, which indicated that there were some indirect modelling of proteins and saturated fatty acids. These are the same characteristics as in previous work on %EPA + DHA estimation in homogenized salmon samples [30, 33]. For the NIR models, the positions around 1701–1706 nm and 1160 nm stood out with high positive weights. The positive weighting around 1701–1706 nm in combination with the negative weighting at 1723 suggested that a shift in the peak around 1723 towards lower wavelengths was important for the model. These characteristics are in accordance with high unsaturation [25,49].

3.6. Raman versus NIR hyperspectral imaging

3.6.1. Performance and robustness

The feasibility of in-line estimation of %EPA + DHA using Raman and NIR spectroscopy, as well as the robustness of the established models, were indicated by the cross validation on the calibration set and the test set performances. These results are summarized in Tables 1 and 2. We show also test set performances when predictions are corrected for bias-and-slope errors. Such errors are oftentimes acceptable for deployment in the industry because models can be recalibrated when new sample types are introduced. However, in certain applications (e.g. genetics studies), performance on new samples should be high without the need of a recalibration. Therefore both uncorrected and corrected test set metrics are relevant to consider. Based on the cross validation on the calibration set, results were excellent for both NIR and Raman. This showed that both methods are viable options for estimation of fatty acid features in salmon fillets at high speeds and indicate that both can handle variations in total fat levels and variations in the ratio between EPA and DHA. Overall, the Raman models needed considerably lower numbers of latent variables than the NIR models to reach similar performances. This is in accordance with observations by Afseth et al. [33] for homogenized salmon and, as they discuss, can be regarded a testimony of the chemical specificity of the Raman spectral features. This makes models more interpretable and might make models less sensitive to interferants. Examples of relevant interferants were signals from water, bone, blood remnants or protein content in fillets, which have more overlapping signals in NIR than for Raman, due to their different nature.

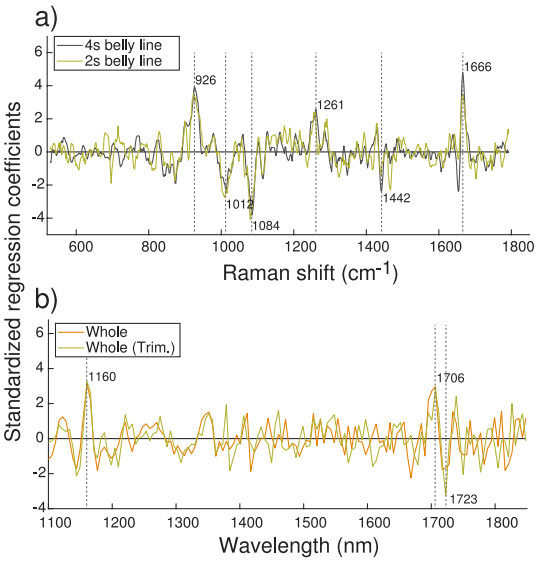

Fig. 4. Standardized regression vectors for the different subsets of Raman data (a) and NIR data (b), as calculated from the calibration set and applied on the test set measurements. For Raman, regression coefficients are shown for both 4s and 2s exposure measurements.

The question was how sensitive these models were to interferants and how dependent they were on conserved correlations between FA parameters in the salmon fillets. This was elucidated by the test set. Predictions on test set samples were generally much less biased for Raman models than the NIR models for which biases were several times higher and varied considerably between different sampling strategies. There was a certain trend (Table 2) that measurements of low fat regions (i.e loin and trimmed fillets) had high biases, while the measurements of high fat regions had lower biases (i.e untrimmed fillets), again reinforcing the impression that higher fat signals decreased the relative spectrum disturbances. The large biases led to odd R2 and RMSEP values. In comparison, biases for the Raman predictions were low and stable for all sampling strategies. In addition, the repeatability of predictions from NIR were overall lower than for Raman, which was reflected by the higher pooled standard deviation of the predictions. For Raman, the repeatability among the different sampling strategies correlated clearly with SNR, and more clearly at 2s exposure time than at 4s ($r_{4s} = -0.83$ and $r_{2s} = -0.94$), which again emphasized the importance of SNR for Raman.

From the bias-and-slope corrected test set predictions, variance errors were identifiable. For both methods, corrected performances were overall excellent. This showed that as long as we assume that slope and bias errors can be corrected during model deployment, NIR is a good option as well. Considering both corrected and uncorrected performances, the best case NIR results were obtained from measurements on untrimmed whole fillets, which stood out with high $R2_{corr}$ values, low bias and the highest repeatability (Table 2). For Raman, the best case result was obtained for line scan on the untrimmed belly, which gave high $R2_{corr}$ values, high repeatability and lowest bias and slope errors (Table 1). For comparison between methods, the Raman measurements at 2s exposure time is most relevant due to the most similar scanning speed as the NIR measuremements. In Fig. 5 we compared the best case test set validation results for NIR and Raman at 2s exposure time. For NIR, R2corr was high for all number of components above 5, but it was evident that some PLS components in the NIR model were particularly disturbing with respect to bias, indicating a more unstable situation than for Raman. In comparison, Raman had high $R2_{corr}$ levels and low bias which were both stable across all components. In addition, there were higher variance errors in the NIR predictions, particularly at low %EPA + DHA levels. This reinforces the importance of high FA signals for NIR. Analysis of variance on the squared test set residuals showed that the best case performance for Raman measurements were significantly higher than NIR at 1% significance level ($p = 0.000013$) when slope-and-bias errors were not corrected, but not significant when residuals were slope-and-bias corrected ($p = 0.28$).

One should keep in mind that, for NIR measurements, differences in water loss due to small deviations in the calibration and test set thawing procedure or differences in sample temperatures might have occurred and influenced results. The repair and recalibration of the NIR instrument between the calibration and test set acquisition could also have an impact. Therefore, any clear conclusion on the comparability of Raman and NIR with respect to robustness of fast in-line %EPA + DHA estimation can not be made. However, this study indicated, in accordance with the nature of the narrow Raman bands versus the broader NIR bands, that Raman is more robust.

3.6.2. Prediction of other fatty acid features

For a broader comparison of the Raman and NIR measurement methods, Fig. C.10 shows predictions of many other FA parameters for

Table 2
PLS regression results for EPA + DHA in salmon fillets (% of total fat), using NIR hyperspectral images. Cross validated results for the calibration set (CV) and test set validation results are shown. For the test set validation, metrics corrected for bias and slope errors are indicated as well (corr).

Sampling method		Calibration set			Test set					Corrected test set	
Fillet version	Region of interest	LV[a]	$R2_{CV}$	$RMSE_{CV}$	R2	RMSEP	Bias	Slope	STD_{pooled}[b]	$R2_{corr}$	$RMSE_{corr}$
–	Loin	13	0.87	0.58	−19.80	12.26	12.19	1.00	0.70	0.80	1.20
untrimmed	Whole	14	0.95	0.37	0.90	0.86	−0.22	1.21	0.19	0.97	0.49
untrimmed	Belly	14	0.97	0.28	−0.08	2.80	−2.72	1.12	0.40	0.97	0.47
trimmed	Whole	16	0.94	0.40	−8.27	8.19	8.15	1.03	0.50	0.93	0.73
trimmed	Belly	15	0.96	0.32	−4.36	6.23	−6.18	1.12	0.51	0.95	0.61

[a] Latent variables.
[b] Pooled standard deviation (repeatability).

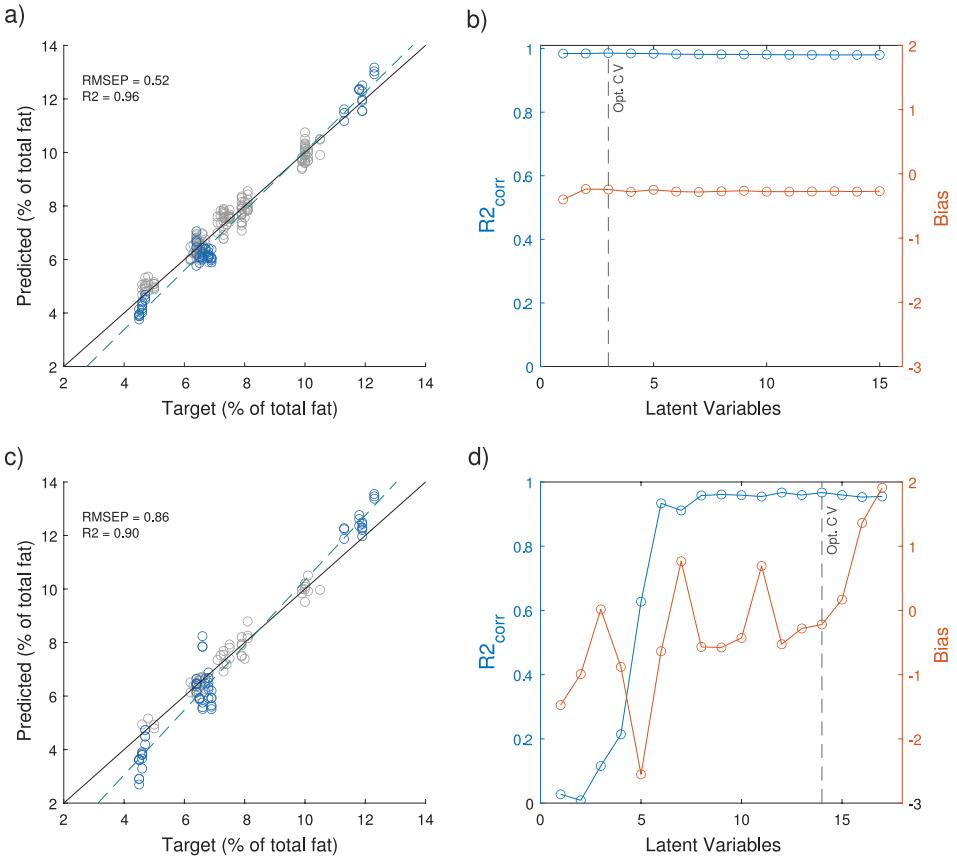

Fig. 5. Overview of the best case results from PLS regression for prediction of %EPA + DHA from Raman measurements at 2s exposure time (a–b) and NIR measurements (c–d). The highest Raman performance was obtained from belly line scans of untrimmed fillet. For NIR, highest performance was obtained for the whole untrimmed fillet. The predicted versus measured EPA + DHA concentrations (a,c) for the test set (blue) is included, and compared with the calibration set (grey). The performances on the test set as a function of latent variables in the models are shown (b,d), including bias and R2 corrected for the bias-and-slope errors. (For interpretation of the references to colour in this figure legend, the reader is referred to the Web version of this article.)

the calibration set. Interpretation of the additional models was out of scope for this article, but it should be noted that predictions for most FAs were high. Covariance between EPA + DHA and other fatty acids or chemical components in the salmon fillets can be an issue if the correlations are different in future samples. In literature, model dependence on conserved correlations has been termed the cage of covariance, and challenges related to this issue for estimation of specific FAs have been demonstrated by Eskildsen et al. and others [21,33,35]. In our calibration samples, the strongest correlations with %EPA + DHA were found for the sum of saturated FAs (r = 0.92), sum of monoenoic FAs (r = −0.91) and the fatty acid 18:3 n-3 (r = −0.94). The correlation with total fat in the samples was low (- 0.17). Furthermore, the correlation between EPA and DHA was moderate (r = 0.74), which showed that they to some extent vary independently across different feeding regimes (Fig.

A.6). In the test set samples, the correlations between the FA properties were overall considerably higher than in the calibration samples (Fig. A.6). Predictions on the calibration set (Fig.C.10) showed that separate DHA models were also excellent for both Raman and NIR, but separate EPA models were less successful (albeit not significantly). However, taking into account the high spectral similarity between these two fatty acids [33] and the moderate correlation between them in the calibration set, we cannot expect them to be predicted independently. Predicting the EPA and DHA as a joint concentration value is a good compromise, keeping also in mind that both have been related to positive health effects.

Berhe et al. [35] found that estimation of specific fatty acids in pork backfat from Raman spectra were indirect and to a large degree dependent on the total FA parameters (i.e Iodine value and total PUFA). In our case, the cross validated IV model and total PUFA model showed poor performances for both Raman and NIR (Fig. C.10), which makes it unlikely that %EPA + DHA was indirectly modelled based on total unsaturation (number of double bonds) or total PUFA content. This corresponds to results recently shown by Afseth et al. [33] for homogenized salmon and illustrates that such issues are dependent on the samples and the variations in the calibration set. It can, however, be noted that the salmon in the work of Afseth et al. [33] were all from the same population and were fed a specific diet, and hence represented a sample set with variations of different origin than the sample set used in our work. Interestingly, slope-and-bias-corrected performances on our test set showed that prediction of IV and total PUFA was considerably improved in comparison to the calibration set (Fig. C.11). This is most likely related to the higher correlations with the individual FAs in the test set samples (Fig.A.6). This suggests that IV and PUFA models were based on correlations with specific FAs. In this work, we successfully removed the issue of indirect modelling on total fat content by a combination of estimating the %EPA + DHA content as percentage of total fat, by the sampling method and by normalising spectra by the EMSC pre-processing. This can be seen by the abysmal cross validated performance of total fat estimation for both Raman and NIR (Fig. C.10). The strategy of estimating the %EPA + DHA content as percentage of total fat was also followed by Berhe et al. [35].

Indirect modelling on other chemical components might be an issue as well. There were few samples within each farming location (i.e feed group) and therefore low variance within each group. This increases the risk that models might rely on other dissimilarities between the groups, such as different fillet structures, composition or water content. Band regions related to proteins were weighted negatively in Raman regression coefficients (i.e. phenylalanine), which might suggest that such indirect modelling on protein content come in to play. For Raman, this region can be removed. For NIR, overlapping bands make such solutions harder to find.

3.6.3. Other practical considerations

Choosing Raman or NIR relies also on practical considerations. The scope of possible applications might be different for the two methods. For example, one is often interested in the total fat content in the fillet and not only the composition of the fat. Estimation of total fat content is undoubtedly possible with NIR [22,23] and have already been implemented in the industry. Raman has been used to measure total fat content previously and showed reasonable laboratory results for heterogeneous salmon by-products [53]. However, it could be more challenging with the indicated Raman scanning procedures in this study, since the whole salmon fillet is not covered and heterogeneity is a challenge. Therefore, a system combining total fat analyses with compositional analyses might be harder to achieve with Raman.

Another practical challenge is sample variations over time. During the seasons, the balance between phospholipids and triglycerides (TAGs) of the fillets can vary due to variation in total fat content, with autumn being the main period for fat deposition and spring the main period for fat burning [54–57]. While the phospholipids are quite stable and high in EPA + DHA composition, the composition of the TAGs are to a large extent dependent on the feed [11,58]. Therefore seasonal variations in the total fat level can still affect the FA composition. This means that fatty fillets may have lower EPA + DHA percentage than lean fillets, when measured as % of total fats, while the quantitative EPA + DHA levels could in fact be higher [59]. This should be taken into account in future strategy developments.

With respect to the practical measurements, the SNR was important for Raman. SNR variations across the different subsets correlated considerably with the corresponding estimation errors, suggesting that SNR is the main motivator in choice of measurement strategy. The results indicated that at high conveyor belt speeds, low fat deposition regions of the fillet (i.e the loin) should be avoided during signal accumulation in order to optimize SNR. In practice, this could be achieved by employing robotic control of the probe to target high fat regions of the fillet (i.e the belly). This presents further system development and additional cost for Raman employment in the industry. Furthermore, it is important to investigate the heterogeneity of the salmon fillets more thoroughly. While we know that total fat levels vary over the fillet [52], uncertainty still remains about how much the composition of the fat vary within a fillet. In the study of Nanton et al. [52] examples (N = 3) of moderate differences in EPA and DHA composition in different parts of salmon fillets were seen. Such spatial variations could potentially challenge the Raman measurements. To the author's knowledge, larger studies on compositional variations over a fillet is lacking in the literature and should be conducted.

4. Conclusion

This work showed that a Raman scanning strategy and NIR hyperspectral imaging are both viable methods for in-line measurements of EPA + DHA concentrations in intact salmon fillets. This study indicated that Raman might be more robust towards matrix effects, which likely means a reduced need for calibration maintenance in comparison to NIR. For Raman, the loin scans exhibited too low SNR and resulted in poor performances. Therefore a robotic solution for Raman measurements in the industry might be needed in order to target high fat areas on the fillet during signal accumulation. In addition, there were indications that reducing the exposure time below 2s might be challenging with respect to spectrum quality. This suggested that at this point in time, Raman might be best suited for fast at-line measurements in applications where robustness is important. NIR hyperspectral imaging is currently best suited for industrial employment, but must likely be followed up more closely with calibration maintenance.

Funding

This work was partially funded by the Research Council of Norway through the projects SFI Digital Food Quality and the Food Pilot Plant [grant numbers 309259, 296,083]; along with The Agricultural and Food Industry Research Funds through the project Precision Food Production [grant number 314111].

Credit author statement

Tiril Aurora Lintvedt: Methodology, Formal analysis, Investigation, Data curation, Writing – Original Draft, Visualization. **Petter Vejle Andersen**: Methodology, Investigation, Writing – Review and Editing. **Nils Kristian Afseth**: Conceptualization, Methodology, Writing – Review and Editing, Supervision. **Karsten Heia**: Methodology, Investigation, Writing – Review and Editing, Supervision. **Stein-Kato Lindberg**: Formal Analysis, Investigation. **Jens Petter Wold:** Conceptualization, Methodology, Writing – Review and Editing, Supervision.

Declaration of competing interest

The authors declare the following financial interests/personal relationships which may be considered as potential competing interests: Tiril Aurora Lintvedt reports equipment, drugs, or supplies was provided by MarqMetrix Inc.

Data availability

Data will be made available on request.

Acknowledgements

We would like to express a special thanks to MarqMetrix Inc. for providing Raman instrumentation through the partnership in the SFI Digital Food Quality project. We also extend our thanks to Thomas Larsson, Arnaud Lefrancois, Tatiana N. Ageeva, Amanda Katrine Karlsen, Samuel Ortega Sarmiento, Gustav Martinsen and Ambjørn Bardal at Nofima for assistance during sample preparation and data acquisition.

Appendix A. Correlations and variation in reference measurements

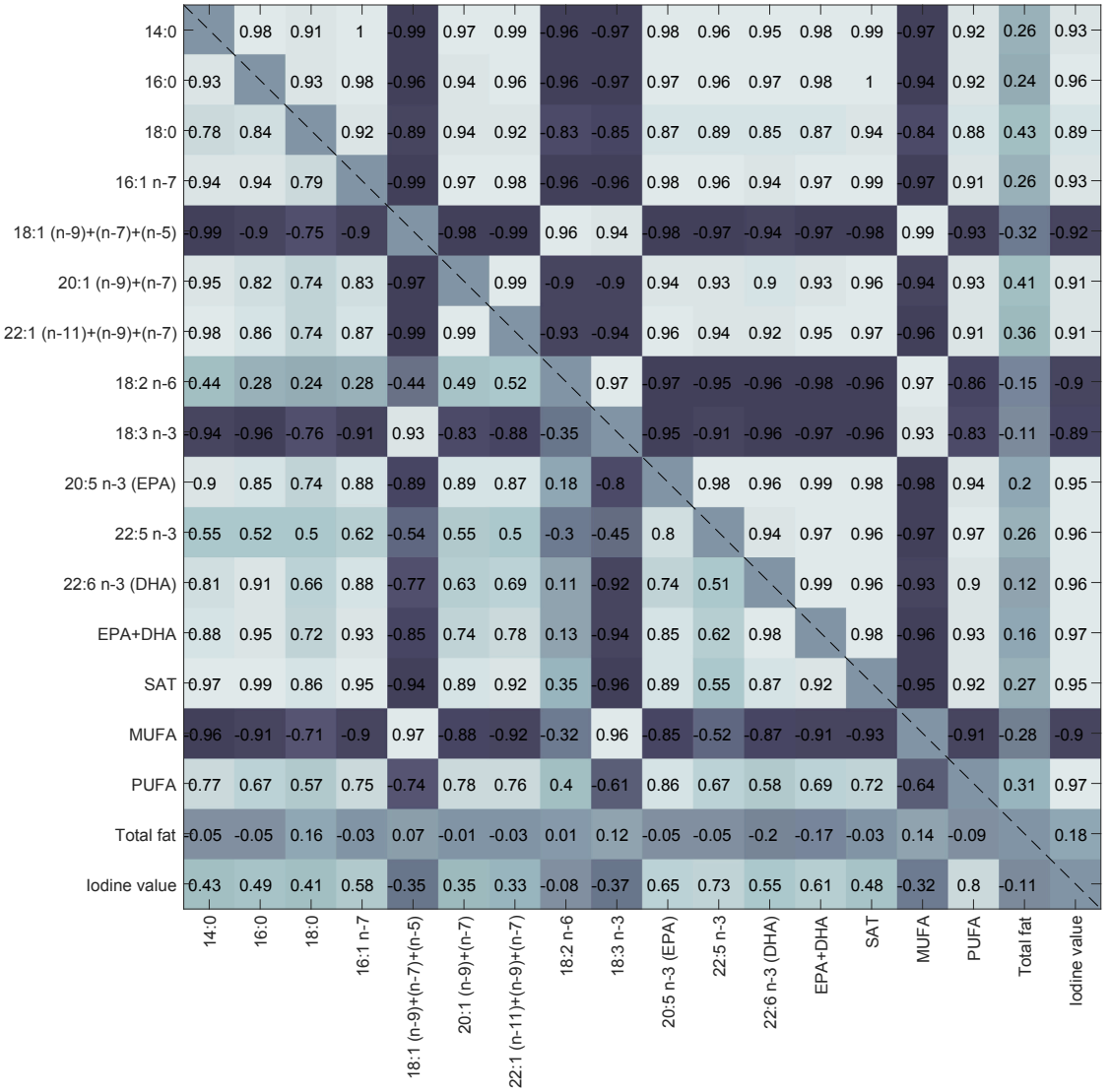

Fig. A.6. Correlation map between reference measurements of the main FAs and total FA parameters for the calibration samples (below diagonal) and the test set samples (above diagonal).

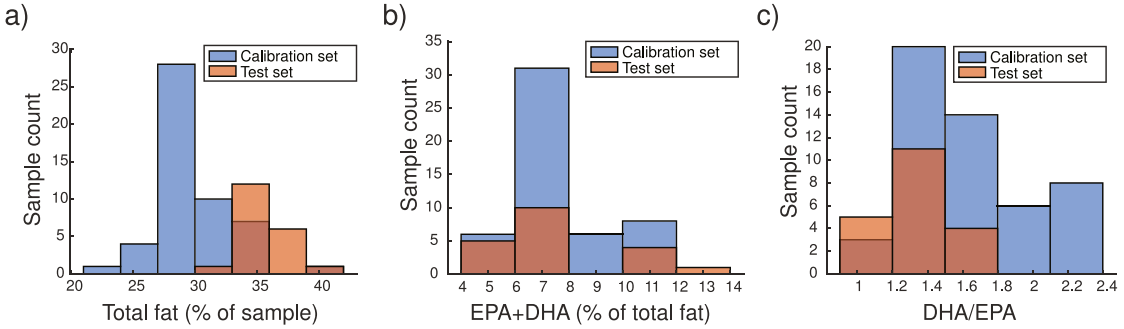

Fig. A.7. Sample distributions of total fat (a), %EPA + DHA (b) and the DHA/EPA ratio, compared between calibration and test set.

Appendix B. Additional spectral data

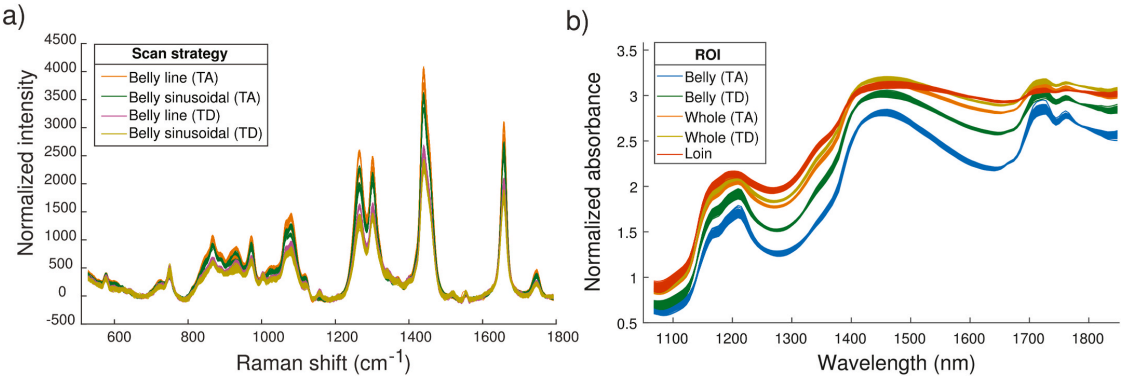

Fig. B.8. Pre-processed Raman test set data (a) and NIR test set data (b).

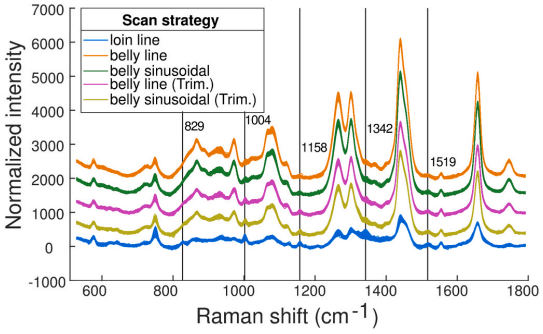

Fig. B.9. Raman measurements of calibration set samples, with introduced offset for clarity.

Appendix C. Modelling additional fatty acid parameters

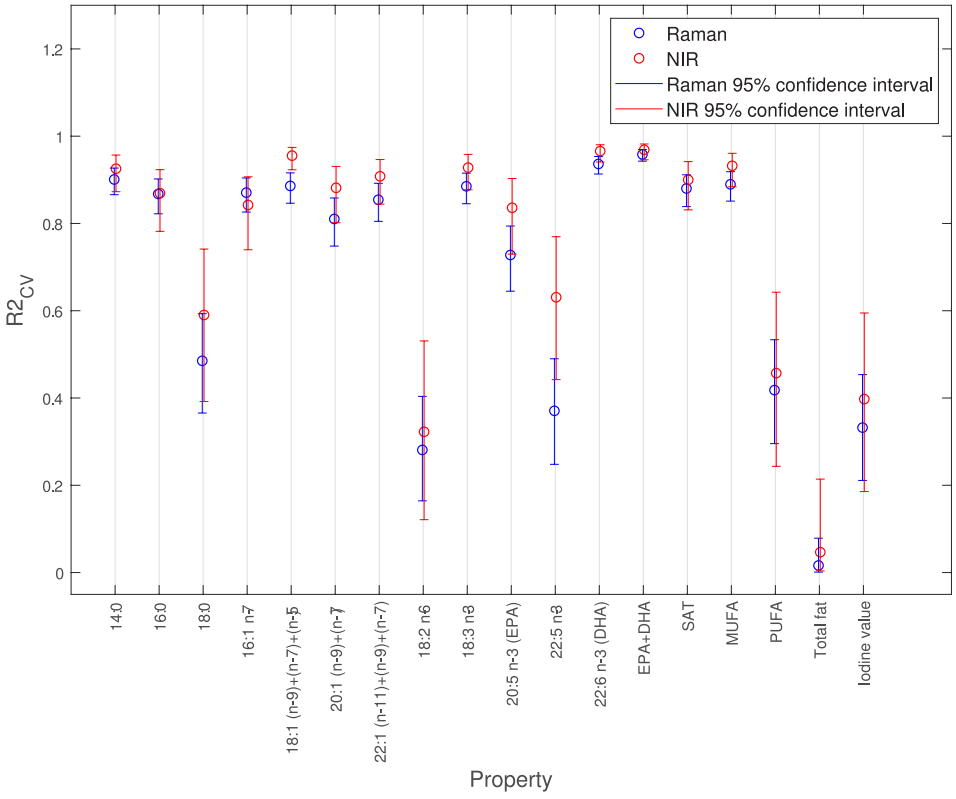

Fig. C.10. Cross validated performances on calibration set for the most important fatty acids parameters, comparing the Raman belly line scans of untrimmed fillet at 2s exposure with the NIR measurements on whole untrimmed fillets. These measurement methods were considered the best case results with respect to %EPA + DHA estimation.

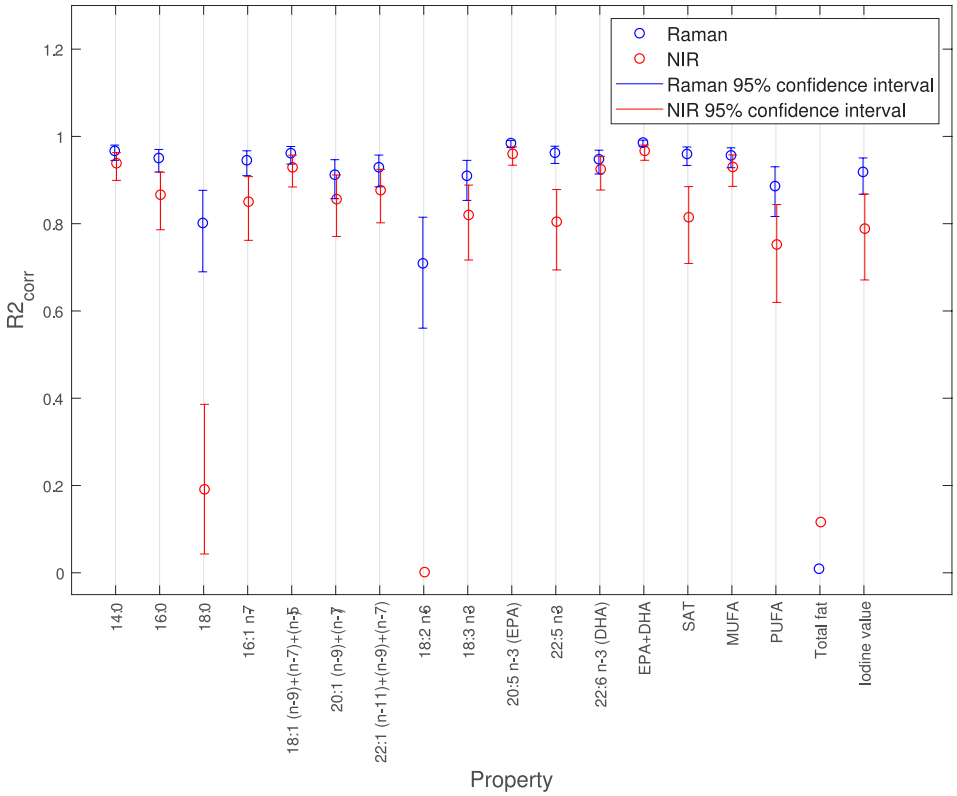

Fig. C.11. Test set performances for estimation of the most important fatty acids parameters, comparing the Raman belly line scans of untrimmed fillet at 2s exposure with the NIR measurements on whole untrimmed fillets. These measurement methods were considered the best case results with respect to %EPA + DHA estimation.

References

[1] P.C. Calder, Marine omega-3 fatty acids and inflammatory processes: effects, mechanisms and clinical relevance, Biochim. Biophys. Acta Mol. Cell Biol. Lipids 1851 (4) (2015) 469–484, https://doi.org/10.1016/j.bbalip.2014.08.010.

[2] A. Eilander, D.C. Hundscheid, S.J. Osendarp, C. Transler, P.L. Zock, Effects of n-3 long chain polyunsaturated fatty acid supplementation on visual and cognitive development throughout childhood: a review of human studies, Prostaglandins Leukot. Essent. Fatty Acids 76 (4) (2007) 189–203, https://doi.org/10.1016/j.plefa.2007.01.003.

[3] M.M. Rogero, P.C. Calder, Obesity, inflammation, toll-like receptor 4 and fatty acids, Nutrients 10 (4) (2018), https://doi.org/10.3390/nu10040432.

[4] C.H. Ruxton, S.C. Reed, M.J. Simpson, K.J. Millington, The Health Benefits of Omega-3 Polyunsaturated Fatty Acids: A Review of the Evidence, oct 2004, https://doi.org/10.1111/j.1365-277X.2004.00552.x.

[5] R.N. Thota, J.J.A. Ferguson, K.A. Abbott, C.B. Dias, M.L. Garg, Science behind the cardio-metabolic benefits of omega-3 polyunsaturated fatty acids: biochemical effects vs. clinical outcomes, Nutrients 9 (7) (2018) 3576–3596, https://doi.org/10.1039/c8fo00348c.

[6] M. Todorčević, L. Hodson, The effect of marine derived n-3 fatty acids on adipose tissue metabolism and function, J. Clin. Med. 5 (1) (2015), https://doi.org/10.3390/jcm5010003.

[7] J.G. Bell, J. McEvoy, D.R. Tocher, F. McGhee, P.J. Campbell, J.R. Sargent, Replacement of fish oil with rapeseed oil in diets of atlantic salmon (salmo salar) affects tissue lipid compositions and hepatocyte fatty acid metabolism, J. Nutr. 131 (5) (2001) 1535–1543, https://doi.org/10.1093/jn/131.5.1535.

[8] J.G. Bell, J. Pratoomyot, F. Strachan, R.J. Henderson, R. Fontanillas, A. Hebard, D. R. Guy, D. Hunter, D.R. Tocher, Growth, flesh adiposity and fatty acid composition of atlantic salmon (salmo salar) families with contrasting flesh adiposity: effects of replacement of dietary fish oil with vegetable oils, Aquaculture 306 (1–4) (2010) 225–232, https://doi.org/10.1016/j.aquaculture.2010.05.021.

[9] B.E. Torstensen, J.G. Bell, G. Rosenlund, R.J. Henderson, I.E. Graff, D.R. Tocher, Ø. Lie, J.R. Sargent, Tailoring of atlantic salmon (salmo salar l.) flesh lipid composition and sensory quality by replacing fish oil with a vegetable oil blend, J. Agric. Food Chem. 53 (26) (2005) 10166–10178, https://doi.org/10.1021/jf051308i.

[10] S.S. Horn, B. Ruyter, T.H.E. Meuwissen, B. Hillestad, A.K. Sonesson, Genetic effects of fatty acid composition in muscle of atlantic salmon, Genet. Sel. Evol. 50 (1) (2018), https://doi.org/10.1186/s12711-018-0394-x.

[11] D.R. Tocher, J.G. Bell, F. McGhee, J.R. Dick, J. Fonseca-Madrigal, Effects of dietary lipid level and vegetable oil on fatty acid metabolism in atlantic salmon (salmo salar l.) over the whole production cycle, Fish Physiol. Biochem. 29 (3) (2003) 193–209, https://doi.org/10.1023/B:FISH.0000045722.44186.ee.

[12] G.M. Turchini, D.S. Francis, R.S.J. Keast, A.J. Sinclair, Transforming salmonid aquaculture from a consumer to a producer of long chain omega-3 fatty acids, Food Chem. 124 (2) (2011) 609–614, https://doi.org/10.1016/j.foodchem.2010.06.083.

[13] T. Ytrestøyl, T.S. Aas, T. Åsgård, Utilisation of feed resources in production of atlantic salmon (salmo salar) in Norway, Aquaculture 448 (2015) 365–374, https://doi.org/10.1016/j.aquaculture.2015.06.023.

[14] P.D. Nichols, B. Glencross, J.R. Petrie, S.P. Singh, Readily available sources of long-chain omega-3 oils: is farmed australian seafood a better source of the good oil than wild-caught seafood? Nutrients 6 (3) (2014) 1063–1079, https://doi.org/10.3390/nu6031063.

[15] M. Sprague, J.R. Dick, D.R. Tocher, Impact of sustainable feeds on omega-3 long-chain fatty acid levels in farmed atlantic salmon, 2006-2015, Sci. Rep. 6 (2016), https://doi.org/10.1038/srep21892.

[16] M. Bou, G.M. Berge, G. Baeverfjord, T. Sigholt, T.K. Østbye, B. Ruyter, Low levels of very-long-chain n-3 pufa in atlantic salmon (salmo salar) diet reduce fish robustness under challenging conditions in sea cages, J. Nutr. Sci. 6 (2017), https://doi.org/10.1017/jns.2017.28.

[17] E. Lutfi, G. M. Berge, G. Bæverfjord, T. Sigholt, M. Bou, T. Larsson, T. Mørkøre, Ø. Evensen, N. H. Sissener, G. Rosenlund, L. Sveen, T.-K. Østbye, B. Ruyter, Increasing

dietary levels of the n-3 long-chain pufa, epa and dha, improves the growth, welfare, robustness and fillet quality of atlantic salmon in sea cages, Br. J. Nutr. 1–19.
[18] M.M. Cascant, C. Breil, A.S. Fabiano-Tixier, F. Chemat, S. Garrigues, M. de la Guardia, Determination of fatty acids and lipid classes in salmon oil by near infrared spectroscopy, Food Chem. 239 (2018) 865–871, https://doi.org/10.1016/j.foodchem.2017.06.158.
[19] M.Y. Bekhit, B. Grung, S.A. Mjøs, Determination of omega-3 fatty acids in fish oil supplements using vibrational spectroscopy and chemometric methods, Appl. Spectrosc. 68 (10) (2014) 1190–1200, https://doi.org/10.1366/13-07210.
[20] M.R. Brown, P.D. Kube, R.S. Taylor, N.G. Elliott, Rapid compositional analysis of atlantic salmon (salmo salar) using visible-near infrared reflectance spectroscopy, Aquacult. Res. 45 (5) (2014) 798–811, https://doi.org/10.1111/are.12021.
[21] C.E. Eskildsen, T. Næs, P.B. Skou, L.E. Solberg, K.R. Dankel, S.A. Basmoen, J. P. Wold, S.S. Horn, B. Hillestad, N.A. Poulsen, M. Christensen, T. Pieper, N. K. Afseth, S.B. Engelsen, Cage of covariance in calibration modeling: regressing multiple and strongly correlated response variables onto a low rank subspace of explanatory variables, Chemometr. Intell. Lab. Syst. 213 (2021), https://doi.org/10.1016/j.chemolab.2021.104311.
[22] T. Isaksson, G. Tøgersen, A. Iversen, K.I. Hildrum, Non-destructive determination of fat, moisture and protein in salmon fillets by use of near-infrared diffuse spectroscopy, J. Sci. Food Agric. 69 (1) (1995) 95–100, https://doi.org/10.1002/jsfa.2740690115.
[23] J.P. Wold, M. Kermit, V.H. Segtnan, Chemical imaging of heterogeneous muscle foods using near-infrared hyperspectral imaging in transmission mode, Appl. Spectrosc. 70 (6) (2016) 953–961, https://doi.org/10.1177/0003702816641260.
[24] V.H. Segtnan, M. Høy, F. Lundby, B. Narum, J.P. Wold, Fat distribution analysis in salmon fillets using non-contact near infrared interactance imaging: a sampling and calibration strategy, J. Near Infrared Spectrosc. 17 (5) (2009) 247–253, https://doi.org/10.1255/jnirs.851.
[25] F. Westad, A. Schmidt, M. Kermit, Incorporating chemical band-assignment in near infrared spectroscopy regression models, J. Near Infrared Spectrosc. 16 (3) (2008) 265–273, https://doi.org/10.1255/jnirs.786.
[26] N.K. Afseth, V.H. Segtnan, B.J. Marquardt, J.P. Wold, Raman and near-infrared spectroscopy for quantification of fat composition in a complex food model system, Appl. Spectrosc. 59 (11) (2005) 1324–1332, https://doi.org/10.1366/000370205774783304.
[27] N.K. Afseth, J.P. Wold, V.H. Segtnan, The potential of Raman spectroscopy for characterisation of the fatty acid unsaturation of salmon, Anal. Chim. Acta 572 (1) (2006) 85–92, https://doi.org/10.1016/j.aca.2006.05.013.
[28] J.R. Beattie, S.E. Bell, C. Borgaard, A. Fearon, B.W. Moss, Prediction of adipose tissue composition using Raman spectroscopy: average properties and individual fatty acids, Lipids 41 (3) (2006) 287–294, https://doi.org/10.1007/s11745-006-5099-1.
[29] D.P. Killeen, S.N. Marshall, E.J. Burgess, K.C. Gordon, N.B. Perry, Raman spectroscopy of fish oil capsules: polyunsaturated fatty acid quantitation plus detection of ethyl esters and oxidation, J. Agric. Food Chem. 65 (17) (2017) 3551–3558, https://doi.org/10.1021/acs.jafc.7b00099.
[30] T.A. Lintvedt, P.V. Andersen, N.K. Afseth, B. Marquardt, L. Gidskehaug, J.P. Wold, Feasibility of in-line Raman spectroscopy for quality assessment in food industry - how fast can we go? Appl. Spectrosc. 76 (5) (2022) 559–568, https://doi.org/10.1177/00037028211056931.
[31] H. Wikström, I.R. Lewis, L.S. Taylor, Comparison of sampling techniques for in-line monitoring using Raman spectroscopy, Appl. Spectrosc. 59 (7) (2005) 934–941, https://doi.org/10.1366/0003702054411553.
[32] Y. Ozaki, C.W. Huck, K.B. Beć, Near-ir spectroscopy and its applications, in: V. Gupta (Ed.), Molecular and Laser Spectroscopy: Advances and Applications, Elsevier, 2018, pp. 11–38, https://doi.org/10.1016/B978-0-12-849883-5.00002-4. Ch. 2.
[33] N.K. Afseth, K. Dankel, P.V. Andersen, G.F. Difford, S.S. Horn, A. Sonesson, B. Hillestad, J.P. Wold, E. Tengstrand, Raman and near infrared spectroscopy for quantification of fatty acids in muscle tissue—a salmon case study, Foods 11 (962) (2022), https://doi.org/10.3390/foods11070962.
[34] E.G. Bligh, W.J. Dyer, A rapid method of total lipid extraction and purification, Can. J. Biochem. Physiol. 37 (8) (1959) 911–917, https://doi.org/10.1139/o59-099.
[35] D.T. Berhe, C.E. Eskildsen, R. Lametsch, M.S. Hviid, F. van den Berg, S.B. Engelsen, Prediction of total fatty acid parameters and individual fatty acids in pork backfat using Raman spectroscopy and chemometrics: understanding the cage of covariance between highly correlated fat parameters, Meat Sci. 111 (2016) 18–26, https://doi.org/10.1016/j.meatsci.2015.08.009.
[36] A. Savitzky, M.J. Golay, Smoothing and differentiation of data by simplified least squares procedures, Anal. Chem. 36 (8) (1964) 1627–1639, https://doi.org/10.1021/ac60214a047.
[37] H. Martens, E. Stark, Extended multiplicative signal correction and spectral interference subtraction: new preprocessing methods for near infrared spectroscopy, J. Pharm. Biomed. Anal. 9 (8) (1991) 625–635, https://doi.org/10.1016/0731-7085(91)80188-F.
[38] K.H. Liland, A. Kohler, N.K. Afseth, Model-based pre-processing in Raman spectroscopy of biological samples, J. Raman Spectrosc. 47 (6) (2016) 643–650, https://doi.org/10.1002/jrs.4886.
[39] P.H.C. Eilers, H.F.M. Boelens, Baseline correction with asymmetric least squares smoothing, Life Sci. (2005) 1–26.
[40] K.H. Liland, T. Almøy, B.H. Mevik, Optimal choice of baseline correction for multivariate calibration of spectra, Appl. Spectrosc. 64 (9) (2010) 1007–1016, https://doi.org/10.1366/000370210792434350.
[41] H. Martens, T. Næs, Multivariate Calibration, second ed., Wiley, Chichester, UK, 1989.
[42] Å. Björck, U.G. Indahl, Fast and stable partial least squares modelling: a benchmark study with theoretical comments, J. Chemom. 31 (8) (2017), https://doi.org/10.1002/cem.2898.
[43] F. Westad, H. Martens, Variable selection in near infrared spectroscopy based on significance testing in partial least squares regression, J. Near Infrared Spectrosc. 8 (2) (2000) 117–124, https://doi.org/10.1255/jnirs.271.
[44] R.A. Fisher, Frequency distribution of the values of the correlation coefficient in samples from an indefinitely large population, Biometrika (1915), https://doi.org/10.2307/2331838.
[45] R.A. Fisher, On the" probable error" of a coefficient of correlation deduced from a small sample, 1, 1921, pp. 3–32.
[46] S. Guo, C. Beleites, U. Neugebauer, S. Abalde-Cela, N.K. Afseth, F. Alsamad, S. Anand, C. Araujo-Andrade, S. Aškrabić, E. Avci, M. Baia, M. Baranska, E. Baria, L.A. Batista De Carvalho, P. De Bettignies, A. Bonifacio, F. Bonnier, E.M. Brauchle, H.J. Byrne, I. Chourpa, R. Cicchi, F. Cuisinier, M. Culha, M. Dahms, C. David, L. Duponchel, S. Duraipandian, S.F. El-Mashtoly, D.I. Ellis, G. Eppe, G. Falgayrac, O. Gamulin, B. Gardner, P. Gardner, K. Gerwert, E.J. Giamarellos-Bourboulis, S. Gizurarson, M. Gnyba, R. Goodacre, P. Grysan, O. Guntinas-Lichius, H. Helgadottir, V.M. Grošev, C. Kendall, R. Kiselev, M. Kölbach, C. Krafft, S. Krishnamoorthy, P. Kubryck, B. Lendl, P. Loza-Alvarez, F.M. Lyng, S. Machill, C. Malherbe, M. Marro, M.P.M. Marques, E. Matuszyk, C.F. Morasso, M. Moreau, H. Muhamadali, V. Mussi, I. Notingher, M.Z. Pacia, F.S. Pavone, G. Penel, D. Petersen, O. Piot, J.V. Rau, M. Richter, M.K. Rybarczyk, H. Salehi, K. Schenke-Layland, S. Schlücker, M. Schosserer, K. Schütze, V. Sergo, F. Sinjab, J. Smulko, G. D. Sockalingum, C. Stiebing, N. Stone, V. Untereiner, R. Vanna, K. Wieland, J. Popp, T. Bocklitz, Comparability of Raman spectroscopic configurations: a large scale cross-laboratory study, Anal. Chem. 92 (24) (2020) 15745–15756, https://doi.org/10.1021/acs.analchem.0c02696.
[47] K. Czamara, K. Majzner, M.Z. Pacia, K. Kochan, A. Kaczor, M. Baranska, Raman spectroscopy of lipids: a review, J. Raman Spectrosc. 46 (1) (2015) 4–20, https://doi.org/10.1002/jrs.4607.
[48] G. Socrates, Alkenes, oximes, imines, amidines, azo compounds: C=c, c=n, n=n groups, in: Infrared and Raman Characteristic Group Frequencies: Tables and Charts, third ed., John Wiley and Sons, 2004, p. 74.
[49] P. Hourant, V. Baeten, M.T. Morales, M. Meurens, R. Aparicio, Oil and fat classification by selected bands of near-infrared spectroscopy, Appl. Spectrosc. 54 (8) (2000) 1168–1174, https://doi.org/10.1366/0003702001950733.
[50] D. Cozzolino, I. Murray, A. Chree, J.R. Scaife, Multivariate determination of free fatty acids and moisture in fish oils by partial least-squares regression and near-infrared spectroscopy, LWT–Food Sci. Technol. 38 (8) (2005) 821–828, https://doi.org/10.1016/j.lwt.2004.10.007.
[51] ABB, Aocs standard procedure for iodine value (iv), Appl. Note 2 (2017).
[52] D.A. Nanton, A. Vegusdal, A.M.B. Rørå, B. Ruyter, G. Baeverfjord, B.E. Torstensen, Muscle lipid storage pattern, composition, and adipocyte distribution in different parts of atlantic salmon (salmo salar) fed fish oil and vegetable oil, Aquaculture 265 (1–4) (2007) 230–243, https://doi.org/10.1016/j.aquaculture.2006.03.053.
[53] P.V. Andersen, J.P. Wold, N.K. Afseth, Assessment of bulk composition of heterogeneous food matrices using Raman spectroscopy, Appl. Spectrosc. (2021), https://doi.org/10.1177/00037028211006150.
[54] J.E. Dessen, R. Weihe, B. Hatlen, M.S. Thomassen, K.A. Rørvik, Different growth performance, lipid deposition, and nutrient utilization in in-season (s1) atlantic salmon post-smolt fed isoenergetic diets differing in protein-to-lipid ratio, Aquaculture 473 (2017) 345–354, https://doi.org/10.1016/j.aquaculture.2017.02.006.
[55] T. Mørkøre, K.A. Rørvik, Seasonal variations in growth, feed utilisation and product quality of farmed atlantic salmon (salmo salar) transferred to seawater as 0 + smolts or 1 + smolts, Aquaculture 199 (1–2) (2001) 145–157, https://doi.org/10.1016/S0044-8486(01)00524-5.
[56] U. Nordgarden, B.E. Torstensen, L. Frøyland, T. Hansen, G.I. Hemre, Seasonally changing metabolism in atlantic salmon (salmo salar l.) ii - β-oxidation capacity and fatty acid composition in muscle tissues and plasma lipoproteins, Aquacult. Nutr. 9 (5) (2003) 295–303, https://doi.org/10.1046/j.1365-2095.2003.00260.x.
[57] F. Oppedal, A. Berg, R.E. Olsen, G.L. Taranger, T. Hansen, Photoperiod in seawater influence seasonal growth and chemical composition in autumn sea-transferred atlantic salmon (salmo salar l.) given two vaccines, Aquaculture 254 (1–4) (2006) 396–410, https://doi.org/10.1016/j.aquaculture.2005.10.026.
[58] B. Ruyter, C. Moya-Falcón, G. Rosenlund, A. Vegusdal, Fat content and morphology of liver and intestine of atlantic salmon (salmo salar): effects of temperature and dietary soybean oil, Aquaculture 252 (2–4) (2006) 441–452, https://doi.org/10.1016/j.aquaculture.2005.07.014.
[59] J.R. Sargent, D.R. Tocher, J.G. Bell, The lipids, in: J.E. Halver, R.W. Hardy (Eds.), Fish Nutrition, Academic Press, 2002.

Appendix C

Paper III

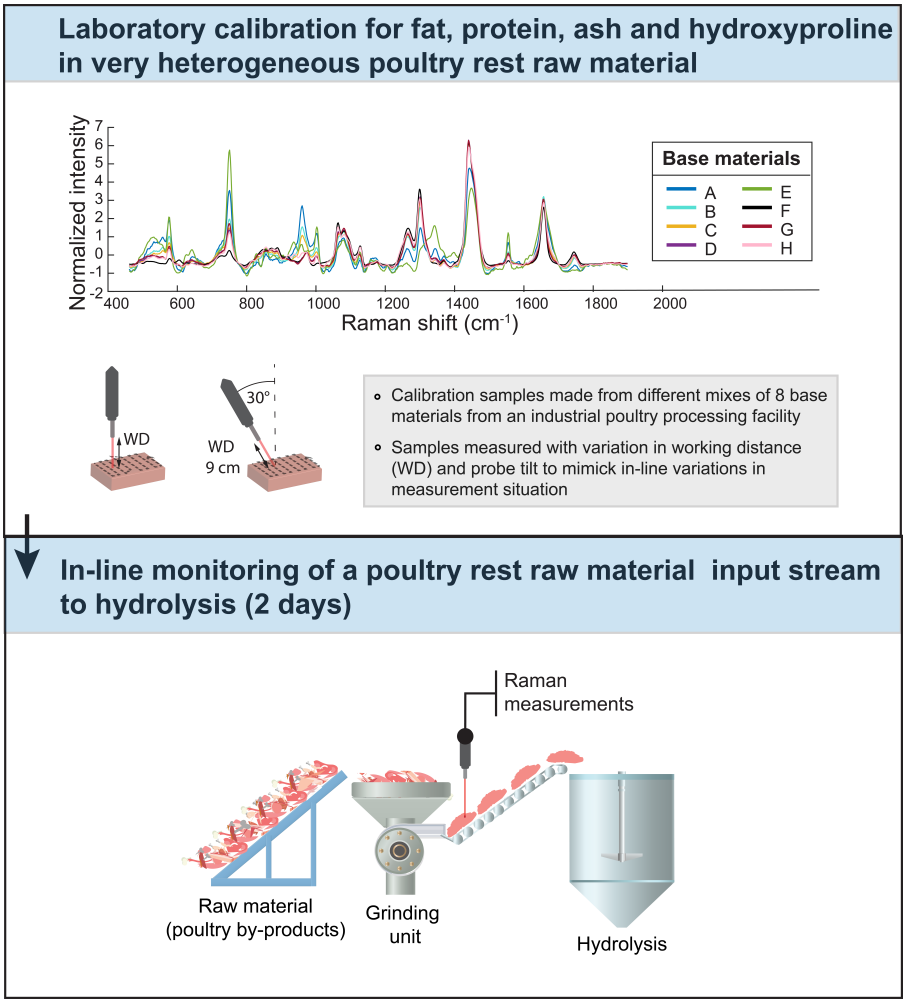

In-line Raman Spectroscopy for Characterization of an Industrial Poultry Raw Material Stream

Tiril Aurora Lintvedt[a,b], Petter Vejle Andersen[a], Nils Kristian Afseth[a], Jens Petter Wold[a]

[a] *Norwegian Institute for Food, Fisheries and Aquaculture Research, Muninbakken 9-13, Breivika, Tromsø, 9291, Norway*
[b] *Faculty of Science and Technology, Norwegian University of Life Sciences, Ås, 1432, Norway*

Abstract

In this work, we evaluated the feasibility of Raman spectroscopy as an in-line raw material characterization tool for industrial process control of the hydrolysis of poultry rest raw material. We established calibrations (N=59) for fat, protein, ash (proxy for bone) and hydroxyproline (proxy for collagen) in ground poultry rest raw material . Calibrations were established in the laboratory using poultry samples with high compositional variation. Samples were measured using a wide area illumination Raman probe at varying working distance (6 cm, 9 cm, 12 cm) and probe tilt angle (0°, 30°) to mimic expected in-line variations in the measurement situation. These moderate variations did not significantly affect performance for any analytes. The obtained calibrations were tested in-line with continuous measurements of the ground poultry by-product stream at a commercial hydrolysis facility over the course of two days. Measurements were acquired under demanding conditions, e.g. large variations in working distance. Reasonable estimates of compositional trends were obtained. Validation samples (N=19) were also reasonably well predicted, with $\mathrm{RMSEP}_{\mathrm{corr}} = [0.14, 1.37, 2.36, 1.51]\%$ for hydroxyproline, protein, fat and ash, respectively. However, there were indications that further calibration development and robustification of pre-processing would be advantageous, particularly with respect to hydroxyproline and protein models. It is the authors' impression that with such efforts, potentially in combination with development of practical measurement setup, the use of Raman spectroscopy as a process control tool for the hydrolysis of poultry rest raw materials is within reach.

Keywords: Raman spectroscopy, Wide Area Illumination (WAI), In-line measurements, Food characterization, Heterogeneous raw materials, Process analytical technology (PAT)
PACS: 0000, 1111
2000 MSC: 0000, 1111

1. Introduction

In recent years, the poultry processing industry have adopted enzymatic protein hydrolysis (EPH) as a strategy to recover constituents from by-products (e.g. carcasses and mechanical deboning residues). In this process, proteins from the by-products are digested and solubilized by proteases. After hydrolysis, the enzyme is inactivated at near-boiling temperatures and the slurry goes into a separator, from which three fractions are recovered; a peptide water phase (i.e. protein hydrolysate), an oil phase and a low value collagen-and-mineral rich solid residue.

Today, recovered constituents from EPH usually end up as lower value feed ingredients (used for e.g. pet food), and for such processes maximising the protein yield is of major importance. In recent years, however, the focus has been shifting towards protein ingredients for higher-paying markets like human consumption. This puts increasing emphasis on protein quality (e.g. producing protein hydrolysates with specific functional or nutritional properties), and not only on protein recovery. The raw materials entering the hydrolysis process are typically very heterogeneous, consisting of different mixes of e.g. water, meat, skin, tendons and bone from chicken and turkey. This variation is a challenge when specific and stable product quality is important. It has been found that poultry raw material variation impacts quality parameters such as peptide size distribution and amino acid composition. [1] Furthermore, the product quality is a function of raw material quality in combination with different process parameters. For instance, collageneous proteins are harder to solubilize than muscle proteins and might require different process settings. [2] Therefore, Wubshet et al. [3] reported a proof-of-concept feed-forward setup, where end-product characteristics (protein yield and average molecular weight) were predicted based on spectroscopic measurements of the raw material in combination with hydrolysis time. They obtained $R^2 = 0.88$ for protein yield and $R^2 = 0.56$ for average molecular weight. These findings illustrate that characterization of the input material has potential to be used in process control for optimization of yield and product quality.

Near-Infrared spectroscopy (NIRS) is a well-established technique for in-line compositional analysis of foods. The technique is particularly suited for estimation of the gross components in foods, such as fat, water and protein. However,

NIRS has clear limitations when it comes to detailed compositional analysis, meaning that targeting detailed chemistry like protein composition can be challenging.[4] Moreover, NIRS models can seldom be transferred directly from laboratory calibration to industry without recalibration or calibration transfer methods. Physical differences between laboratory and industry samples and sampling situation usually lead to large biases.[5, 6] This makes the calibration development and practical application labour intensive. Raman spectroscopy, on the other hand, is a technique that might ease some of these challenges. Raman spectroscopy is a promising spectroscopic technique for in-line food analysis, with the advantage that both gross components, including fat,[7] proteins[7] and bone[8, 9], can be targeted at the same time as more detailed information on protein composition, e.g. the concentration of collagen.[4] In general, recent work have indicated that Raman might be more robust with respect to tackling sample variation than NIRS,[10, 11] due to more unique and non-overlapping analyte fingerprints. This raises the hypothesis that Raman might require less calibration maintenance and could potentially tackle more direct calibration transfer.

A main limitation for in-line compositional analysis with Raman spectroscopy for a heterogeneous raw material stream, is the small sampling volume obtained with the laser. By using Wide Area Illumination (WAI) probes, the laser spot is widened (3-6 mm diameter) compared to traditional Raman probes, which is an advantage when aiming to cover the surface of more heterogeneous materials. As reviewed by Shin and Chung,[12] the WAI probes can improve the accuracy of Raman spectroscopic analysis for a variety of heterogeneous samples (e.g. in the pharmaceutical, polymer and agricultural domains) due to their effective enhancement in sample representation (surface area and depth) and reproducibility in the spectral collection. Using such a probe, Lintvedt et al.[9] scanned heterogeneous and homogenized poultry samples and found that the estimation of ash from the two sample versions gave similar performance. This showed that employment of WAI Raman probes are promising with respect to robust measurements of heterogeneous streams of poultry by-products. For in-line measurements, variations in working distance is expected in addition to heterogeneity. Other studies[13, 14] have shown that the WAI Raman probes are good alternatives to traditional Raman probes when moderate variations in working distance are expected. This is because the WAI Raman probes do not employ strongly focused lasers. Although studies have indicated that moderate variations in working distance impact spectrum intensity less for WAI probes, the critical variation in working distance will most likely depend on the pre-processing of spectra, material properties and the analyte of interest. This motivates a study on how variation in working distance affects the estimation of fat, protein, bone and collagen in ground poultry rest raw material.

The main aim of the present study was to use in-line Raman spectroscopy for characterisation of an industrial poultry raw material stream. In the work, calibrations based on Raman measurements of fat, protein, ash (proxy for bone) and hydroxyproline (HYP, proxy for collagen) in ground poultry rest raw material were established. All samples were measured using a WAI Raman probe at varying working distance (6 cm, 9 cm, 12 cm) and probe tilt angles (0°, 30°) to mimic expected in-line variations. All calibrations were based on sample designs with high chemical variation measured in a laboratory environment. Subsequently, the obtained calibrations were tested for continuous monitoring of a ground poultry by-product stream at a commercial hydrolysis facility over the course of two days. To the best of our knowledge, this is the first time a WAI Raman probe has been tested in-line under relevant measurement conditions in the food industry.

2. Material and methods

2.1. Sample materials

Calibrations (N=59) were made based on 49 designed samples and 10 samples acquired directly from the input stream of a commercial hydrolysis process (Bioco, Hærland, Norway). For the process samples, the mix ratio of two separate input streams for turkey and chicken were varied in the range of 100% chicken - 25 % chicken. The designed calibration samples were based on a variety of raw materials acquired from the associated poultry processing plant (Nortura, Hærland, Norway). The samples were made by mixing the following ground base materials,

A: Mechanical deboning residues from chicken by-products

B: Chicken by-products prior to mechanical deboning

C: Turkey by-products prior to mechanical deboning

D: Mechanically deboned chicken meat

E: Chicken fillet

F: Chicken skin

G: Approximately 60% material D and 40 % tap water

H: Tendons and skin

Mechanical deboning is a process where the remaining meat on the carcasses after filleting is separated from the bones, resulting in two fractions: The mechanically deboned meat, containing mostly meat, and the mechanical deboning residues containing more bone. The batches of chicken skin (F) and tendon-skin-mix (H) were difficult to grind fresh and were frozen before being ground. All other base materials were taken from the process line and vacuum packed in smaller bags to keep as fresh as possible throughout the 3 experiment days. Each calibration sample was made by mixing six sub-samples of the available base blends A-H in shares according to the sample design (See section 2.2 and Tab.A.2). The samples were made consecutively during the experiment and the base blends were kept in a cold room (0 - 4 °C) throughout the whole experiment. Measurements of the samples were done in

room temperature.

A validation set (N=19) was obtained based on samples acquired from the commercial process during in-line measurements at the hydrolysis facility. Six of the samples were made by adding other materials, which could be relevant for long-term variation, manually to the grinder. These materials were acquired from the poultry production line at Nortura, and corresponded with material groups C, B, F mixed with the in-line stream and finally C mixed with in-line stream. The sampling was done with help of a half-cylinder tool, which allowed measurements to be done on the material simultaneously with the sampling. This resulted in a large sampling volume, from which the illuminated surface layer was collected (ca 300-500g). The samples were immediately vacuum packed and frozen. Later, the samples were half thawed and homogenized to be measured again under controlled conditions in the laboratory.

2.2. Calibration sample design

The target analytes fat, protein, HYP and ash content may typically covary in this kind of material. To reduce these correlations and to elucidate how independently we could model the different analytes, we carefully designed the sample set. Prior knowledge of the approximate composition of each base materials (A-H) were found from previous analyses on similar samples or in the literature and used to estimate expected sample composition of all possible mixes of the eight base materials. From the candidate samples, 49 samples were selected using the Kennard-Stone algorithm to obtain samples with large variation and low covariance between the analytes. Water was added in material G to introduce samples with lower concentrations of both fat and protein, in order to break covariances between these two analytes in the sample set. The final sample design is provided in Tab.A.2.

2.3. Measurements and data analysis

2.3.1. Raman measurements for calibration set

A MarqMetrix All-in-One (AIO) Raman system covering a Raman shift range of 100-3250 cm^{-1} was employed for all Raman measurements. The system was equipped with a 785 nm laser operating at 450 mW power and the sampling optic was a wide area illumination (D = 3mm) Proximal Ball-Probe HV stand-off Raman probe (MarqMetrix Inc., Seattle, WA, USA). Calibration samples were measured in the laboratory. Samples were placed in a rectangular aluminum sample holder (20cm × 15cm × 2cm). The surface of each sample were scanned with the Raman probe, accumulating a signal with a 6s x 5 exposure time, as illustrated in Fig.1. To mimic variations in the measurement situation that can be expected to occur in a real raw material stream, we measured all samples at a working distance of 6, 9 and 12 cm. For the optimum working distance of 9 cm, we also acquired measurements with a 30 °tilt of the Raman probe (Fig.1). Three replicate measurements were acquired for each measurement setup.

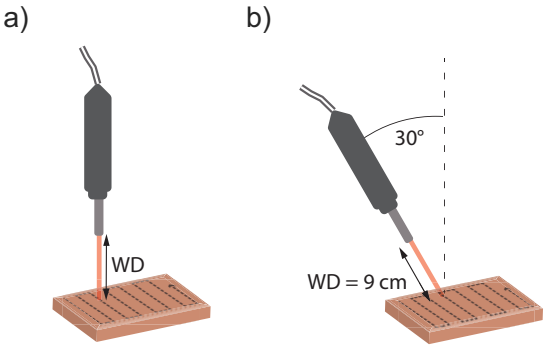

Figure 1: Laboratory measurement setup for calibration samples, illustrating the usual backscattering setup for which we acquired measurements at varying working distances (WD) (a) and the probe tilt setup measured at a 9 cm working distance (b).

2.3.2. Raman measurements for validation set

Continuous in-line measurements for testing of the laboratory calibrations were done at the poultry hydrolysis facility over 2 days. The Raman probe was placed at the outlet of a grinder, i.e at the input stream to the hydrolysis process. Fig.2 shows the hydrolysis process as well as the Raman measurement location. The probe was placed at a working distance of approximately 8 cm when the output stream was at maximum. However, the working distance varied in correspondence with the output volume, alternating from maximum stream and optimal working distance to no stream at all. This certainly affected the quality of the collected spectra, and a method for filtering out low quality spectra was needed.

Different exposure times from those used during calibration was employed in-line. This was due to the alternating grinding which provided a maximum output volume only for a limited time. The exposure time for each spectrum was set to 6s x 2 on the first day. It was adjusted to 5s x 3 on the second day to avoid saturation of the detector due to higher fluorescence levels from the material. A dark measurement was acquired approximately every 30 minutes. The software Aspen Process Pulse (Aspen Technology Inc., Bedford, MA, USA) was used for real-time analysis of the analytes. Later, the acquired samples were measured again under controlled conditions in the laboratory employing a working distance of 9 cm and an exposure time of 4s x 10, with the same scanning strategy as illustrated in Fig.1a. The further decrease in exposure time compared to previous measurements was needed due to increased fluorescence associated with sample degradation.

2.3.3. Reference measurements

Samples taken directly from the input stream to the hydrolysis were quite coarse and were therefore homogenized before reference analyses. The samples were first frozen at -20 °C and homogenized in half frozen state (10000 RPM for 6s x 4 times). Reference analyses were carried out at an external

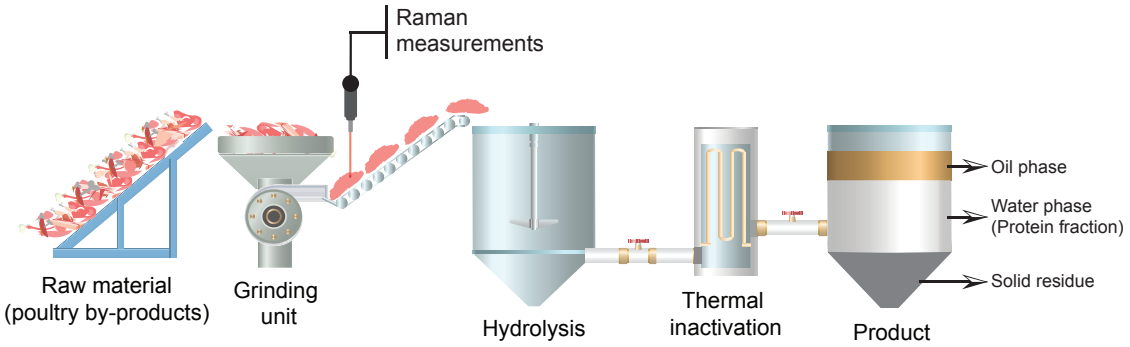

Figure 2: Schematic illustration of the hydrolysis process, with the Raman measurement location indicated. Adapted from Wubshet et al.[3]

laboratory (ALS Laboratory Group, Oslo, Norway). Determination of ash concentration (% of wet weight) were carried out by gravimetric analysis (BS 4401 Part1 1998 Commision Regulation (EC) 152/2009 MU 6.5%). Fat concentrations (percent of wet weight) were determined by pulsed NMR analysis (MU 6.5%). HYP concentrations (% of wet weight) were determined by oxidizing HYP using chloramine T and subsequently producing chromophores by the product's reaction with 4-dimethylaminobenzaldehyde (based on BS 4401-11:1995). The chromophores were measured spectrophotometrically and finally compared with standard HYP solutions. Protein concentrations (% of wet weight) were estimated from the nitrogen content using a conversion factor of 6.25. Nitrogen was determined by complete combustion of the sample in the presence of oxygen.

2.3.4. Pre-processing of spectral data

The Raman shift range 520-1800 cm^{-1} was used in the data analyses. Cosmic ray spikes were removed by a simple spike detection algorithm based on derivatives. Subsequently Savitsky-Golay (SG) smoothing (polynomial order 2 and window size 9) [15] was applied, and a baseline correction was done by the Asymmetric Least Squares (ALS) algorithm [16, 17]. The baseline correction employed a smoothing parameter of 4 and an asymmetric weighting parameter (of the residuals) of 0.01. Finally, each spectrum was normalized by the intensity of the sapphire peak at 750 cm^{-1}, mainly with the aim to correct for intensity variations due to varying working distances or potential laser fluctuations. The sapphire signal originates from the sapphire in the probe optics.

2.3.5. Data modeling

Partial least squares regression (PLSR)[18, 19] was used for model development. For the calibration set, separate models were made for the different combinations of working distance and probe tilt. The separate models were compared with a combined data set which included all measurement variations. To establish whether the estimation errors acquired were significantly different, cross validation (CV) together with a three-way analysis of variance (ANOVA) of the squared residuals (unbalanced design) was employed, as adapted from Indahl and Næs. [20] The factors included were the sample number, the calibration model and the measurement setup. In the CV, one sample (including replicate measurements) was held out in the same CV segment to avoid overfitting. A simple criterion using a 4% punish factor, as described by Westad and Martens, [21] was used to determine the number of components for the calibration models. For the in-line testing, the calibrations based on all working distances and probe tilts were used. Due to light pollution from an LCD screen at the measurement location, some regions in the in-line spectra had to be removed from the calibration, including 628-648, 832-852, 862-880, 994-1010, 1769-1788 cm^{-1}. For the calibration, we report performance through the coefficient of determination (R^2) and the root mean squared error (RMSE). For the in-line and laboratory validation, we also report these metrics when corrected for slope and bias errors, to emphasize what performance could be achieved if the cause of these errors is identified and corrected for.

2.3.6. Filtering of low quality in-line spectra

To remove in-line spectra acquired when there were little to no output stream at the grinder and spectra that were close to detector saturation, spectra with low signal-to-noise (SNR) were filtered out. For calculating the SNR, the spectra were first preprocessed as described in section 2.3.4. Then, the SNR of each spectrum was calculated as the ratio between the average spectrum intensity and the standard deviation of the estimated noise, according to Eq.1.

$$SNR = \frac{mean(I)}{sd(I_n)}, \tag{1}$$

where I is the spectrum intensity and I_n is the estimated noise intensity. Noise was estimated by subtracting a smoothed version of the spectrum from the original spectrum. For smoothing we used SG with polynomial order 2 and window size 9. This is similar to Guo et al.[22] and same as in previous work.[9] Spectra with SNR lower than 23 were discarded. This threshold was chosen so that all validation sample spectra could be

categorized of sufficient quality, since large working distances were not expected during sampling.

3. Results and discussion

3.1. Sample variation

An overview of sample variations and analyte correlations in the calibration and validation set can be found in the appendix (Fig. A.8). The calibration samples had large variations in chemistry: 1) HYP: 0.1-1.3 %, 2) Water: 51-76 %, 3) Protein: 10-22 %, 4) Fat: 2-37 % and 5) Ash: 0.5-6.2%. Several of the design samples could be considered extreme with respect to expected in-line variations. For instance, several samples contained mainly skin (very high fat) while others consisted mainly of the tendons-skin mix or chicken fillets only. Although an aim was to include large variations in composition while keeping the covariance between the different analytes at a minimum, some analytes still had considerable correlations. Fat and protein concentrations had the highest correlation (r = -0.73), followed by HYP and ash (r = 0.42). The tendon-skin samples were important to break correlations between ash and HYP (the correlation increased to r = 0.75 when they were not included). The extreme skin and fillet samples were the main reason why the correlation between fat and protein was still considerable. When removing the most high-fat and high-protein samples ($y_{fat} > 25\%$ and $y_{protein} > 18\%$) correlation could be reduced to r = -0.33. However, this led to an increased correlation between protein and ash (r = 0.48). As a high degree of heterogeneity of material should be expected in-line over time and be accounted for, we chose to not remove any extreme samples from the main analyses in this work. However, it is important to note that this did indeed impact the calibration set correlations and could impact model robustness.

With respect to the validation samples acquired in-line, a reasonable variation in most analytes were obtained (Fig.A.8), partially thanks to the manual addition of extra material. Interestingly, the variation in HYP concentration covered a different range compared to the calibration set, i.e lacking the low concentrations. The variation in ash concentration was moderate (3-6 %), with the exception of one sample at approx 13%.

3.2. Spectral features

Fig.3 shows spectra from each of the 8 base materials used in the calibration sample design. There were clear differences in the spectral fingerprints. Material E (chicken fillets) mainly exhibit spectral features associated with protein, while material F (skin) mainly shows spectral features associated with lipids. Material A has high bone (ash) content and material H has high collagen (HYP) content. Important Raman active groups associated with lipids include the out-of-phase aliphatic C-C stretch (1064 cm^{-1}), the liquid aliphatic C-C stretch in gauche (1080 cm^{-1}), the methylene twisting deformation (1301 cm^{-1}), the methylene scissor deformation (1440 cm^{-1}), the in-plane cis olefinic hydrogen bend (1267 cm^{-1}) and the cis olefinic stretch (1657 cm^{-1}). [23, 24] As Fig.3 suggests, several bands associated with protein overlap with lipid related bands, for example the C-H deformation (1450 cm^{-1}), the Amide I (1657 cm^{-1}) and the Amide III (1250, 1270 cm^{-1}).[25] Other notable bands associated with proteins originate from phenylalanine (1002cm^{-1}), tryptophan (958, 1342, 1555 cm^{-1}), tyrosine (641, 829, 856 cm^{-1}), peptide C-N bonds (1125 cm^{-1}), peptide backbone $N - C_\alpha - C$ (936 cm^{-1}) and disulfide bonds (532 cm^{-1}).[25] With respect to bone content, the main Raman band of interest was found at 960 cm^{-1}, which is associated with phosphate. The importance of this band originates from the high correlation between ash and calcium, since calcium is a major bone mineral and exists mainly as a phosphate salt.[8] The band at 750 cm^{-1} originates from sapphire in the Raman optics.

3.3. Calibration

3.3.1. Regression models

Fig.4 shows the regression results and the regression coefficients obtained for the different analytes. Here, spectra from all working distances and probe tilts were included in a single calibration for each analyte. Overall, the performance was high for all analytes ($R^2_{CV} > 0.8$). The ash model was dominated by the 960 cm^{-1} phosphate band, but included a weaker negative weighting of the 1657 band, associated with fat. This corresponded to the moderate negative correlation between fat and ash seen in the calibration set. Similar regression coefficients have been obtained in previously published work. [8] The fat model had a low degree of complexity (LV=3) and exhibited expected features, consisting mainly of positive weighting of bands associated with lipids (1080, 1306, 1437, 1655 cm^{-1}) and negative weighting of bands associated with protein (e.g. 940, 1129 cm^{-1}) . The model was dominated by bands related with saturated fat, as seen by the strong weighting of saturated modes (1080, 1306, 1437 cm^{-1}) and weaker weighting of unsaturated modes (1267, 1655 cm^{-1}). This was reasonable since a majority of the fat in these samples is saturated. The protein model was more complex (LV=7), but the model corresponded well with expectations. The main positively weighted bands are associated with the disulfide bonds (528 cm^{-1}), tyrosine (823,854 cm^{-1}), the peptide backbone $N - C_\alpha - C$ (936 cm^{-1}), tryptophan (958, 1340, 1555 cm^{-1}), phenylalanine (1002 cm^{-1}), the peptide C-N bonds (1127 cm^{-1}), and C-H deformation (1454,1466 cm^{-1}). [25] The main negatively weighted regions were associated with lipids (1266, 1302, 1442, 1659 cm^{-1}) and this indirect modelling was most likely a consequence of the considerable negative correlation between fat and protein in the calibration set. The correlation between HYP and protein was low, and the HYP model was clearly different from the total protein model, emphasizing the uniqueness of the HYP spectral fingerprint from other proteins. The main differences from the protein model were the relatively stronger weighting of the Amide I component at 1678 cm^{-1}), the weaker weighting of the C-N band at 1129 cm^{-1} and tryptophan (indole ring) at 1555 cm^{-1} and the relatively stronger weight of the peptide backbone component at 919 cm^{-1} ($N - C_\alpha - C$). These observations are in accordance

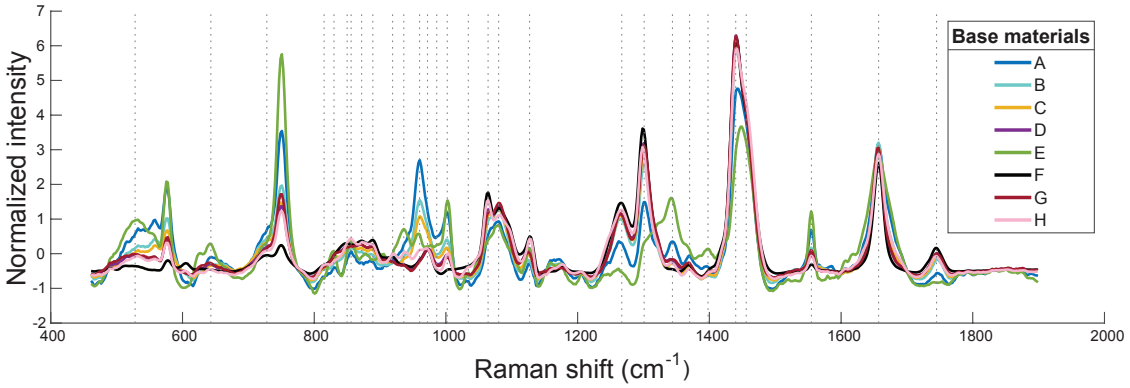

Figure 3: Baseline corrected and normalized (SNV) spectra from the 8 different poultry base materials used in the designed calibration samples, elucidating the difference in their spectral signatures. Important peaks and shoulders are indicated (dashed lines). The apparently large variation in the sapphire peak at 750 cm^{-1} is mainly an effect of the normalization procedure applied here for illustration purposes.

with characteristics for collagens. [25] A relatively stronger weight of the amide III band (1245 cm^{-1}) compared to the protein model was also found. Another interesting observation was that while protein models weighted the tyrosine doublet (827, 856 cm^{-1}) positively, the HYP models weighted the 827 cm^{-1} band negatively and the 856 cm^{-1} band positively, indicating the importance of the ratio between exposed and buried tyrosine. Overall, the obtained regression coefficients corresponded well with previous work on similar material.[4]

3.3.2. Implication of moderate variations in measurement situation

Cross validated regression models based on Raman measurements employing different working distances and probe tilts, are shown in Tab.1. The performance based on the model with all measurement setups merged was not significantly (α = 10%) different from the performance of models based on separate measurement setups, for any analytes. This demonstrated that the WAI Raman probe tackled moderate variations in working distance and probe tilt well. However, while the fat models had a stable number of components suggested across all measurement setups, the other analytes had more variations. This could indicate that the fat model was less influenced by variation in measurement situation than HYP, protein and ash models. Moreover, fat is the analyte largely dominating the overall Raman signals in the spectra (due to a combined Raman scattering efficiency and concentration effect). This could also therefore explain the effects seen in the table. Interestingly, the set including all variations in measurement setups consistently suggested the highest number of components. This could either indicate an increased complexity to compensate for effects of varying working distance or simply that employing this many components might be overfitting.

Our hypothesis was that normalization by the sapphire peak should correct for intensity differences as a function of working distance. Indeed, the SNR and average normalized spectrum intensity was little affected by the moderate variations in working distance, with SNR between 45-48 and average intensity between 0.30 - 0.31. The effect was moderate even when omitting the normalization, which showed that the WAI probe tackled the variations in working distance well. Hence, the mentioned hypothesis was not properly tested during these lab calibrations. However, when this normalization was omitted, a strong negative regression coefficient for the sapphire peak was produced for all analytes (except HYP). Although this only moderately impacted the performances, it greatly altered the regression coefficients. Although the negative weighting was stronger for the set combining measurements of different working distances, it was still present in varying degrees also for the other sets where working distances were constant. This showed that there might be other factors influencing the sapphire peak as well, and that further elucidation of this normalization strategy is of interest.

3.4. In-line validation

3.4.1. Model adjustments

As discussed in section 3.3.1, the regression coefficients acquired for the cross-validated calibrations represented models which corresponded well with literature. However, for the validation samples, employing models of the suggested complexity did not provide optimal results. The number of latent variables employed in the PLSR were instead decided based on a criteria that slope should be close to 1 and that the RMSEP corrected for slope-and-bias errors should be as low as possible. Fig.C.11 shows the regression coefficients that were employed, both for the in-line measurements and the control laboratory measurements. For the fat models, the number of components was unchanged in both cases, again emphasizing the stability and robustness of these models. For ash, a moderate decrease from 5 to 4 components was observed in both cases , indicating slight overfitting in the calibration set. The number of LVs were more critically adjusted for HYP and protein models. The number of LVs in the protein model was

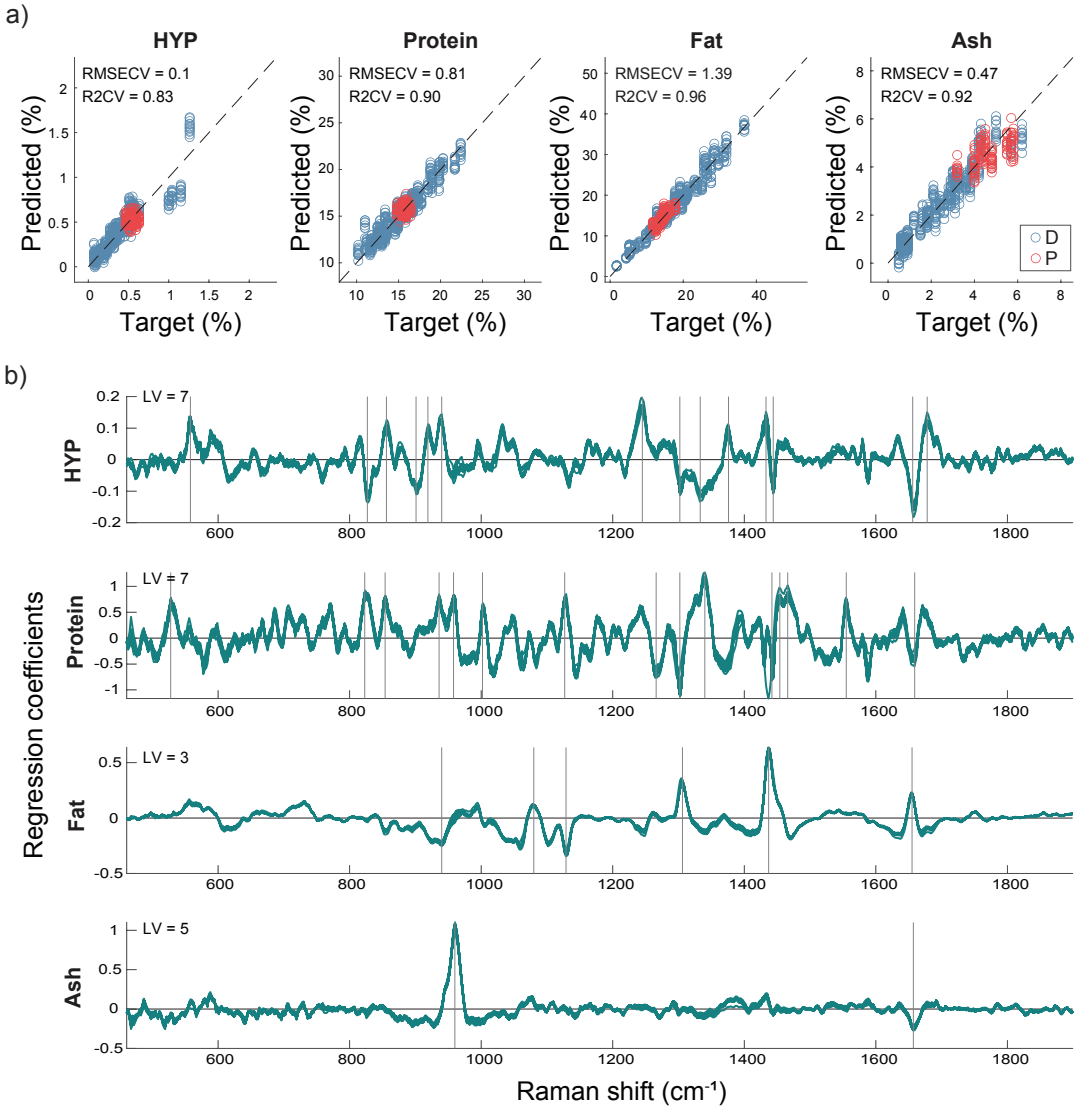

Figure 4: Predicted versus target values (a) for the calibration set including measurements in all working distances and probe tilts, with corresponding regression vectors for fat, protein, ash and HYP (b). Important regions are marked (lines). The number of latent variables (LV) employed in the respective PLSR models is indicated. Distinction is made between the design (D) and process (P) calibration samples.

Table 1: Cross validated PLSR performance for fat, protein, ash and HYP estimation, using the calibration samples and varying measurement setups.

Measurement setup		**Performance**											
WD[a]	Tilt angle	HYP			Protein			Fat			Ash		
		$RMSE_{CV}$	R^2_{CV}	LV[b]	$RMSE_{CV}$	R^2_{CV}	LV	$RMSE_{CV}$	R^2_{CV}	LV	$RMSE_{CV}$	R^2_{CV}	LV
6 cm	0 °	0.12	0.78	5	0.85	0.89	4	1.29	0.97	3	0.50	0.91	2
9 cm	0 °	0.11	0.81	7	0.88	0.89	4	1.30	0.96	3	0.48	0.92	5
9 cm	30 °	0.10	0.83	6	0.79	0.91	6	1.34	0.96	3	0.48	0.92	5
12 cm	0 °	0.11	0.80	5	0.71	0.93	7	1.39	0.96	3	0.50	0.91	4
all	all	0.10	0.83	7	0.81	0.91	7	1.39	0.96	3	0.47	0.92	5

[a] working distance
[b] number of latent variables employed in the PLS model.

decreased from 7 to 2-and-3, respectively. The main effect of this was stronger indirect modelling on bands associated with other analytes, i.e fat and ash. For the in-line HYP model, the number of LVs were reduced from 7 to 3 and overall became more similar to the protein models. This was not the case for the HYP model based on controlled laboratory measurements, which only had a moderate decrease from 7 to 6 LVs.

Several factors might have contributed to the model changes that were observed between the calibration and validation set as well as the discrepancies between the in-line and laboratory models. Overfitting of the calibration set might be one factor, but another important factor was the light pollution from the LCD screen during in-line measurements. The signals consisted of narrow peaks which varied in intensity and resulted in mismatches in the dark subtraction, and the corresponding regions needed to be discarded. This had little effect on the fat and ash models, as the regions did not correspond to any important bands associated with these analytes. The protein and HYP models were more affected, as the discarded regions were associated with e.g. phenylalanine (994-1010 cm^{-1}), tyrosine (832-852, 862-880 cm^{-1}) and tryptophan (862-880 cm^{-1} cm^{-1}). The choice of number of LVs for the controlled laboratory measurements could potentially also be affected by the homogenization of the samples.

3.4.2. Filtering out low quality spectra

Fig. 5a shows the in-line spectra that were filtered out by the SNR thresholding routine. The low quality spectra included many low intensity spectra corresponding to large working distances or no material stream at the grinder. A few high intensity spectra were also filtered out, due to strong fluorescence that lead to a large shot noise component combined with near-saturation effects. The in-line variations in working distances were much larger (ca 4-30 cm) than accounted for in the calibration (6-12 cm). There was still a large range of intensities among the accepted spectra (Fig. 5a,b). This could potentially be explained by chemistry alone, but could also potentially be related to working distance intensity fluctuations not accounted for by the sapphire normalisation.

The filtering routine was based on a simple thresholding of the spectrum SNR. In the calibration set, the SNR and average spectrum intensity was little affected by the moderate variations in working distance. Since the variations were much larger during in-line measurements, the SNR did vary with the alternating working distance (Fig. B.9). However, the SNR could also be influenced by other phenomena that changes either the average Raman signal intensity (e.g. chemistry) or the noise level (e.g. shot noise from fluorescence). For example, a high fat sample measured at a large working distance could yield similar SNR as a low fat sample measured at shorter working distance. Therefore, this method might not be the best choice if one wants to specifically diagnose and filter out spectra with large working distances. Overall, further elucidation of specific spectral diagnosis and sapphire normalization dependence on working distance is of high interest.

3.4.3. Predictions

After filtering out low SNR spectra, predictions of all analytes were performed, and considerable variations around the average trend line were still present in predictions (Fig.C.10). These variations are most likely real and first of all a consequence of heterogeneity of the material stream. Identifying the main trends in material composition is the most interesting with respect to process control, as one set of hydrolysis settings would be applied to a large volume of material. The hydrolysis of the material typically runs for 45 minutes, and potential process adjustments based on material composition should be made within this time frame. In that regard the variations in predictions over a smaller time interval (e.g. 5 min) might not be critical for process control. By employing a 15 min moving average, temporal variations in the predicted material composition was evident (Fig. 6). By comparing the qualitative trends, expected patterns were observed. For instance higher fat concentrations were often accompanied by lower concentrations in other analytes. Around time index 800-850 (day 2), a sudden change in predicted protein, fat and ash concentration was observed, which corresponded with the extra materials that were added manually. The correlations between the predicted analyte trends corresponded well with the measured values for validation samples in case of fat-protein ($r_{val} = -0.56, r_{pred} = -0.56$), protein-hyp ($r_{val} = 0.4, r_{pred} = 0.34$) and ash-fat ($r_{val} = -0.33, r_{pred} = -0.17$). As expected due to the larger adjustments in the HYP and protein models, dis-

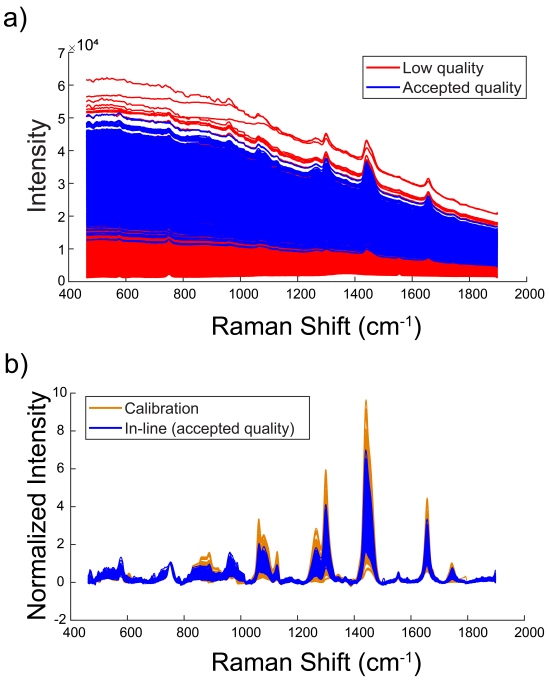

Figure 5: All raw spectra acquired in-line at the hydrolysis plant, showing low quality spectra which were filtered out and the spectra with sufficient quality used for predictions (a) and the pre-processed version of the accepted spectra compared to calibration spectra (b).

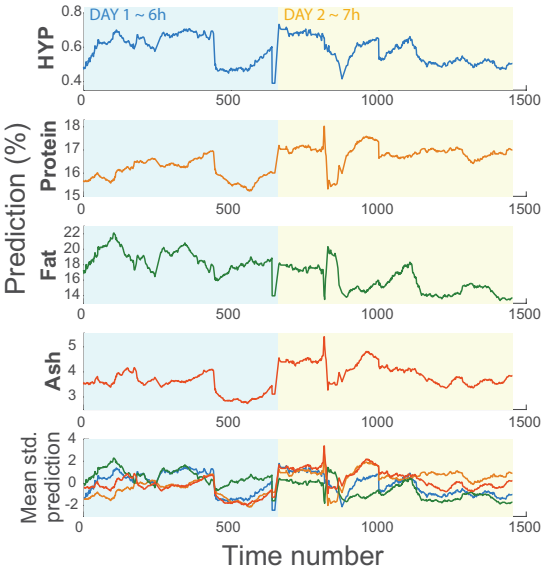

Figure 6: Predicted trends over the two measurement days for HYP, protein, fat and ash (a-d) and the mean standardized predictions of these compounds for better comparison of qualitative trends (e). The trends are calculated as a 15 min moving average.

cussed in section 3.4.1, the HYP and protein correlations with other analytes were higher, i.e between fat-HYP ($r_{val} = -0.04, r_{pred} = 0.56$), ash-HYP ($r_{val} = 0.5, r_{pred} = 0.61$) and protein-ash ($r_{val} = 0.31, r_{pred} = 0.8$) Although HYP and protein models exhibited a larger degree of indirect modelling on fat and bone than wanted, the overall prediction trends indicated that we were able to measure chemistry in spite of the challenging measurement conditions.

3.4.4. Performance for validation samples

Fig. 7 shows the predicted versus measured values of the validation samples measured in-line and later in the laboratory. Overall, there was a certain degree of bias and slope errors for most analytes, but they were not extreme, and the results are very promising. Assuming these systematic errors can be resolved, the corrected prediction errors ($RMSEP_{corr}$) were still overall larger than for the cross-validated calibration set. One source of error for the in-line measurement was the sampling. Since the collected samples were large and the illumination area small, the spectra-to-reference correspondence was likely poorer compared to the control laboratory measurements. This was probably part of the reason why the corrected prediction errors were generally smaller for the controlled laboratory measurements. Moreover, this likely explains why the one sample with high ash concentration was considerably better predicted from the laboratory measurement (Fig.7), as this sample was collected under demanding sampling conditions.

Although the corrected prediction errors were smaller for the laboratory measurements, there were similar bias and slope errors as for the in-line measurements, indicating weaknesses in the calibration models. This was, as discussed, particularly expected for protein and HYP models. For instance, the same two samples were underestimated with respect to protein concentration (Fig.7) in both cases. In particular the protein predictions were affected by variations in fat concentrations, as was evident from the increased correlation between predicted protein and fat concentrations ($r_{inline} = -0.76$) compared to the true values ($r = -0.56$). This revealed robustness issues, i.e dependence on conserved correlations with fat, which was not clear from the predictions over the full time span discussed in section 3.4.3. The HYP performance mainly had bias and slope issues, while the $RMSEP_{corr}$ was similar to those obtained in the calibration set. The former errors could be related to the lack of samples with moderate-to-high HYP concentrations in the calibration set. Other factors that could contribute to the prediction errors could be variations between calibration and validation samples, e.g. pressure applied during grinding, homogenization, freezing and thawing. Overall, further calibration development is advantageous, particularly with respect to robustification of HYP and protein models.

Another source of error for in-line measurements could be the challenging measurement conditions. For example the re-

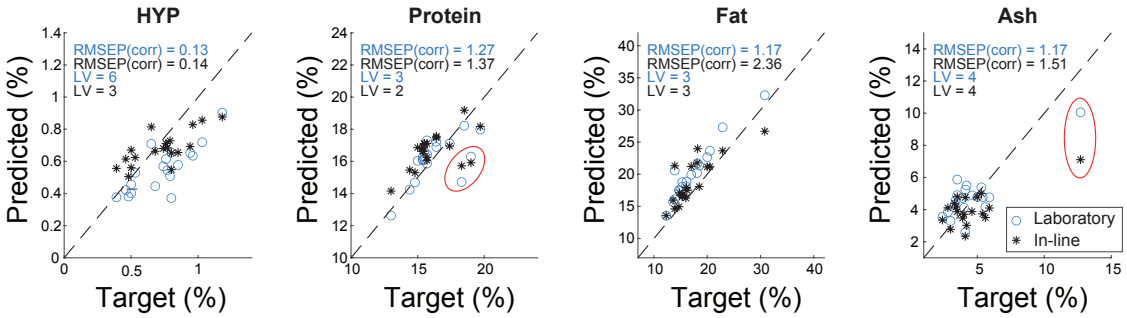

Figure 7: Predicted versus target values for each analyte, using in-line measurements (black) and laboratory measurements (blue). Note that the reported RMSEP values are corrected for bias-and-slope errors, while the plotted predicted values themselves are not corrected. Predictions for samples which are discussed in the text are marked (red circle).

duced exposure time led to reduced SNR (ca.30) compared to the calibration and laboratory validation spectra (ca.50). This might be another reason why the corrected prediction errors were higher for the in-line measurements. Secondly, the large variations in working distance could possibly contribute with errors, depending on the robustness of the pre-processing. It was assumed that the sapphire normalization could handle the variations present in exposure times and working distances, which could not be completely confirmed. After pre-processing, the intensities were lower for the in-line spectra compared to the calibration spectra (Fig. 5b) Although this could be expected due to the more extreme samples in the calibration set, the full extent of the intensity differences might not be justified by the differences in chemistry (i.e. 2% - 37% fat in calibration compared to 12%-31% fat for validation samples). This could be indicative of a pre-processing issue or an issue with calibration transfer from laboratory (room temp) to hydrolysis facility (6-8 °C). Notably, the temperatures at the hydrolysis facility were lower than the listed operating temperature (15-33 °C) for the instrument. In the future, it is of interest to look into robustification of the pre-processing as well as exploring if more custom pre-processing for different analytes could be advantageous.

4. Future potential

We have demonstrated that WAI Raman spectroscopy has potential as a tool for characterization of very heterogeneous streams of raw material, in an in-line industrial environment. Although this was demonstrated through measurements of a poultry rest raw material stream in this study, this indicates that there are many other prospective applications in the food industry. Today, in-line sensor systems in the food industry mainly employ NIRS. Such systems have the advantage that they are cheaper, have relatively simple assembly in the process-line, are insensitive to ambient light and have much better sample coverage. In contrast, Raman spectroscopy based systems will require more careful development of practical measurement setup. For instance one might need shielding from ambient light. However, WAI Raman opens up for more sophisticated sensor systems which could target more detailed chemistry and quality parameters. Due to the more unique Raman fingerprints compared to NIRS, Raman might also be more robust with respect to variations in absorption and scattering properties within a sample or between samples and have a lower degree of dependence on conserved correlations with other compounds. This potentially means that Raman based models can be more easily maintained in the industry. Overall, WAI Raman spectroscopy may be a good alternative to NIRS for industrial food quality monitoring, particularly in applications where more detailed chemical analysis is needed.

5. Conclusion

In this work, the cross validated calibration set showed that moderate variations in working distance (6-12 cm) or probe tilt (0, 30°) did not significantly affect the performance of fat, protein, ash and hydroxyproline estimation for poultry rest raw material. The in-line test of the acquired models represented demanding measurement conditions, including light pollution, large variations in working distance and variations in exposure time. Even so, reasonable variations in average trends of raw material composition were predicted. It is the authors' impression that with further efforts in calibration development, potentially in combination with development of practical measurement setup, the use of Raman spectroscopy as a process control tool in the hydrolysis of poultry rest raw materials is within reach.

6. Data availability statement

All data that support the findings of this study are available from the corresponding author, upon request.

7. Funding

This work was partially funded by the Research Council of Norway through the projects SFI Digital Food Quality and the

Food Pilot Plant [grant numbers 309259, 296083]; along with the Norwegian Agricultural Food Research Foundation through the project Precision Food Production [grant number 314111].

8. Acknowledgements

We would like to express a special thanks to MarqMetrix Inc. for providing Raman instrumentation through the partnership in the SFI Digital Food Quality project. We also extend our thanks to Katinka Dankel, Lene Øverby, Ulrike Böcker and Erik Tengstrand at Nofima for assistance during sample preparation and data acquisition.

Appendix A. Sample composition

Appendix B. Filtering of low quality spectra

Appendix C. In-line predictions

Table A.2: The sample design for the calibration set, made from raw material A-H. One sample part was defined as 1 dl of the respective material.

Sample number	**Part 1/6**	**Part 2/6**	**Part 3/6**	**Part 4/6**	**Part 5/6**	**Part 6/6**
1	A	A	A	A	A	A
2	B	B	B	B	B	B
3	C	C	C	C	C	C
4	D	D	D	D	D	D
5	E	E	E	E	E	E
6	F	F	F	F	F	F
7	G	G	G	G	G	G
8	H	H	H	H	H	H
9	A	A	C	E	F	G
10	D	D	D	F	F	F
11	E	E	G	G	G	G
12	F	F	G	G	G	G
13	C	C	C	C	C	F
14	E	F	F	F	F	F
15	D	E	E	E	E	F
16	F	G	G	G	G	G
17	A	B	E	E	E	G
18	D	D	D	D	D	F
19	D	D	D	D	F	F
20	B	B	C	G	G	G
21	B	B	B	C	C	C
22	C	C	C	C	F	F
23	F	F	F	F	G	G
24	F	F	F	G	G	G
25	B	B	B	E	G	G
26	D	D	D	D	G	G
27	A	B	B	B	D	D
28	B	C	F	G	G	G
29	B	C	F	F	F	F
30	C	F	F	F	F	F
31	C	D	E	E	E	F
32	A	C	C	E	E	E
33	C	C	C	E	F	G

Table A.2 continued:

Sample number	Part 1/6	Part 2/6	Part 3/6	Part 4/6	Part 5/6	Part 6/6
34	E	E	E	F	G	G
35	B	C	F	F	G	G
36	B	B	B	B	C	F
37	B	C	C	F	F	F
38	C	E	E	E	E	E
39	C	C	C	G	G	G
40	D	E	E	E	F	F
41	D	E	E	E	G	G
42	C	C	D	E	F	F
43	D	E	G	G	G	G
44	B	D	E	F	G	H
45	F	F	F	F	H	H
46	B	B	B	G	H	H
47	C	C	C	F	H	H
48	C	E	E	F	H	H
49	A	A	E	E	E	H

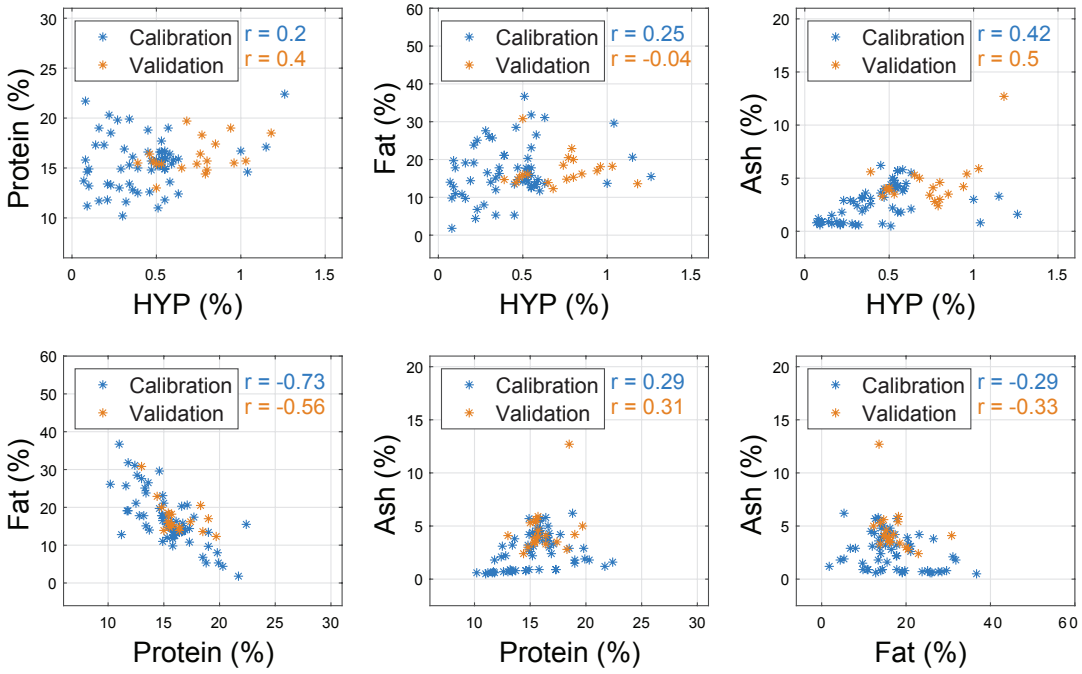

Figure A.8: Variation in analytes and their correlation in the calibration set compared to in-line validation set.

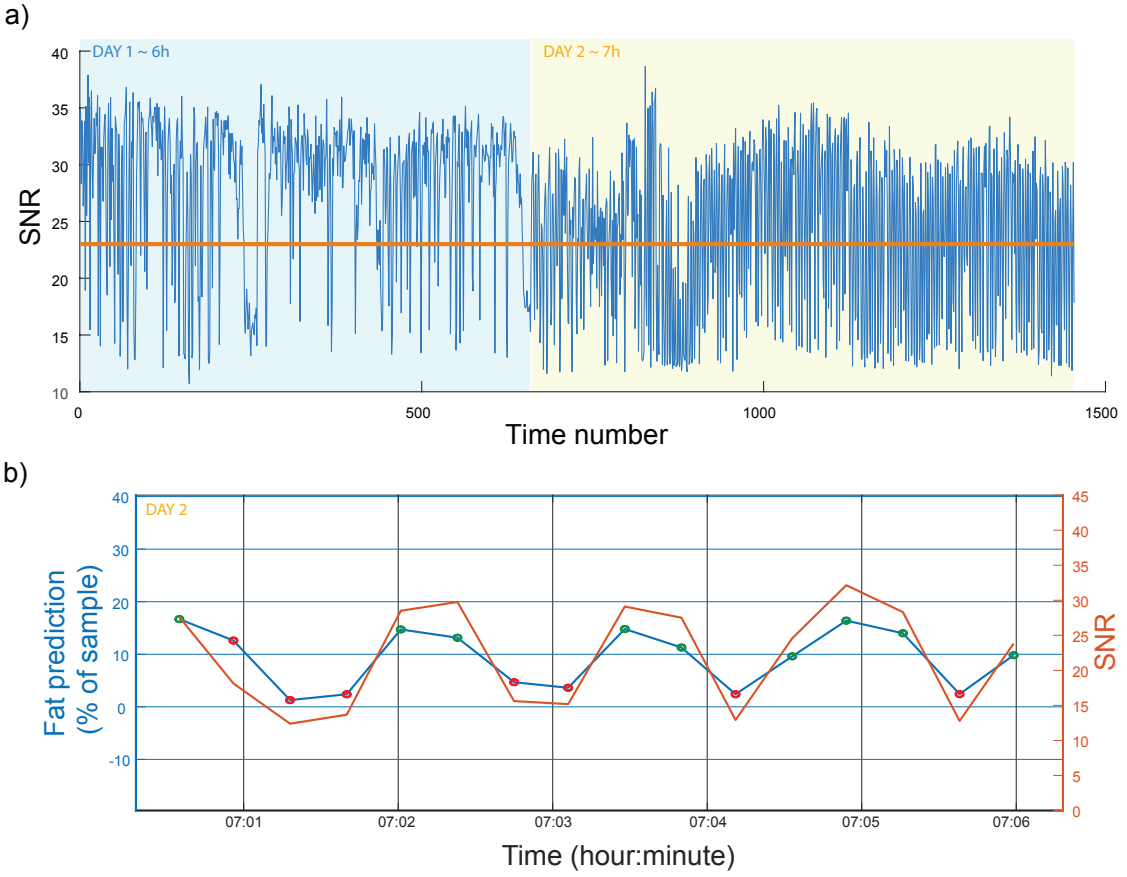

Figure B.9: Variation in SNR over time, with the threshold used to filter out low quality spectra indicated (a). An example of how fat predictions and SNR alternated within a shorter time span is shown (b). There were clearly periodic variations which corresponded with the alternating output volume (i.e working distance) at the grinder. Predictions associated with discarded predictions are marked (red), while predictions based on spectra with accepted quality are marked (green).

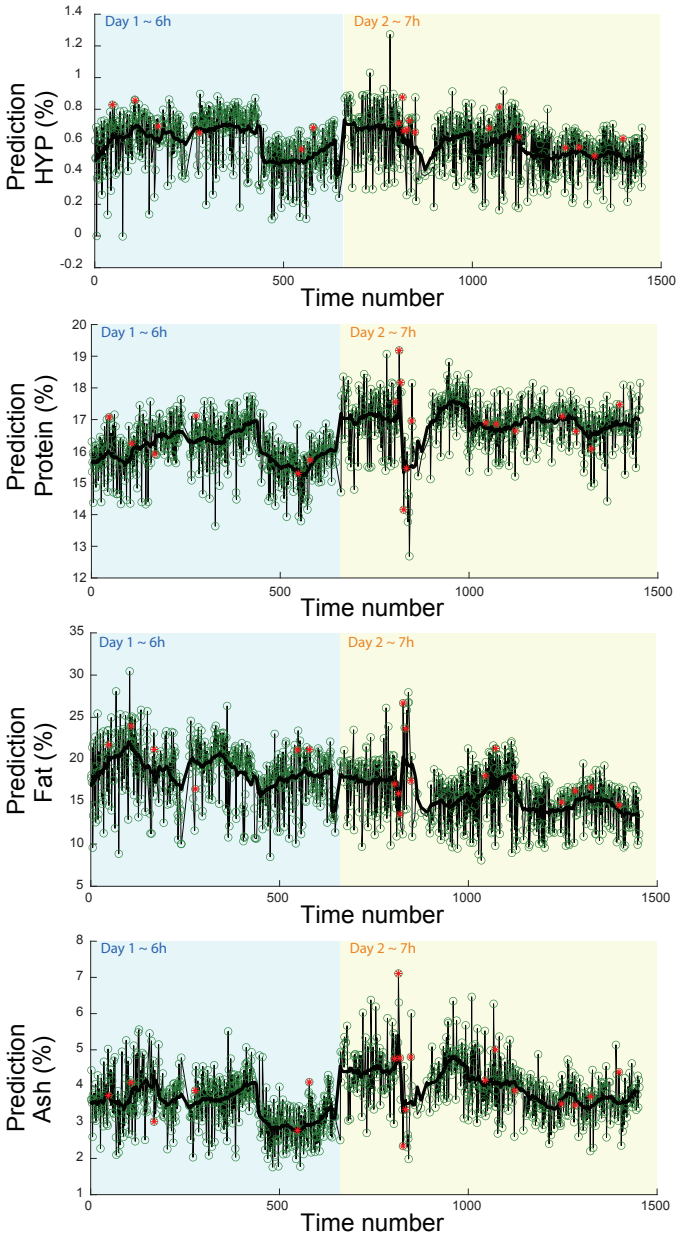

Figure C.10: All in-line predictions based on spectra with accepted quality. Times for reference sampling and corresponding predictions are marked (red *). The black lines show the average trends, calculated as a 15 min moving average.

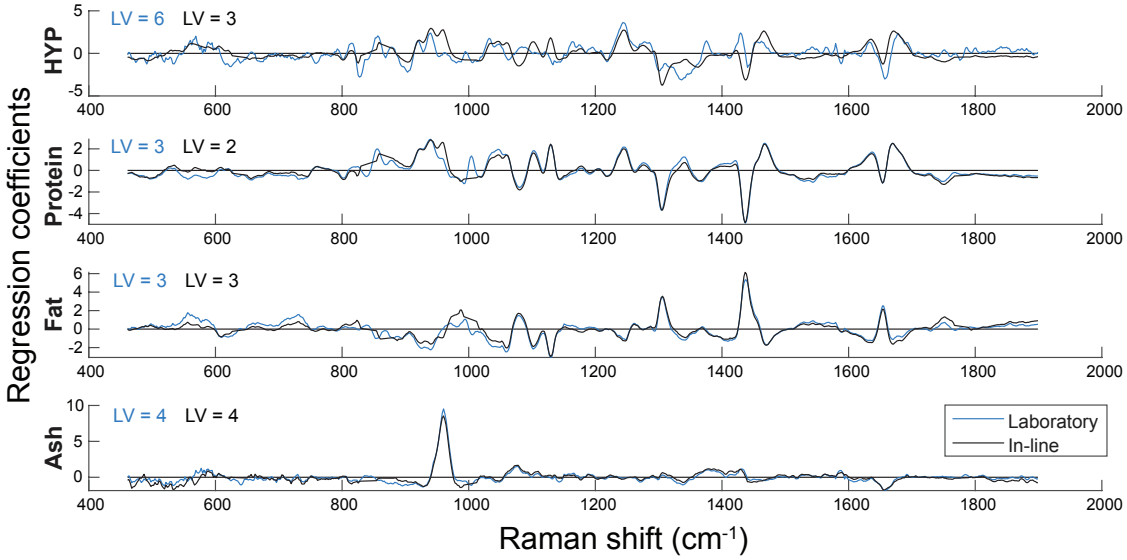

Figure C.11: Regression coefficients used for the validation, based on in-line measurements (black) and laboratory measurements (blue). The number of latent variables (LV) employed in the respective PLSR models is indicated.

References

[1] D. Lindberg, K. A. Kristoffersen, H. de Vogel-van den Bosch, S. G. Wubshet, U. Böcker, A. Rieder, E. Fricke, N. K. Afseth, Effects of Poultry Raw Material Variation and Choice of Protease on Protein Hydrolysate Quality, Process Biochemistry 110 (2021) 85–93. doi:10.1016/j.procbio.2021.07.014.

[2] D. Lindberg, K. A. Kristoffersen, S. G. Wubshet, L. M. G. Hunnes, M. Dalsnes, K. R. Dankel, V. Høst, N. K. Afseth, Exploring Effects of Protease Choice and Protease Combinations in Enzymatic Protein Hydrolysis of Poultry By-Products, Molecules 26 (17) (2021) 5280. doi:10.3390/molecules26175280.

[3] S. G. Wubshet, J. P. Wold, N. K. Afseth, U. Böcker, D. Lindberg, F. N. Ihunegbo, I. Måge, Feed-Forward Prediction of Product Qualities in Enzymatic Protein Hydrolysis of Poultry By-products: a Spectroscopic Approach, Food and Bioprocess Technology 11 (2018) 2032–2043. doi:10.1007/s11947-018-2161-y.

[4] O. Monago-Maraña, J. P. Wold, R. Rødbotten, K. R. Dankel, N. K. Afseth, Raman, Near-Infrared and Fluorescence Spectroscopy for Determination of Collagen Content in Ground Meat and Poultry By-Products, Food Science and Technology 95 (2019) 267–273. doi:10.1016/j.lwt.2020.110592.

[5] Y. Dixit, M. P. Casado-Gavalda, R. Cama-Moncunill, P. J. Cullen, C. Sullivan, Challenges in Model Development for Meat Composition Using Multipoint NIR Spectroscopy from At-Line to In-Line Monitoring, Journal of Food Science 82 (7) (2017) 1557–1562. doi:10.1111/1750-3841.13770.

[6] P. Mishra, R. Klont, T. Verkleij, S. Wisse, Translating Near-Infrared Spectroscopy from Laboratory to Commercial Slaughterhouse: Existing Challenges and Solutions (2021). doi:10.1016/j.infrared.2021.103918.

[7] P. V. Andersen, J. P. Wold, N. K. Afseth, Assessment of Bulk Composition of Heterogeneous Food Matrices Using Raman Spectroscopy, Applied Spectroscopy 75 (10) (2021) 1278–1287. doi:10.1177/00037028211006150.

[8] S. G. Wubshet, J. P. Wold, U. Böcker, K. W. Sanden, N. K. Afseth, Raman Spectroscopy for Quantification of Residual Calcium and Total Ash in Mechanically Deboned Chicken Meat, Food Control 95 (2019) 267–273. doi:10.1016/j.foodcont.2018.08.017.

[9] T. A. Lintvedt, P. V. Andersen, N. K. Afseth, B. Marquardt, L. Gidskehaug, J. P. Wold, Feasibility of In-line Raman Spectroscopy for Quality Assessment in Food Industry - How Fast Can We Go?, Applied Spectroscopy 76 (5) (2022) 559–568. doi:10.1177/00037028211056931.

[10] T. A. Lintvedt, P. V. Andersen, N. K. Afseth, K. Heia, S.-K. Lindberg, J. P. Wold, Raman Spectroscopy and NIR Hyperspectral Imaging for In-line Estimation of Fatty Acid Features in Salmon Fillets, Talanta 254 (2023) 124113. doi:10.1016/j.talanta.2022.124113.

[11] N. K. Afseth, K. Dankel, P. V. Andersen, G. F. Difford, S. S. Horn, A. Sonesson, B. Hillestad, J. P. Wold, E. Tengstrand, Raman and near Infrared Spectroscopy for Quantification of Fatty Acids in Muscle Tissue—A Salmon Case Study, Foods 11 (7) (2022) 962. doi:10.3390/foods11070962.

[12] K. Shin, H. Chung, Wide Area Coverage Raman Spectroscopy for Reliable Quantitative Analysis and its Applications (2013). doi:10.1039/c3an36843b.

[13] H. Wikström, I. R. Lewis, L. S. Taylor, Comparison of Sampling Techniques for In-line Monitoring using Raman Spectroscopy, Applied Spectroscopy 59 (7) (2005) 934–941. doi:10.1366/0003702054411553.

[14] I. Latka, S. Dochow, C. Krafft, B. Dietzek, J. Popp, Fiber Optic Probes for Linear and Nonlinear Raman Applications - Current Trends and Future Development, Laser and Photonics Reviews 7 (5) (2013) 698–731. doi:10.1002/lpor.201200049.

[15] A. Savitzky, M. J. Golay, Smoothing and Differentiation of Data by Simplified Least Squares Procedures, Analytical Chemistry 36 (8) (1964) 1627–1639. doi:10.1021/ac60214a047.

[16] P. H. C. Eilers, H. F. M. Boelens, A Perfect Smoother, Life Sciences 75 (14) (2003) 3631–3636. doi:10.1021/ac034173t.

[17] K. H. Liland, T. Almøy, B. H. Mevik, Optimal Choice of Baseline Correction for Multivariate Calibration of Spectra, Applied Spectroscopy 64 (9) (2010) 1007–1016. doi:10.1366/000370210792434350.

[18] H. Martens, T. Næs, Multivariate Calibration, 2nd Edition, Wiley, Chichester, UK, 1989.

[19] Å. Björck, U. G. Indahl, Fast and Stable Partial Least Squares Modelling: A Benchmark Study with Theoretical Comments, Journal of Chemometrics 31 (8) (aug 2017). doi:10.1002/cem.2898.

[20] U. G. Indahl, T. Næs, Evaluation of Alternative Spectral Feature Extraction Methods of Textural Images for Multivariate Modelling, Journal of Chemometrics 12 (4) (1998) 261–278. doi:10.1002/(SICI)1099-128X(199807/08)12:4<261::AID-CEM513>3.3.CO;2-Q.

[21] F. Westad, H. Martens, Variable Selection in Near Infrared Spectroscopy Based on Significance Testing in Partial Least Squares Regression, Journal of Near Infrared Spectroscopy 8 (2) (2000) 117–124. doi:10.1255/jnirs.271.

[22] S. Guo, C. Beleites, U. Neugebauer, S. Abalde-Cela, N. K. Afseth, F. Alsamad, S. Anand, C. Araujo-Andrade, S. Aškrabić, E. Avci, M. Baia, M. Baranska, E. Baria, L. A. E. Batista de Carvalho, P. de Bettignies, A. Bonifacio, F. Bonnier, E. M. Brauchle, H. J. Byrne, I. Chourpa, R. Cicchi, F. Cuisinier, M. Culha, M. Dahms, C. David, L. Duponchel, S. Duraipandian, S. F. El-Mashtoly, D. I. Ellis, G. Eppe, G. Falgayrac, O. Gamulin, B. Gardner, P. Gardner, K. Gerwert, E. J. Giamarellos-Bourboulis, S. Gizurarson, M. Gnyba, R. Goodacre, P. Grysan, O. Guntinas-Lichius, H. Helgadottir, V. M. Grošev, C. Kendall, R. Kiselev, M. Kölbach, C. Krafft, S. Krishnamoorthy, P. Kubryck, B. Lendl, P. Loza-Alvarez, F. M. Lyng, S. Machill, C. Malherbe, M. Marro, M. P. M. Marques, E. Matuszyk, C. F. Morasso, M. Moreau, H. Muhamadali, V. Mussi, I. Notingher, M. Z. Pacia, F. S. Pavone, G. Penel, D. Petersen, O. Piot, J. V. Rau, M. Richter, M. K. Rybarczyk, H. Salehi, K. Schenke-Layland, S. Schlücker, M. Schosserer, K. Schütze, V. Sergo, F. Sinjab, J. Smulko, G. D. Sockalingum, C. Stiebing, N. Stone, V. Untereiner, R. Vanna, K. Wieland, J. Popp, T. Bocklitz, Comparability of Raman Spectroscopic Configurations: A Large Scale Cross-Laboratory Study, Analytical Chemistry 92 (24) (2020) 15745–15756. doi:10.1021/acs.analchem.0c02696.

[23] N. K. Afseth, J. P. Wold, V. H. Segtnan, The Potential of Raman Spectroscopy for Characterisation of the Fatty Acid Unsaturation of Salmon, Analytica Chimica Acta 572 (1) (2006) 85–92. doi:10.1016/j.aca.2006.05.013.

[24] J. R. Beattie, S. E. J. Bell, C. Borgaard, A. Fearon, B. W. Moss, Prediction of Adipose Tissue Composition using Raman Spectroscopy: Average Properties and Individual Fatty Acids, Lipids 41 (3) (2006) 287–294. doi:10.1007/s11745-006-5099-1.

[25] A. Rygula, K. Majzner, K. M. Marzec, A. Kaczor, M. Pilarczyk, M. Baranska, Raman Spectroscopy of Proteins: A Review, Journal of Raman Spectroscopy 44 (8) (2013) 1061–1076. doi:10.1002/jrs.4335.

ISBN: 978-82-575-2033-5
ISSN: 1894-6402

Nofima
Postboks 6122
NO-9291 Tromsø
nofima.no

Norwegian University
of Life Sciences

Postboks 5003
NO-1432 Ås, Norway
+47 67 23 00 00
www.nmbu.no

116573 / ANDVORDGRAFISK.NO